EXPERIMENTAL AND MODELING EVALUATION OF PROPPANT TRANSPORT IN COMPLEX FRACTURES

by

Abla Rhouma

A thesis submitted to the Faculty and the Board of Trustees of the Colorado School of Mines in partial fulfillment of the requirements for the degree of Doctor of Philosophy (Petroleum Engineering).

Golden, Colorado

Date: _____

Signed: _____

Abla Rhouma

Signed: _____

Dr. Jennifer Miskimins
Advisor

Signed: _____

Dr. Hazim Abass
Co-Advisor

Golden, Colorado

Date: _____

Signed: _____

Dr. Erdal Ozkan
Professor and Head
Department of Petroleum Engineering

ABSTRACT

Hydraulic fracturing (HF) is widely used to stimulate and produce hydrocarbons from both conventional and unconventional reservoirs. Hydraulic fracturing creates thin but long fractures that frequently connect to pre-existing natural fractures or newly created micro-fractures resulting from the HF process in the formation; thus, creating a complex fracture network. The transport, placement, and distribution of the proppant in these complex fractures is dependent on the proppant type, size, density, the fluid viscosity and the slurry injection rate. The fracturing fluid and the proppants affect the productivity and conductivity of the complex fracture network created by the HF process. A 2015 study by Alotaibi at the Colorado School of Mines used inter-connected orthogonal fractures sets with water as the transport fluid. In this thesis, Alotaibi's results are extended to a complex fracture network consisting of non-orthogonal fractures of unequal width with 'slickwater' used as the transport fluid.

A complex fracture network made of Plexiglas® slots was constructed to simulate a prototype of an en echelon natural fracture system; thus, the fractures were not exactly parallel. The ultimate purpose of this research is to improve our understanding of proppant transport in complex fracture network using slickwater at various concentration of friction reducer, different proppant types (size and density), and different injection rates.

The following was completed during this thesis: 1) a new laboratory apparatus was built to conduct proppant transport studies in a complex fracture system consisting of a main fracture, three sub-fractures branches or groups, and two open perforations; 2) using this apparatus, the minimum slurry velocity in the entrance of each branch of the fracture network at seven locations was determined; 3) computational fluid dynamics (CFD) software from ANSYS simulated the proppant placement, distribution and trajectory inside the complex fracture networks for three slickwater compositions, two proppant types, three proppant sizes, nine hybrid proppants, and two injection rates; and 4) experiments were also performed by alternately closing the top and bottom main entry points.

Proppant dune development measurements were obtained in regard to dune height, dune area, and proppant distribution. Evaluations were made to the effects of proppant size, proppant density, fluid properties and injection rates on slickwater transport in the main as well as the sub-

fracture groups, plus evaluations of transport using hybrid proppants mixtures. The results are reported for the transport mechanisms as a function of perforation location height.

This research found that higher viscosity fluids resulted in proppant transportability increasing from 20% to 36% into the sub-fracture groups. Higher flow rates, going from 1 gal/min to 2 gal/min yielded higher velocities that transported proppants of all sizes further in the fracture network and yielded longer propped areas. The increased flow rates improved transport from 3% to 13%. The diameter of the proppants did hinder the transport of proppants when the median diameter was doubled as the change in dune height was decreased by 9.4%. The sieve analysis showed that 100 mesh had 35% more segregation than the 40/70 mesh while hybrid proppants of different sizes provided a 40% better coverage of the fractures of different widths. In vertically propped areas, hybrid proppants with different densities provided a 70% better propped area in each fracture.

Comparisons were made between lab experiments and simulated results from ANSYS Fluent computer modeling and found to be very close. The results showed that higher concentrations of friction reducer combined with higher slurry velocity have a great impact on the distribution of the proppant into the sub-fracture groups including the quaternary fracture.

The results from the numerical modeling indicated that the fracture width and fluid viscosity had the most significant impact on proppant placement, while the sand size and density had a lesser impact on the distribution of the proppant in fractures. The fracture network geometry, such as bends and angles, had the least impact on the proppant transport and settling.

TABLE OF CONTENTS

LIST OF FIGURES

LIST OF TABLES

ACKNOWLEDGMENTS

To my advisor, Dr. Jennifer Miskimins, I would like to express my sincerest gratitude for the motivation, patience, and immense knowledge throughout the two and a half years of my Ph.D. program at Colorado School of Mines. Her counsel aided me during the time of research and writing of this thesis. I couldn't begin to describe the endless support you have given me. Through your guidance, teaching, and advice, this project materialized into what it is today. It has been a great honor to work with you and I will always be grateful for your time and expertise.

To Dr. Ramona Graves, with your funding and instruction, I have been able to complete my doctorate degree. I will always be grateful to you and fortunate to have had you. Thank you for granting me this opportunity to do my Ph.D. degree and for your financial support.

I would also like to extend my sincerest appreciation to my minor advisor, Dr. Steven Sonnenberg, and my co-advisor Dr. Hazim Abass. The door to your office was always open to me. Without their passionate participation and input, I would not have been able to successfully complete this project. I was fortunate to have had the chance to work with you and gain from your mastery and perception.

Furthermore, I would like to thank my committee members, Dr. Manika Prasad, Dr. Mansur Ermila, and Dr. Jessica Smith for their insight into this project. You all made yourselves available for advice and helped widen my research from the various perspectives you have provided for me.

I also want to thank the Petroleum Engineering Department at Colorado School of Mines for the help and support throughout my research.

Lastly, I would like to thank my family for supporting me to travel to the United States to conduct my Ph.D. at Colorado School of Mines. To my mother, Mabrouka Alzredi, and my father, Abdulsalam Rhouma, without your prayers, nurturing and sacrifices that you have made on my behalf, I would never be where I am today. I would also like to thank my friends in the United States for supporting me throughout my research and helping me reach my goals.

DEDICATIONS

This dissertation is dedicated to my loving parents, Mabrouka Alzredi and Abdulsalam Rhouma, who have been the source of my motivation, encouragement, and support. I would also like to dedicate my Ph.D. work to my brothers and sisters who have supported me and kept me grounded throughout my years in the United States.

CHAPTER 1

INTRODUCTION

Hydraulic fracturing is an important technique that has enhanced the production of hydrocarbons from oil and gas bearing formations. Since its inception in 1947, fracturing technology has improved dramatically. Hydraulic fracturing in unconventional reservoirs began to take off in 1981, when Mitchell Energy developed gas production using hydraulic fracturing in the Barnett Shale in the Fort Worth Basin (Curtis 2002). Since then, the technology has advanced to where it has become the primary means to extract hydrocarbons from low permeability formations. Between Texas, Oklahoma, Pennsylvania, Wyoming, and Louisiana, hydraulic fracturing accounted for 65% of the total production of natural gas in the United States in 2015 (Smith and Montgomery, 2015). Hydraulic fracturing techniques have helped develop unconventional gas fields such as the Marcellus Shale in the Appalachian Basin across the Eastern United States, the Haynesville Shale in Louisiana, and the Fayetteville Shale in Arkansas (see Figure 1.1).

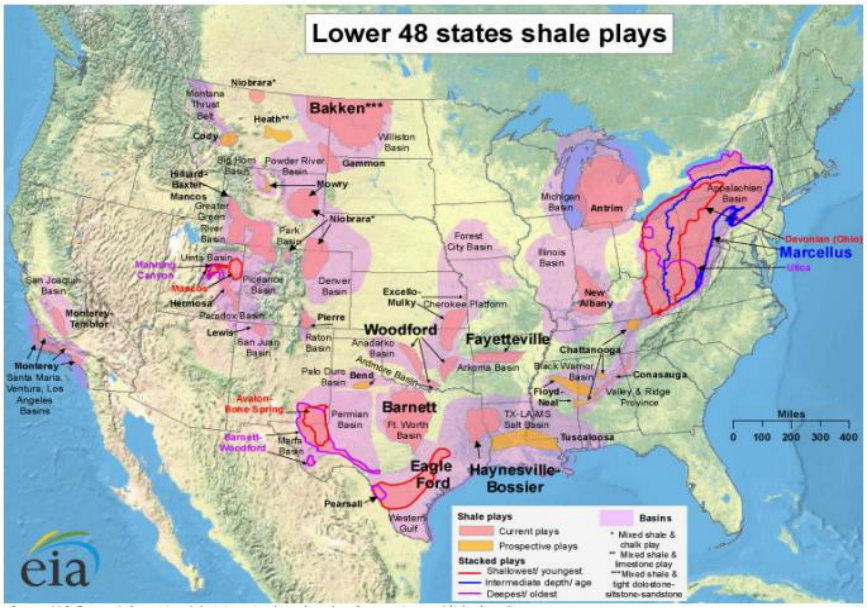

Figure 1.1: United States shale plays (from EIA 2011).

Commercial gas production from unconventional shale reservoirs began in the 2000s with the Barnett Shale located in Texas and initially developed by Mitchell Energy and Development Corporation (U.S Energy Information Administration 2011). Due to the success of Mitchell Energy in the Barnett Shale, many other shale natural gas plays were and are being developed. The

United States has 200 trillion cubic feet of proven shale gas resources and 623 trillion cubic feet of unproved technically recoverable (EIA 2011) as shown in Table 1.1 that likely will need fracturing for commercial extraction.

Table 1.1: United States Shale Gas Plays (from EIA, 2011)

Shale Gas Play	Active Area (sq. mi)	Recoverable Gas (Tcf)
Haynesville	3,574	74.70
Barnett-Woodford	2,691	32.15
Fayetteville	9,000	31.96
Barnett	4,075	23.81
Mancos	6,589	21.02
Antrim	12,000	19.93
Woodford	2,900	19.26
Devonian Low thermal	45,844	13.53
Lewis	7,506	11.63
New Albany	1,600	10.95
Greater Siltstone	22,914	8.46
Devonian Big Sandy	8,675	7.40
Cana-Woodford	688	5.72
Eagle Ford	200	4.38
Floyd-Neal	2,429	4.37
Hilliard-Baxter Mancos	16,416	3.77

Shale is a fissile and laminated sedimentary rock that can contain natural gas or oil. Kerogen, the complex organic material in shale, generates oil and gas in large volumes (Boggs et al. 2002). This large volume of oil and gas creates pressures larger than the in-situ stress which generate natural fractures in the formation. However, the shale rock must also be hydraulically fractured to make the well economically viable.

In order to carry the proppant downhole and into the fractures, various fluids have been designed and engineered for the hydraulic fracturing process. These fluids are selected in accordance to the downhole conditions, especially in regard to temperature. Another determining factor is whether the formation is ultra-low or moderate permeability which affects the leak-off behavior. Guar-based fluids are used in wells with temperatures less than 300˚ F. Other polymers are used for their stability in higher temperatures up to 450˚F including the use of polyacrylamide (PAM) based polymers. High density brines have been used to increase the hydrostatic pressure

by 30%. Slickwater is also used, which generally uses drag-reducing agents (PAM based polymers) to minimize the friction (Al-Muntasheri 2015). In this research work, slickwater is the subject fluid.

A common stimulation treatment for shale reservoirs includes: 1) an acid stage where diluted acid is pumped into the wellbore to dissolve carbonate minerals, 2) a pad stage where slickwater with additives is pumped in to initiate the fracture and create space for the proppant, and 3) a proppant injection stage where slurry, consisting of fluid and proppant, is pumped into the pad space to prop the fracture. This slurry stage can account for 70% of the treatment volume. The concentration of proppant in slickwater treatments generally ranges from 0.1 to 2.0 lb/gal.

The flush stage is the last stage of the stimulation treatment and flushes excess proppant from the wellbore. If the flush stage is not done properly, it could affect the conductivity near the wellbore (Abass et al. 2006).

Slickwater fluids are pumped at high rates (> 60 bpm) and generate narrow fractures with low proppant concentration. These treatments have become a standard practice in fracture stimulation in the United States (Kundert and Mullen 2009). Common chemicals for friction reducers (FR) are polyacrylamide derivatives and copolymers added to water at low concentrations. Additional additives for slickwater fluids may include biocides, surfactants (wettability modification), and scale inhibitors. Friction reducers in slickwater fluids are typically less sensitive to mix-water quality which is a tremendous advantage over many conventional gelled fracturing fluids. However, in high-salinity mix-water, many friction reduction additives may be inefficient (King 2010).

Since the development of the Barnett Shale by Mitchell Energy in 1981, friction reducers have proven themselves to be the most common additive in slickwater slurries. Friction reducers are used to minimize the friction pressure, enabling higher bottom hole pressure generation from the same number of pump trucks (Mack et al. 2014). Friction reducers have a typical loading range from 0.25 gallon of friction reducer per one thousand gallons (gpt) of water to six gallons per one thousand gallons of water. There are three types of polyacrylamide friction reducers: anionic, cationic, and nonionic (Mack et al. 2014). They have thermal stability up to about 400 °F and easily decompose after 550°F. Chemical and thermal deterioration of the polymer lowers their

performance (Carman and Cawiezel 2007). For the purpose of this research, an anionic polyacrylamide was procured and used to carry out experimental work at different concentrations and the associated effects on proppant transport.

The research described in this dissertation pertains to proppant transport and the impact such parameters as proppant sizes, proppant flow and slickwater fluid rheology have on transport in hydraulic fractures. Even though there has been other research done on slickwater slurries up to the present time, there still exists the need to go further in this field to research the slickwater slurry proppant pack in tertiary and quaternary fractures which simulate fracture networks that exist in the field. This has not been done until now and is the motivation of this thesis.

1.1 Project Motivation and Contribution

Research studies conducted on slickwater proppant transport in complex fractures are limited. Most of such research has been in the simulation modeling of complex fractures, but there are limited experimental lab results. This phenomenon needs more research in order to understand this transport and achieve a better proppant pack in complex fracture networks. Two experimental studies have come from the Colorado School of Mines. One study was produced by Sahai et al. (2014). It was based on slickwater proppant transport in primary and secondary fractures. A continuation of this study was done by Alotaibi (2015), with further research on primary, secondary and tertiary fractures. Alotaibi also introduced roughness to the fracture slot walls. Both studies were performed using a water system with no added chemicals or orthogonal slot angles.

This PhD research project expands the work of these two studies by including various slot widths, complex slots at obtuse and acute angles, a quaternary slot, ultra-light weight ceramic proppant, and the introduction of chemical friction reducer at various concentrations to the base case water systems. This research study further explores proppant flow in complex fracture systems.

The industry has a shortage of experimental demonstrations of the physical proppant settlement with regards to the settling velocities, proppant dune height and area occupied inside the fractures. The focal point of this research study is to estimate dune height, dune area, and proppant distribution in complex fracture networks and compare the experimental values to

modeled results using ANSYS simulation software. These comparisons are based on the proppant type, proppant size, proppant density, fluid viscosity, and slurry injection rates. Using this model, the settling velocity, Reynold's number, fluid flow type and fluid rheology can be determined. The goal of the model is to see if the effects of the above parameters on the proppant transport and settlement are in a range that is close to the results of the experiments.

This research study contributes to the industry by improving the accuracy of proppant transport and assisting in hydraulic fracturing treatments for enhanced oil and gas recovery. An improved understanding of the impacts of slurry flow rate, proppant type, proppant size, proppant density, and fluid viscosity on proppant transport will help to obtain the optimal proppant height and area. This study further explores the settled proppant size distributions in a complex fracture system through the addition of tertiary fractures and is the first experiment to study proppant flow in a quaternary fracture. Because this approach simulates natural fracture systems, similar to an en echelon fractures that are not exactly parallel, this provides realistic transport results that can be used in the field.

1.2 Research Objectives

This research is a continuation of studies on slickwater proppant transport in complex fractures, conducted by Sahai et al. (2014) and Alotaibi (2015). The focus of this study is unconventional shale wells that must be hydraulically fractured to be economically viable. This study focuses on slickwater fracturing treatments and tests slickwater at a laboratory scale to provide a performance comparison of the proppant transport in different slickwater solutions. This research consists of laboratory studies and simulations using a series of slot configurations that represent different complex fracture scenarios. These slot systems consist of a main slot fracture with a varying number of secondary slots placed at different angles to the main slot, tertiary slots that protrude from the secondary slots, and a quaternary slot placed from the tertiary slots.

In the laboratory, proppant transport was studied with two proppant densities, nine hybrid proppant types, three proppant sizes, three fluid systems, two injection rates, and one complex fracture network with sub-fractures attached to the main fractures at various angles. In addition to the laboratory experiments, a computational fluids dynamics simulation was used to study the proppant placement and distribution in the fracture networks. The motion of the particles flowing

with the fluid was simulated using ANSYS software at different slurry injection rates, proppant sizes, proppant densities, and fluid viscosities. The following objectives are addressed in this thesis:

1. Design a complex fracture model with primary, secondary, tertiary, and quaternary slots of different widths and varying angles to simulate fracture angles such as those found in shale formations (multiple varying angles to the main fracture).
2. Study the effect of proppant density, proppant size, specific gravity, slurry injection rates, and fluid viscosities on proppant transport in the complex fracture networks.
3. Study proppant settlement coverage and distribution in the slot systems.
4. Study the effect of perforation location (height) relative to the main fracture, specifically at the top and bottom of the main slot; and,
5. Use computational fluid dynamics software to simulate proppant placement, distribution, and trajectory inside the complex fracture networks. These modeling results are used to validate the laboratory experiments.

CHAPTER 2

LITERATURE REVIEW

Hydraulic fracturing in horizontal wells has given the U.S. energy supply a boost in its oil independence. Since 1947, when the first vertically fractured well in Kansas done by Stanolind Oil, which was to create a small fracture for improved oil recovery, until today where fracturing is used to create multiple fractures in a horizontal shale well, proppants are used to keep the fractures open.

As mentioned in Chapter 1, the idea of hydraulic fracturing in shale reservoirs began to take shape in 1981 with Mitchell Energy where the potential commercialization of gas from the Barnett Shale in the Fort Worth Basin was investigated (Steward 2013). After a couple of decades of field trials and improvements in technology, it was in the early 2000's that technology made it economically viable to recover hydrocarbons from these low permeable shale formations. Through the years, technology and research have shown that slickwater fracturing technology is frequently the preferred choice of the industry due to its economics combined with much less contamination of the reservoir formation allowing for quicker cleanup and better production (Schein et al. 2004). Although gelled systems are better at transporting the proppant because of their higher viscosity, the industry frequently uses slickwater, which doesn't always carry the proppant as well as gelled fluids (Brannon et al. 2006). The main driving factors that influence the use of slickwater over gelled fluids are: 1) the decline of gas prices in North America combined with the lower cost of the slickwater systems; and 2) reservoirs are not able to clean up the gel systems because of the low permeability and low-pressure differences that can be generated. Slickwater causes very little to no gel damage to the proppant pack (Cipolla et al. 2008).

Chapter 2 is a summary of the published literature on the following topics which include both experimental and field applications. The summary includes: (1) shale formations containing oil and gas, (2) proppant types in hydraulic fracturing, (3) fracturing fluids, (4) complex fracture network orientation, (5) hydraulic fracturing injection rates and slurry velocities, (6) proppant transport and conductivity, (7) proppant transport mechanisms, (8) proppant transport mechanisms plus modeling, and (9) potential research areas.

2.1 Shale Formations Containing Oil and Gas

Shale gas can be found in clay minerals with high organic matter. Shale gas formations are highly saturated with water as a result of their cage-typed pore spaces. It is important to note that in the shale gas system, there are no conventional gas traps. Therefore, natural gas is stored directly in the shale formation. Shale gas formations are abundant resources that are hard to retrieve due to the low permeability and reservoir quality (Zhong et al. 2016).

Shale gas formations usually have natural fractures as a result of the pressure build up due to the generation of new hydrocarbons. These fractures have permeability and porosity and store a lot of hydrocarbons. The natural fractures also help the hydraulic fracturing process. The permeability of the matrix is low (Zhang et al. 2017).

2.2 Proppant Types in Hydraulic Fracturing

The sizes and types of proppants are important to proppant transport and the creation of fracture conductivity. Sand and ceramic proppants are the most common proppants used in the hydraulic fracturing process. In general, larger size proppant increases fracture conductivity and smaller proppants transport better. The sizes of the proppants are determined by using meshing sizes. Ottawa sand is widely used in fracturing treatments. It is well-rounded, monocrystalline, and maintains conductivity even when subjected to high stress (Rickards et al. 2003).

Liu and Sharma (2005) state that increasing the diameter of the proppant increases the settling rate of the proppant. This reduces the transportability of the proppant as larger proppants are heavier. The high settling rate creates larger proppant dune areas. They noted that larger grains interact more with themselves and the walls of the fracture which causes more settling and higher dunes.

In 2015, Alotaibi observed during his experiments that: (1) slickwater can transport smaller particles into the fracture. At the first stage of the experiment, the Equilibrium Dune Length (EDL) increases with decreasing proppant size because more particles travel via a hindered settling mechanism. That is with larger proppants the lateral distance covered by proppants in the fracture is shorter. For example, while using 100 mesh, he observed the following: (1) 1.45% increase in EDL with an 11% increase in velocity, (2) higher velocity erosional effect, (3) lower concentration

is better for dune erosion, and (4) at higher velocities 100 mesh does not lose erosional power (Alotaibi 2015).

Chang et al. (2016) explains that larger proppants increase conductivity. He observed that ceramic proppants have a higher conductivity than sand of similar sizes. This is a result of the higher unit pack permeability of the ceramic proppants. The propped-open stimulated reservoir volume (PSRV) reduces with the ceramic proppants. The concentration of the proppants effects the conductivity of the fracture in the sense that the decreased concentration produces increased conductivity. He used two different proppant sizes, 40/70 mesh (midsize) and 100 mesh (fine size). From his experiments, he observed that larger proppants (40/70) are essential to maintaining the fracture conductivity, but 100 mesh had a higher PSRV. He suggested the viscosity of 8 cp and 100 mesh as the optimal treatment for adequate conductivity and transport, under scenarios with 100' by 200' natural fracture spacing. He claims that increasing the viscosity of the fluid improves the benefits of the smaller proppants. The low settling velocity of 100 mesh creates longer and higher proppant dunes. After his research, Chang et al. (2016) recommends using a mixed-size proppant schedule for good conductivity and effective transport.

Angular grains like sand grains are more susceptible to drag forces than rounder grains. This increases the slurry velocity and proppant transport. Angular grains have higher drag coefficients and shape factors (Wu and Wang 2006). Angular grains interact more with the walls and therefore have higher settling tendencies Southard (2006). The rounder, more spherical grains reduce the erosional effect of the slurry. In the first two stages of the Alotaibi (2015) experiment, the height and length of the dune decreased with the rounded and spherical grains.

Higher proppant concentration increases the settling rate and creates larger dunes. To reduce the height of the bed, Woodworth and Miskimins (2007) recommended lowering the concentration of the proppant. More concentration reduces the available area for slurry flow, which increases particle-wall interaction. The interaction between the wall and the proppant particle increases the drag force which causes it to settle and create dunes (Gadde and Sharma 2005).

Barree and Conway (1995) stated that increasing proppant concentration over 10% moves particles away from the highest flow velocity point and reduces their average velocity. Alotaibi

(2015) agrees that increasing proppant concentration causes more settling and reduces transport distance in the fracture especially with the larger grains.

2.3 Fracturing Fluids

Fracturing fluids carry proppants into the fracture to develop conductivity. It is important for fracturing fluids to have the right density, viscosity, and pressure for the designed treatment. There are five categories of fracture fluids including: water-based fluid, oil-based fluid, alcohol-based fluid, foam-based fluid, and energized fluid. Water-based fluids are low cost and work well with additives. There are three groups of water-based fluids: slickwater, linear and cross-linked fluids. Linear water-based fluids are controllable but sensitive to acidity, temperature, and salinity. Cross-linked fluids are less sensitive to depth, temperature, acidity, and salinity. Slickwater is vital for shale formations where large propped areas are essential for sustainable fracture conductivity (Palisch et al. 2010).

There are several reasons that slickwater is preferred in low permeability applications. These reasons include: activation of fractures, optimal fracture conductivity, economics, minimal leak-off, and zero gel residue (Woodworth and Miskimins 2007). Fracture conductivity is the ratio of the ability of the fracture to flow to the ability of the reservoir to fuel the fracture. In slickwater systems, low concentrations of proppants are recommended and surfactants, friction reducers, and clay stabilizers are typically added to the base water.

The density contrasts between fluids may bring about the denser fluid flowing under the lighter fluid or the lighter fluid superseding the denser fluid. This occurrence, known as convection or gravitational flow is essential in numerous fields (e.g. - saltwater intrusion under fresh water, as sourced in Ghyben (1988) and Herzberg (1901). In fracturing, it may be relevant if a high- density slurry stage flows under a previously pumped stage or pad, as well as for other 2D aspects of fluid flow such as those considered by Clifton and Wang (1988). An expression for average fluid velocity between two parallel plates is the classical solution derived from the Navier-Stokes equations and boundary conditions. It describes the laminar flow of incompressible fluid. Considering Newtonian fluid flowing laterally through a narrow slit (e.g., a fracture), the pressure drops δp along the length δx of the channel, fluid flow is given by the parallel plate law (Tomac and Gutierrez 2016). The fluid flow equations for a Newtonian fluid can be written as:

$$u_x = \frac{-w^2}{12\mu} * \frac{\delta p}{\delta x} \tag{2.1}$$

$$u_y = \frac{-w^2}{12\mu} * \left(\frac{\delta p}{\delta x} + pg\right) \tag{2.2}$$

$$\left(\frac{\delta(wu_x)}{\delta x} * \frac{\delta(wu_y)}{\delta y}\right) + \frac{\delta w}{\delta t} + 2u_L = 0 \tag{2.3}$$

Substituting Eq.2.2 and 2.3 obtains,

$$\frac{1}{12\mu} * \left(\frac{\delta^2 w^3 p}{\delta x^2} * \frac{\delta^3 w^3 p}{\delta y^2}\right) = \frac{\delta w}{\delta t} + 2u_L - \frac{1}{12\mu} * \frac{\delta w^3 \rho g}{\delta y} \tag{2.4}$$

Where;

δy = change in the velocity in the fracture in the y-direction (ft) [Length]

δx = change in the velocity in the fracture in the x-direction (ft) [Length]

δw = change in the velocity with respect to the fracture width (ft) [Length]

δt = change in the velocity with time (seconds) [Time]

p = pressure (psi) [$\frac{\text{Force}}{\text{Area}}$]

uL = velocity in the slurry (ft/sec) [$\frac{\text{Length}}{\text{Time}}$]

ρ = density of the fluid (lb/gal) [$\frac{\text{Mass}}{\text{Volume}}$]

The last (gravitational) term on the right-hand side of Eq. 2.4 is the convective term for vertical-slot flow. This can be treated as a source term, just as the other two terms are storage or sink terms, resulting from width change and leak-off. Barree and Conway (1994), Unwin and Hammond (1995) and Smith and Klein (1995) showed that the gravitational term is generally not significant for most properly designed fracturing treatments. Smith and Klein (1995) showed that if excess pad was pumped, the fluid flow after pumping stops (i.e. after flow) and could lead to convection until the pad leaked off. Also Eq. 2.4 shows the extreme sensitivity of convection to fracture width. If the width is large (e.g. in a low-modulus rock), convection may be more critical. Fortunately, such low moduli are usually associated with high permeability reservoirs in which case tip screen-out (TSO) designs and rapid leak off after shut-in effectively prevent convection. Cleary and Fonseca (1992) presented a dimensionless number that reflects the ratio of buoyant and viscous forces. This ratio can be used to estimate the effect of different conditions on the severity

of convection. Clark and Courington's (1994) and Clark and Zhu's (1994) experiments on convection verify the theoretical and numerical results described here.

For the most part, the viscosity of a proppant-laden slurry is higher than that of the carrying fluid base alone. Experimental relations are well established for Newtonian fluids, but much less so for power law fluids. Nolte (1988) showed that relations for power law fluids could be obtained by using the relations for Newtonian fluids and raising them to the power of n. For example, the viscosity ratio μr for vertical-slot flow could be obtained as:

$$\mu_r = \frac{\mu_{slurry}}{\mu_{base}} = \frac{1}{\left(1-\frac{f_v}{f_{VM}}\right)^{2.5n}} \tag{2.5}$$

Where;

f_v = proppant volume fraction (unitless)

f_{vM} = the maximum fraction for a mobile slurry (unitless)

μ_{slurry} = the viscosity of the slurry (cp) [$\frac{\text{Mass}}{\text{Lenth x Time}}$]

μ_{base} = the viscosity of the base fluid (cp) [$\frac{\text{Mass}}{\text{Lenth x Time}}$]

Southard (2006) stated that increasing the viscosity of the fluid increases the drag force which transports the proppant further into the fracture. The viscous fluid can suspend proppant which makes it easier to transport into subsidiary fractures. At low velocities, there is very little suspended load when slickwater is being used.

Slickwater proppant transport depends on proppant density. Sand settles readily in slick-water. The smaller the density ratio between the proppant and the fluid, the better the efficiency of the transport system. Increasing viscosity and decreasing proppant density will enhance proppant transport (Alotaibi 2015).

Chang et al. (2016) in their experiments, show that increasing the viscosity of the fluid increases the PSRV. The fracture conductivity decreases with higher fluid viscosity. They state that viscosity of 8 cp has higher PSRVs and PSRV/SRV because of the lower proppant settling. Lower viscosity increases the slurry flow velocity. Also, conductivity increases because at the

bottom of the fracture, there are thick concentrated banks of proppants: the low viscosity fluids cause more settling of proppants. The optimal case for increased fracture conductivity according to Chang et al. (2016) is: low pumping rate, small pay thickness, low viscosity and sand proppants. To increase efficiency, fluid viscosity can be increased.

2.4 Complex Fracture Network Orientation

Kern et al. (1959) studied proppant transport in water. Their work shows that at early stages of injection, proppant settled near the wellbore. They observed that developed proppant dunes kept increasing in height until equilibrium, where all injected proppant moved further into the fracture. The experimental results of Sahai et al. (2014), Brannon et al. (2006) and Barree and Conway (1995), all coincide with the result of Kern et al. (1959).

In 2014, Sahai et al. evaluated proppant transport in subsidiary fractures. They utilized Plexiglas® sheets which were first used by Babcock et al. (1967) to create primary fracture and secondary fractures. They stated that proppant flows into the secondary fractures by turning a corner with the effects of gravity and fluid flow rate. Sahai et al. (2014) observed that smaller proppants were dominate in the secondary fracture slots and the larger proppant were found in the main fracture. Thus, some operators and engineers pump in larger proppant at the beginning of the treatment (Palisch et al. 2010).

Li et al. (2016) performed experiments using primary fracture and secondary fractures at different angles. They investigated the proppant transport into different sub-fractures at different angles. They used three flow rates: 1.32 gal/min, 1.98 gal/min, and 2.64 gal/min to investigate the height and area of proppant in the fractures. These are the observations made from the experiments: (1) changing the angles of the secondary fracture, greatly affected the proppant distribution, (2) the lower the flow rate, the higher the proppant in secondary fracture, (3) increasing the angle at which the secondary fracture is connected to main fracture, reduces the proppant in the secondary fracture and affects the amount of proppant in the main fracture, (4) using smaller particles, shorter dune heights were observed, (5) increasing the injection rate, reduces proppant in main fracture but increases proppant in the subsidiary fracture, and (6) larger diameter proppant and increased injection rate increases slurry in secondary fracture, but reduces propped area (Li et al. 2016).

Figure 2.1 shows the result of the treatments conducted by Kresse et al. (2013). It displays the UFM simulated fracture geometry and width for gel and slickwater fractures. The perforations triggered planar hydraulic fractures. These fractures propagate as longitudinal fractures because the direction of the well-bore is parallel to the orientation of the fracture.

For cross-linked gel treatments, the longitudinal fracture intersected the natural fractures that are approximately orthogonal to the direction of the fracture. OpenT is an analytical model developed to evaluate the impact of flow rate and fluid viscosity on the complex fracture network crossing behavior. The natural fractures open and accept fracturing fluid when the fluid pressure exceeds the normal stress acting on the natural fractures. The UFM model predicts a significant planar trend along the well with a very narrow network width. This prediction is consistent with the microseismic observation shown in Figure 2.1.

For the slickwater treatment, the OpenT crossing model predicts non-crossing conditions when a hydraulic fracture intercepts a natural fracture. As a result, there is a wider fracture network width when the fractures extend as demonstrated in Figure 2.1. The width of the network is 1700 ft wide, approximately equal to the width indicated by the microseismic data as shown in Figure 2.1.

In his experiments, Alotaibi observed that secondary fractures had large dune area, but the tertiary fractures did not. The EDL in the secondary fracture depends on the total amount of proppants injected into the fracture. The figure below shows that slickwater can transfer proppant into secondary fractures and the tertiary fractures of the secondary fractures closer to the wellbore.

2.5 Hydraulic Fracturing Injection Rates and Slurry Velocity

Brannon et al. (2006) stated that higher slurry velocities transport proppants better, create shorter heights, and longer proppant dunes. The higher slurry velocities increase the drag and lifting forces exerted by the carrying fluid. Brannon et al. (2006) studied the effect of increased slurry velocity on equilibrium dune height. They observed that dune height reduced with increased lateral flow velocity.

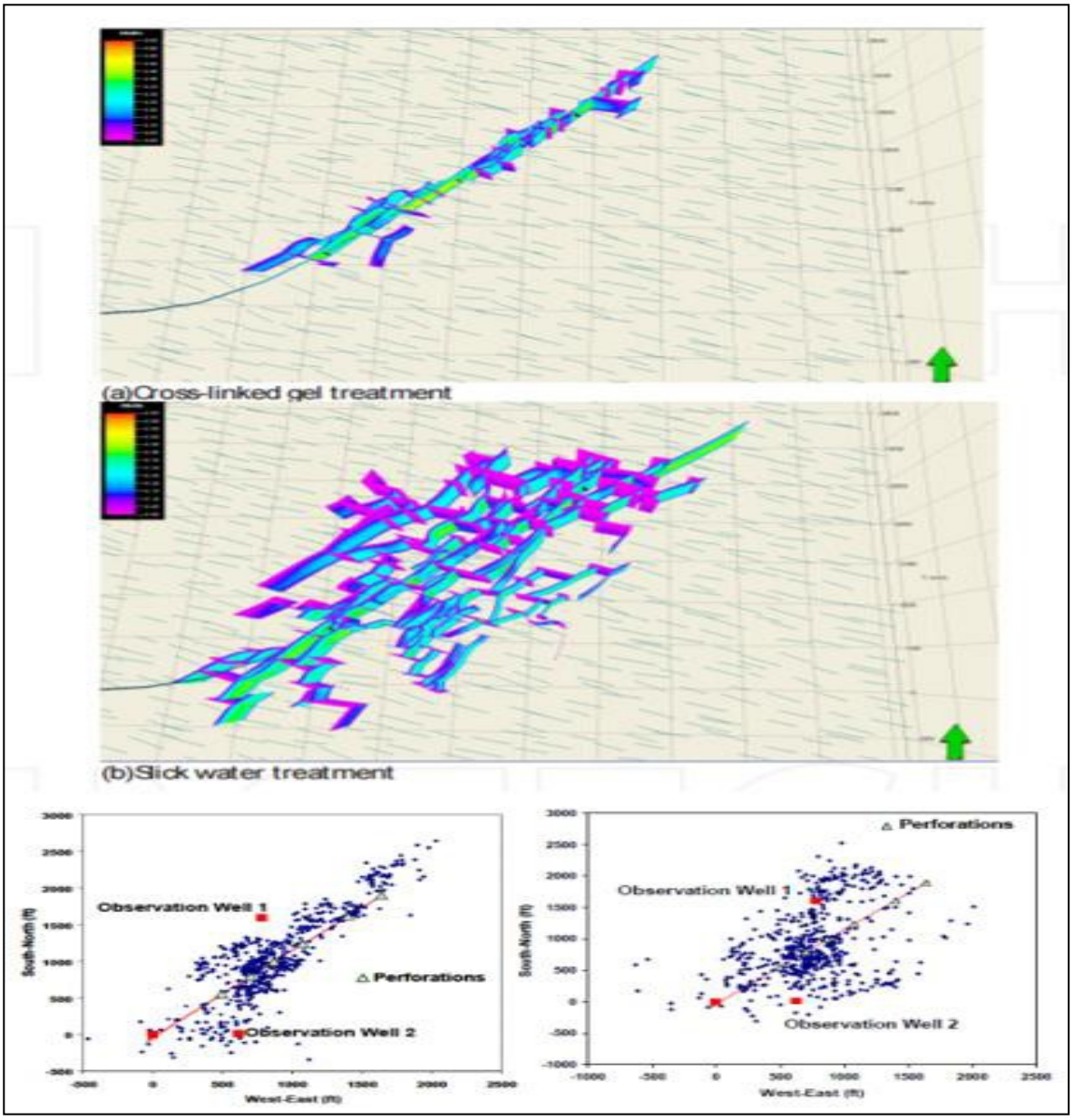

Figure 2.1: UFM simulation results for the Barnett case, (from Kresse et al. 2013) and microseismic event location for XL gel stimulation and water-frac refracturing treatment of horizontal Barnett Shale well (From Warpinski et al. 2005).

Table 2.1: The proppant dune area for all the primary, secondary, and tertiary fractures (from Alotaibi 2015)

Fracture type	Dune Area, ft^2	Dune to fracture area ratio (DFA), %
Primary	61,901	81.8
S-1	18,705	90.6
S-2	17,048	82.6
S-3	10,545	51.1
T-1	4,795	23.2
T-2	305	1.5
Total	113,300	

The following are the results of Alotaibi's (2015) experiment: (1) the height of the dune depends on the velocity of the slurry, (2) higher velocity increases erosional effect on the proppant dune, (3) higher velocity improves the transport of proppant into subsidiary fractures, and (4) the higher velocity reduced the observed angle of the dune. His results show that increasing velocity by 11% caused a 0.7% reduction of the equilibrium dune length. Doubling the flow rate resulted in approximately 5% reduction of EDL. Alotaibi (2015) concluded that increasing the velocity does not significantly affect the settling tendencies of slickwater. At higher velocities, the dune loses its' erosional power due to the nearly horizontal dune surface. His recommendation for optimum results is the increase of flow rate and decrease of proppant concentration.

2.6 Proppant Transport and Conductivity

Proppant transport and proper placement is essential to the success of the hydraulic fracturing treatment. Proper placement of proppant in the fracture is required for viable fracture conductivity. Reserve recovery and production depend on the conductivity of the propped area.

Biot and Medlin (1985) stated that proppants in slickwater have four modes of transportation: turbulent transport, viscous drag transport, bed load transport, and stationary deposited bank. They also stated that the most important aspect of proppant transport is the slurry flow velocity and settling velocity. They developed a ratio for the settling velocity and fluid flow velocity; a ratio larger than 0.9, the proppant movements are rolling and sliding. If less than 0.9 but higher than 0.1 then bed load transport dominates. If less than 0.1, then suspension is the main mode of proppant transport.

In 1977, Novotny concluded that settling velocity is the most important factor in determining proper transport and placement of proppant. Cabrejos and Klinzing (1994) concluded that the movement of proppant is highly dependent on the slurry velocity. The slurry velocity changes to modify the shape of the dunes. Their work supports the conclusion made by Biot and Medlin (1985). Mobbs and Hammond's (2001) work shows that when convection is strong there is more settlement of proppant. They stated that convection is stronger in the middle of the fracture. Convection depends on buoyancy; the lower the buoyancy, the higher the convective behavior.

Proppant settles to the bottom of the fracture and begins to form a dune of proppant. The proppant dune develops and rises until the gap between the highest point of the dune and the top of the fracture is small. The slurry velocity increases as the gap decreases until it reaches the critical velocity. At and above, the critical velocity of the proppant is then transported until a new equilibrium height is formed. Transport is sliding, rolling, and suspension of the proppant particles. At and above the critical velocity, the proppant particles are transported to the end of the fracture (Kern et al. 1959 and Patankar et al. 2002).

Gadde et al. (2004) concluded that the settling velocity reduces with increased turbulence and enhances the proppant transport. Nabi et al. (2012) used experimental work and modeling to suggest that gravitational force and flow rate are the most important factors for proppant transport and deposition. Mack et al. (2014) performed experiments in a complex system and stated that the change in proppant diameter affects proppant transport more than gravity or other forces. They concluded that saltation is the most important transport mechanism. Proppant was transported into secondary slots at lower and higher flow rates with different mechanisms.

Tsai et al. (2013) found that if the density of the proppant is equal to the carrying fluid, then proppant can be transported further into the fracture. If the proppant has a higher specific gravity, then the proppant settles and forms dunes quicker. They stated that an increase in flow rate will decrease the settling of the proppant by increasing the drag forces. They concluded that smaller proppant should be injected before heavier proppant to maintain conductivity near the wellbore.

Sahai et al. (2014) studied the behavior of proppant transport in complex fracture networks. In this work they stated that: (1) proppant settlement affected the concentration of the proppant, (2) suspended slurry did not turn into secondary slots at lower velocities, (3) proppant dune height is independent of slurry concentration but dependent on flow rate, and (4) smaller proppant travel into secondary slots better than larger proppant.

2.7 Proppant Transport Mechanisms

Dey (1999) states that rolling, and sliding are the slowest transport mechanism. He also states that high drag and lifting forces of the slurry cause the settled proppant to roll forward in the direction of the slurry. The rolling and sliding mechanism starts where slurry velocity is high enough to exert enough drag and lifting forces. When the bed-shear stress exerted on a particle is more than the Shields parameter it moves by rolling. When rolling, particles move in the direction of the flow and keep contact with the bottom of the fracture. An increase in the bed shear velocity and the particle moves in the form of jumps. At this point, turbulence tries to lift the particle into suspended motion. When bed-shear velocity exceeds the settling velocity of the article, it is left in suspension and moves in a suspended motion.

Saltation requires higher slurry velocity that applies enough lifting force to overcome the weight of the proppant grain. The grain loses it is upward motion and falls while traveling with the direction of the slurry Southard (2006).

When the carrying fluid exerts high enough drag and lifting forces, the proppant grains travel as a suspended load. The smaller grains travel via suspension because their grain weight is not sufficient enough to overcome the forces exerted by the fluid Patankar et al. (2002).

A detailed experiment was conducted by Alotaibi (2015) using a primary slot and secondary slots. In his experiment he observed the three transport mechanisms: rolling, saltation, and suspension. The lowest dune level (0-10%) is the first stage of dune formation. It is between 0-10 percent of the total equilibrium dune length. The slurry velocity is not high enough, and the proppants move by hindered settling. The dune angle at this level is 2.4%. The dune angle is the angle between the horizontal plane and the particle settling direction. The larger particles in this stage experience more gravity, have short lateral travel distance, and have higher settling angles. The dune has an upward increasing proppant size distribution. For this first stage, the smaller particles are at the bottom of the fracture and therefore the conductivity will likely be lower. The initial flow rate was 14.5 ft/min but increased to 256.7 ft/min when the dune is fully developed as demonstrated in Figure 2.2.

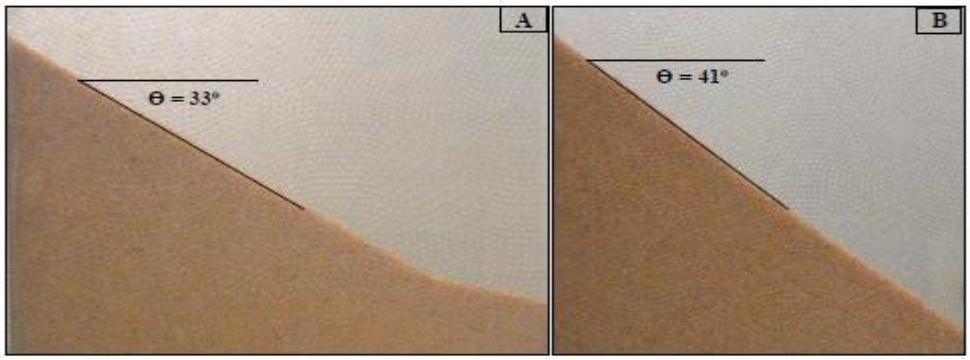

Figure 2.2: The beginning and end of Stage 2 of the dune developing process (from Alotaibi 2015).

At the second stage of the dune development, the linear dune slope increases. The slurry velocity increases at this stage which increases the proppant transport. The increased velocity increases the drag force exerted by the fluid. Because of the increased slope of the dune, the gravitational force is enhanced. The mechanism for Stage 2 is rolling and free settling. Stage 2 has the highest dune development rate of all the proppant. In this stage, the larger grains roll, and the smaller grains are in suspension. At the third stage of the development (75-97% of EDL), there is reduced area for slurry to flow. This increases the slurry velocity further and creates the vertical eddies seen in Stage 3 as demonstrated in

Figure 2.3. The transport mechanism at this stage is rolling, suspension, and free settling. In Stage 3, the highest conductivity will likely be at the top of the fracture. Stage 4 is when the remaining 3% of the EDL is formed as demonstrated in

Figure 2.4. The proppant is transported via rolling and saltation. The largest grains settle in this section. The sorting of the proppant is important to the hydraulic fracture conductivity as demonstrated in Figure 2.5.

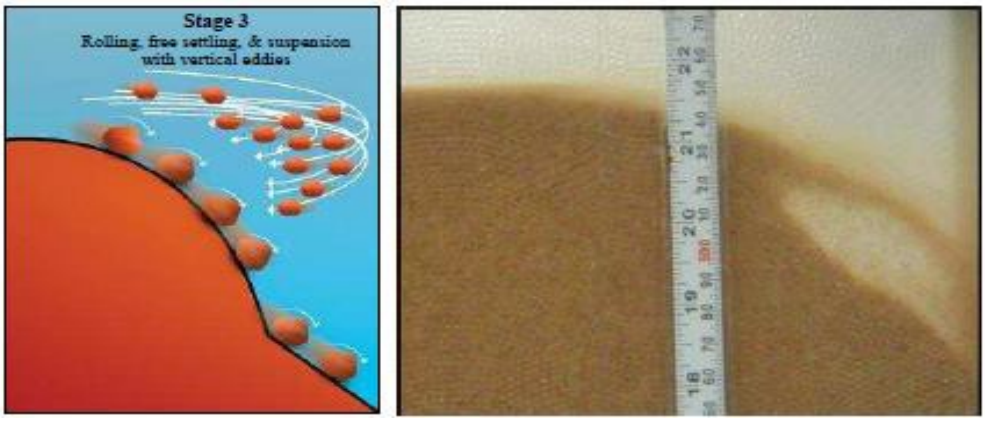

Figure 2.3: Stage 3 of the EDL (from Alotaibi 2015).

Stage	EDL, %	Dune shape	Transport mechanism	Relative proppant size range	Proppant size distribution	
					Vertically	Horizontally
1	0-10		Hindered settling	Smallest size range	Increasing	No change
2	10-75		Free settling + Rolling	Mostly mid to large size range	Layers of small and large proppant with a downward slope	
3	75-97	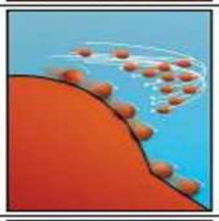	Rolling + free settling + Suspension	Mostly large with partially mid-size range	No certain sorting was observed	
4	97-100		Rolling + Saltation	The largest size range		

Figure 2.4: The stages of the equilibrium dune development (from Alotaibi 2015).

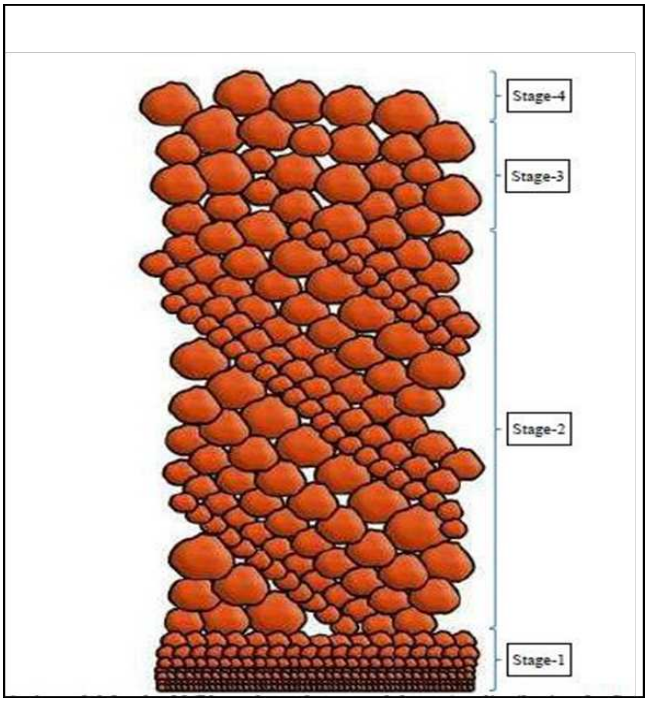

Figure 2.5: Dune size distribution of medium sized proppant at the different stages (from Alotaibi 2015).

2.8 Proppant Transport Mechanisms and Modeling

The simulation of proppant transport and placement in the fracture is important in the field and for research purposes. In modeling proppant transport, three stages should be considered: (1) the surface creep which involves the rolling or sliding of proppant particles across the surface of the stationary proppant bed; (2) saltation which occurs as the flow rate increases and proppant particles are carried off the stationary bed; and (3) suspension, which occurs when the velocity is high enough for the proppant to be suspended and carried by the fluid (Mack et al. 2014).

Slurry transport was modeled using fracture shear and leak-off of the fracturing fluids without considering the gravitational effect, particle-particle, fluid-particle interaction (Miller et al. 2008). Tsai et al. (2013) studied proppant transport using the effect that particles have on each other and the effects fluids have on particles. Blyton et al. (2015) investigated the proppant distribution in a fracture using a CFD-DEM coupling method. Their method involved using a modified Navier-Stokes equation, the momentum equation, and the continuity equation as shown in Equation 2.6 below:

$$\rho_f \frac{\partial \varepsilon}{\partial t} + \rho_f v.\nabla(\varepsilon v) = -\varepsilon \nabla p + \mu \nabla^2(\varepsilon v) + f_b \tag{2.6}$$

Where,

ρ_f = fluid mass density in kg/m^3 [$\frac{\text{Mass}}{\text{Volume}}$]

ε = porosity

t = time in seconds

v = fluid velocity in m/s [$\frac{\text{Length}}{\text{Time}}$]

p = pressure in pascal [$\frac{\text{Force}}{\text{Area}}$]

μ = fluid dynamic viscosity pa s [$\frac{\text{Mass}}{\text{Length x Time}}$]

f_b = particle body force per unit volume in N [$\frac{\text{Force}}{\text{Volume}}$]

Miller et al. (2008) and Tsai et al. (2013) modeled the interaction between particles and fluids using the force of the particle on the fluid and the force of the fluid on the particle for every cell.

Zhang et al. (2017) used a rectangular domain with non-slip boundaries to model proppant transport mechanisms. They observed that when proppant is injected, it settles at the bottom of the fracture and a proppant dune forms. Due to the size of the domain, the proppant settles in a small amount of time. They used high injection rates that caused the dune to be flat and wide-spread across the fracture. The initial results of Zhang et al. (2017) show a settled proppant bed-load, a high concentration of slurry above the bed-load and a clear fluid layer. They characterized the transport as suspension, fluidization and settlement.

High viscosity fluid created wider dunes and caused a stronger fluidization mechanism. This will increase the time it takes for the proppant dune to achieve equilibrium height. Proppant transport is heavily dependent on fluid viscosity. A small change in viscosity can affect placement and transport of proppant (Zhang et al. 2017). Chang et al. (2016) also observed from their results that higher viscosity enhanced transport and lower viscosity enhanced fracture conductivity.

The drag force of the fluid controls the horizontal transport of the proppant. This means that at a higher injection rate, the proppant is dragged for a longer distance. With higher pump rates, the location near the wellbore is free of settled proppant because of the erosional power of

the high velocity slurry entering the fracture. The downside of using high injection rates will be the reduction of fracture conductivity near the wellbore (Zhang et al. 2017). Chang et al. (2016) also indicates that higher injection rates enables proppant to travel longer distance before settling. Lower treatment rate results in higher conductivity of the proppant. Also, higher treatment rate reduces the treatment time. Chang et al. (2016) observes longer flatter dunes with higher flow rates and increased horizontal propped area.

For this simulation, an open-hole wellbore is utilized. It involved pumping the slurry from the whole left side boundary of the rectangular domain. Zhang et al. (2017) experimented using an open-hole wellbore. The first group of injected proppants settled at the bottom of the fracture tip. With time, the tip fracture is blocked, and the simulation is forced to stop at a premature time. Proppant transport mechanism is dependent on the injection rate, fluid viscosity, perforations and proppant characteristics (Zhang et al. 2017).

The presence of pre-existing fractures and joints is to be taken into account to adequately capture the proppant transport process. Mack et al. (2014) observed that proppant flowed more readily into sub-fractures that were orthogonal to the direction of the flow in the main fracture at high flow-rates. Lab results from Sahai et al. (2014) shows that below the threshold velocity, suspended proppant will not turn into the sub-fractures. Proppant with a smaller diameter has a higher chance of being transported into sub-fractures.

A minimum velocity is required to transport proppant into the sub-fractures. The minimum velocity is dependent on fracture width and particle size. When the particle gets to an intersection, it is subjected to a drag force that is related to the diverging flow into the sub-fracture. The particle begins to move in the direction of the drag flow, if the drag force is strong enough, then the particle goes into the sub-fracture (Chang et al. 2016).

2.9 Potential Research Area

Although various research studies have been performed on assorted topics corresponding to slickwater proppant transport, the clear majority of research areas have yet to be explored or improved. Sections 2.9.1 - 2.9.6 relate the unexplored areas addressed in this PhD thesis.

2.9.1 Experimental Apparatus

Related studies were conducted on proppant transport by Sahai et al. 2014. Their experiments used smooth surface plexiglass slotted walls with slickwater proppant, and the proppant flow was introduced into secondary fractures. Continuous study in this research area was conducted by Alotaibi 2015, which included the addition of tertiary fractures with roughness added to the plexiglass slotted walls. Both research experiments were performed using orthogonal slot angles, as well as a water-based system without chemical additives. This PhD research focused on evaluating proppant transport by including various slot widths, complex slots at obtuse and acute angles to simulate a prototype of an en echelon natural fracture system and fracture not exactly parallel as by Smith et al. 2015. In this PhD thesis, an apparatus with rough slot walls was designed to conduct experiments and obtain the required lab data to develop comparisons with a computational fluid dynamic (CFD) software.

2.9.2 Proppant Diameter and Density

As presented by Alotaibi (2015), proppant diameters impact the exerted fluid flow and fracture wall drag forces. The effect of proppant transport and dune height development was researched by Alotaibi (2015). He used proppant sizes 100, 30/70, and 20/40 mesh for both brown and white sand. This PhD thesis' scope is to evaluate the proppant diameter and density effects on slickwater proppant transport using white sand 100 and 40/70 mesh and ultra-light weight proppant 14/40 mesh. Since these proppants have different densities, an evaluation of proppant and carrying fluid densities can be done. Included in this evaluation are the determination of the net force between gravity and buoyancy forces acting on the proppant, which must be performed to optimize the fracture treatments.

2.9.3 Proppant Concentration and Flow Rates

An increase in the proppant concentration is found to develop larger dunes and proppant settling rates. STIM-Lab Inc. produced experiment results relating the lower proppant concentration in fluidization of the settled proppant bed to reducing the dune height development (Woodworth and Miskimins 2007). Slickwater operators often pump large amounts of water in with the proppant at higher rates. Avoiding high rates of settling, the slurry concentration is

reduced. In this PhD study, the effect of flow rate was evaluated at the lower ranges of flow rates being 1 gal/min and 2 gal/min (gpm). The concentration is kept constant at 2 lb/gal based on King's (2010) study, where he stated that proppant concentration in shale formations ranging from 0.25 to 2.5 lbs/gal is needed to evaluate the proppant dune development as well as the behavior of the proppant transport.

2.9.4 Fluid Viscosity

High settling velocity causes proppant depositional rate in the low viscosity fluid to increase. The equation of terminal velocity displays a relationship between the lower fluid viscosity value when the terminal velocity increases. This is due to the drag force mechanisms affecting the particle decreasing because of the thinning agent. Shear forces also affect the particles by charging longer distances to balance momentum causing a higher terminal velocity. Because of the described mechanisms above, proppant transport in a thinner fluid leads to an accumulation of proppant from the suspended slurry at the bottom of the fracture. According to the research done by Sahai et al. (2014) and Alotaibi (2015), they used a water-based system to evaluate the proppant transport mechanisms. In this PhD research, the fluid types are investigated using three different concentrations of friction reducers on proppant dune development and proppant transport mechanisms.

2.9.5 Proppant Transports in Subsidiary Fractures

Studies published by Sahai et al. (2014) and Alotaibi (2015) were based on proppant transports and settling rates in orthogonal secondary and tertiary fractures. For the quaternary fractures, there was no previous published work in this area located during this literature review. The design of the apparatus in this research project includes a network of secondary, tertiary and quaternary fractures at obtuse and acute angles.

2.9.6 Proppant Transport Modeling

The reviewed literature shows limited experimental research work on slickwater proppant transport mechanisms and placement in fractures combined with modeling. In fact, most of the modeling was built based on simulation without experimental work done previously. The purpose of this PhD research work is to study the proppant transport mechanism in complex fracture

networks to simulate a prototype of an en echelon natural fracture system by fracturing fluid using computational fluid dynamics (CFD).

CHAPTER 3

METHODOLOGY

In this thesis, experiments and modeling were conducted to study the transport and placement of proppant in complex fracture systems. To investigate the different factors that impact the proppant transport, a structure that mimics the complex fracture networks found in unconventional reservoirs was created. This chapter focuses on the experimental setup, test materials, test parameters, experimental procedure, and modeling which were used to achieve the results analyzed in Chapters 4 and 5.

3.1 Experimental Setup

The laboratory apparatus was built in the FAST Consortium research center at the Colorado School of Mines. Experiments were conducted to study the transport and placement of proppant in complex fracture networks. To investigate the different factors that impacted the proppant transport, a structure that mimicked the complex fracture networks found in the unconventional reservoirs had to be created. The following sections discuss the specific components of the experimental setup.

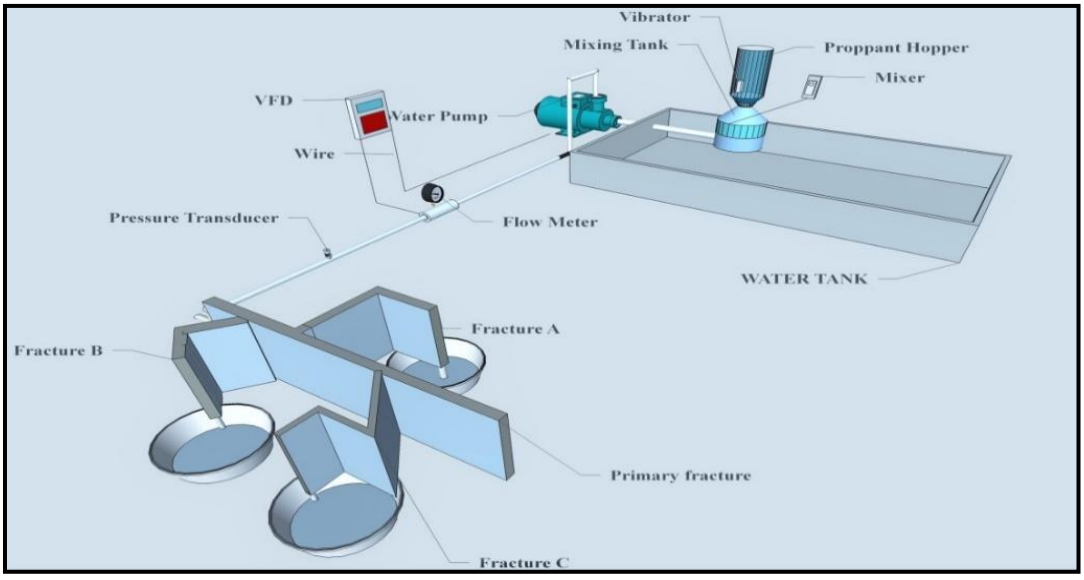

Figure 3.1: Schematic of the laboratory apparatus.

3.1.1 Experimental Apparatus

Figure 3.1 shows the equipment used in the laboratory. The apparatus consisted of a mixing tank, proppant hopper, mixer, water tank, vibrator, water pump, VFD, flow meter, and pressure transducer.

3.1.1.1 Proppant Hopper

The proppant hopper holds approximately 100 lbs of proppant and regulates the proppant mass flow rate with a disk located at the bottom of the hopper. There is a funnel underneath the disk that regulates the transfer of proppant from the disk ports into the mixing tank. The disk ports are perforations that measure the mass flow rate of the proppant into the mixing tank. The hopper is cylindrical and is built with Plexiglas® materials, as shown in Figure 3.2. To prevent blockage at the outlets and maximize proppant flow, a proppant vibrator is attached to the proppant hopper.

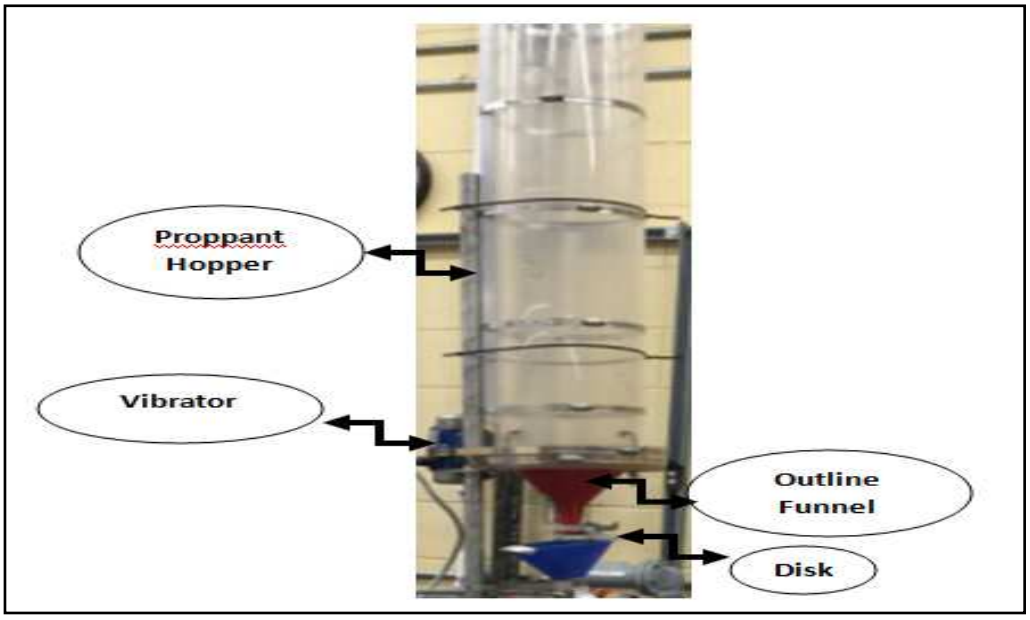

Figure 3.2: Proppant hopper.

3.1.1.2 Proppant Mixer

The proppant mixer is comprised of the mixing tank and the drive mixer, as shown in Figure 3.3. The mixing tank has four openings that are 2 inches wide. The drive mixer has three propellers that make the slurry by mixing water and proppant. The slurry is transported through a 1-inch PVC pipe that connects the mixer tank to the slurry pump.

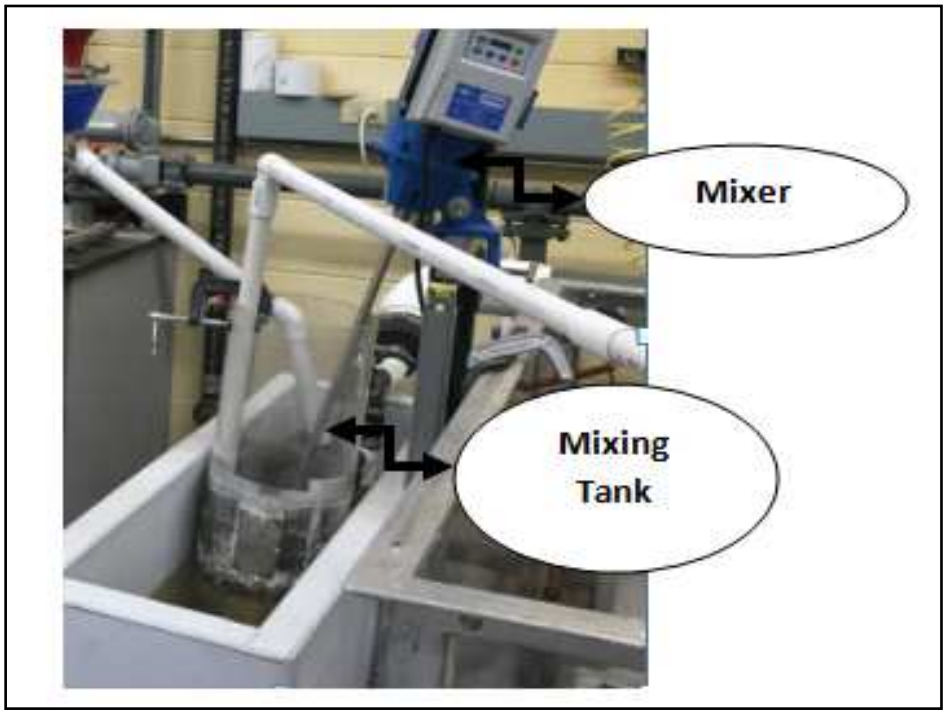

Figure 3.3:Proppant mixer and mixing tank.

3.1.1.3 Slurry Pump

In Figure 3.4, it shows the centrifugal pump that is used to carry the slurry into the fracture slots. There is an impeller that applies centrifugal force to create a pressure drop across the inlet and outlet of the pump. The pressure drop is directly proportional to the RPM of the impeller. There is a silicon carbide seal in the pump that enables it to handle the mixture of solid particles and fluid.

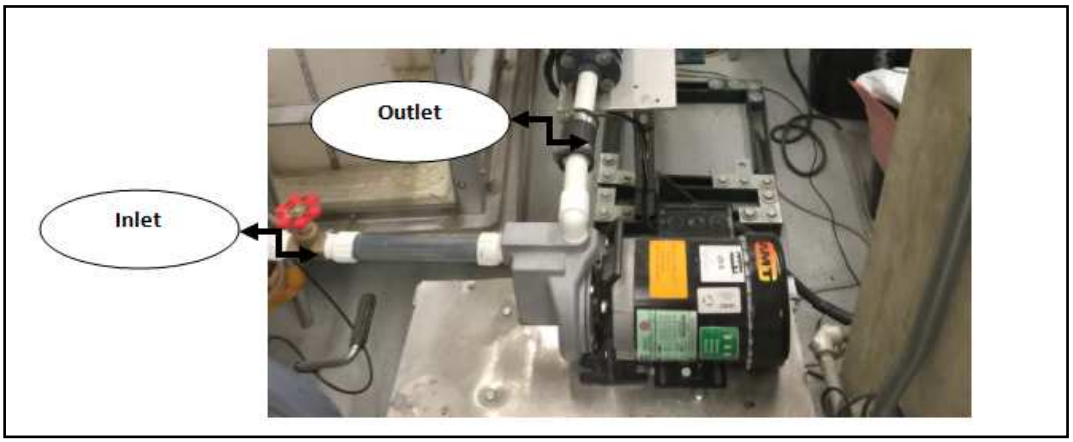

Figure 3.4:Slurry pump.

3.1.1.4 Flow Meter

The flow meter displayed in flow measures the flow rate at which the slurry is injected into the main slot. As the slurry flows through the pipe, a magnetic field is created. Then the flow meter uses Faraday's law of induction (Equation 3.1) to calculate the velocity of the slurry and converts this velocity to a volumetric flow rate.

$$E = -B \times l \times VF \times K \tag{3.1}$$

Where,

E= Induced voltage, (volts) $E = [\frac{\text{Mass} \times \text{Length}^2}{\text{Time}^2 \times \text{Electric charge}}]$

l = Distance between the two electrodes, (meter) [Length]

B = Magnetic field strength, (volt × s$[\frac{\text{Mass} \times \text{Length}^2}{\text{Time}^2 \times \text{Electric charge}}]$)

V_F = Fluid velocity, (m/s) $[\frac{\text{Length}}{\text{Time}}]$

K = Factory set-calibration factor, ($1/m^2$) $[\frac{1}{\text{Length}^2}]$

Figure 3.5: Flow meter used to monitor the slurry flow.

3.1.1.5 Variable Frequency Drive

Since the accuracy of the experimental results depends on pumping the slurry at a consistent flow rate, a Variable Frequency Drive (VFD) was added to the system. The VFD stabilizes the flow rate by reading the output of the flow meter while adjusting the pump RPM. The VFD adjusts the RPM by controlling the electrical frequency received by the pump.

Figure 3.6: Variable Frequency Drive (VFD).

3.1.1.6 Pressure Transducer

The model P265 pressure transducer is based on Kavlico's field proven ceramic capacitive technology. The P265 is designed for general use wherever a rugged and reliable pressure transducer is required. The P265 is offered with a variety of seal materials and is suitable for many diverse applications. The P265 delivers a cost-effective solution without compromising performance or reliability. The pressure transducer reads the pressure from 0 to 20 psi.

Figure 3.7: Pressure transducer model P265.

A new setup was recommended by the FAST Consortium members to test the effect of various concentrations of friction reducer on proppant transport. To accommodate this suggestion, a new equipment design was developed, and the necessary physical components were assembled. The new experimental setup was comprised of a water tank, mixing tank, mixer, slurry pump, flow meter, flow line, and the fracture slots. Adding the batch mixing technique to the experiment allowed for the addition of friction reducer to the fracturing fluid. Figure 3.8 presents the schematic of the new and improved design.

3.1.2 Fracture Slots Network

The slot configurations were designed to duplicate a complex fracture network found in some unconventional reservoirs. The complex fracture network was created to simulate a prototype of an en echelon natural fracture system; therefore, the fractures were not exactly parallel (Smith et al. 2015). Features on the surface of a fracture provide information about the fracture's origin. It describes a set of extension fractures that are aligned en echelon and rotated away from the joint axis. A plumose structure, or hackle plume, has a characteristic feather pattern. Rib marks are curved features perpendicular to the lines of hackle of the fracture face. All these features indicate extensional fracturing, as opposed to slickenside lineation, which indicate shear fracturing. Fractures are associated with faults, folds, and igneous intrusions. Conjugate shear fractures are two sets of small-scale shear fractures that form in fault zones at roughly 60° to each other. At the center of a syncline, fractures are often parallel to the fold axis, making a low angle with the bedding, whereas folds at the peak of an anticline make a high angle roughly 120° with the bedding. Columnar, sheet, foliation, and lineation are all associated with igneous intrusions. Based on the above, chosen experimental angles were 60°, 90°, and 120°.

The network has one primary fracture, three secondary fractures, three tertiary fractures, and one quaternary fracture (see Figure 3.9: Fracture slot networks). Plexiglas was utilized to construct the fracture slots. The fracture slots were designed at a uniform height of 12 inches but had varying lengths and widths. The primary fracture was three feet long, while the lengths of the secondary, tertiary, and quaternary fractures have different lengths in each sub-fracture group (see Table 3.1).

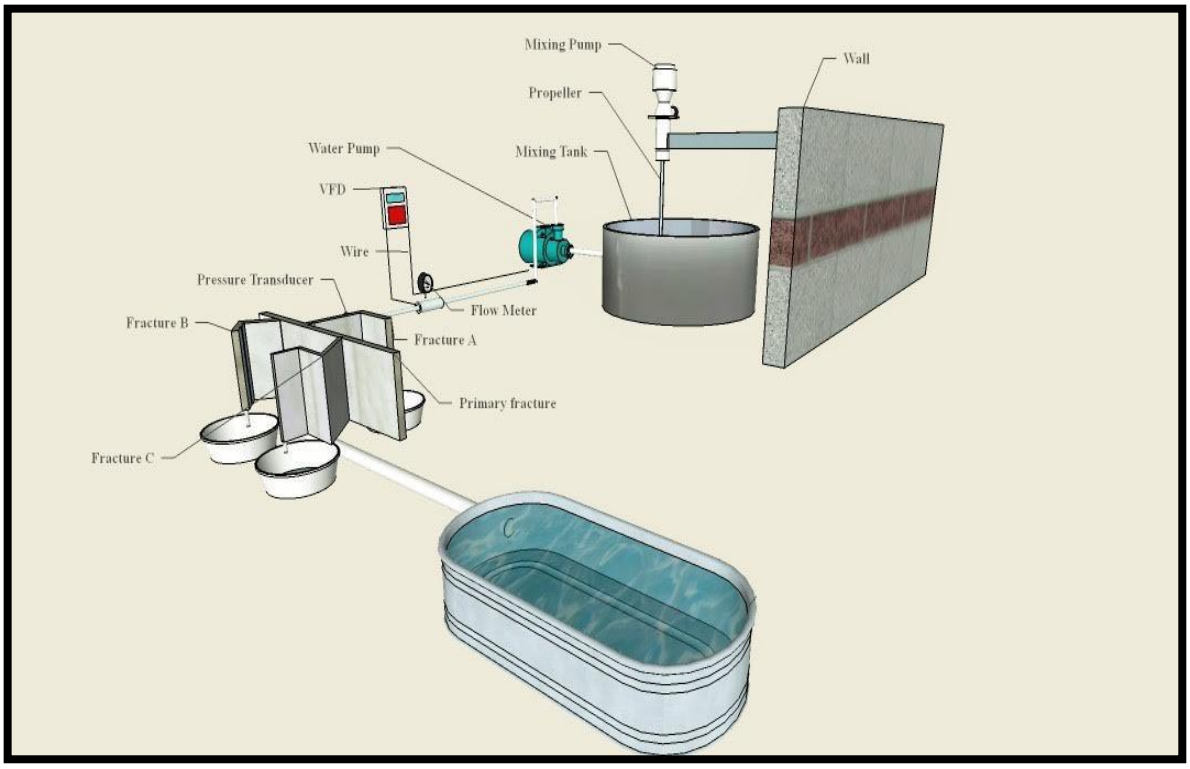

Figure 3.8: Schematic of the proppant transport testing second apparatus.

The width of the primary fracture slot measures 0.2 inch, set to replicate the hydraulic fracture widths published by Palisch et al. (2010), as well as Alotaibi, (2015). Secondary, tertiary and quaternary fractures were set at 0.1 inch as published by Alotaibi, (2015). Although the subsidiary fractures are larger than the average natural fractures, results found by Liu and Sharma (2005) determined that increasing the width has an effect of 5% or less on the proppant settlement rate. This was based on fracture widths with size 2.5 times the particle diameters. In addition to this, to maintain the integrity of the resulting experimental data that was compared to the results obtained, the fracture widths were set to the same sizes. See Table 3.1 and Figure 3.9 for the lengths, width and angles of the secondary, tertiary, and quaternary slots. Based on the Liu and Sharma work, a width of 0.1 inch was sufficient for the sub-slots. Also, this thesis is a continuation of the research conducted by Sahai (2012) and Alotaibi, (2015) and they both used 0.2-inch width for the primary slot. Alotaibi used 0.1 inch for the secondary and tertiary slots.

Table 3.1: Model parameters of the sub- fractures

Characteristic	Sub-Fracture (A)	Sub-Fracture (B)	Sub-Fracture (C)
Angle (deg)	90˚	60˚/ 120˚	60˚ / 90˚ / 120˚
Length (ft)	1.5	1.25	1.75
Width (in.)	0.1	0.1	0.1
Height (ft)	1.0	1.0	1.0

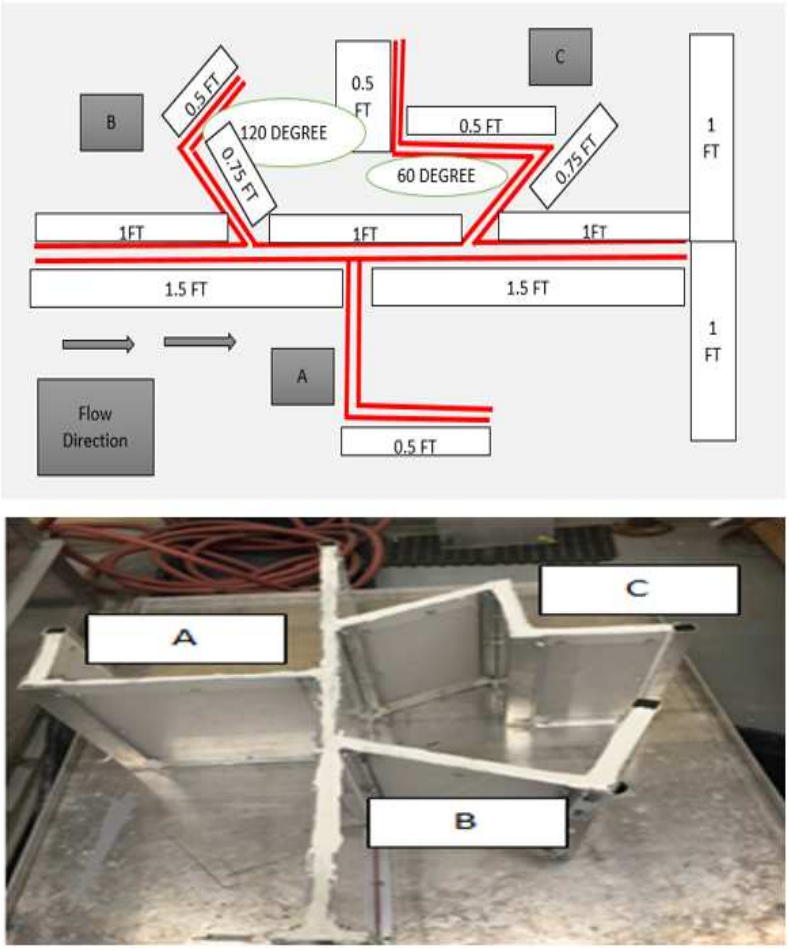

Figure 3.9: Fracture slot networks.

Taking frictional effects on proppant settling into consideration, roughness was added to each wall of the slots. Figure 3.10 shows the pattern of the grooves added to the Plexiglas® to attain the desired roughness.

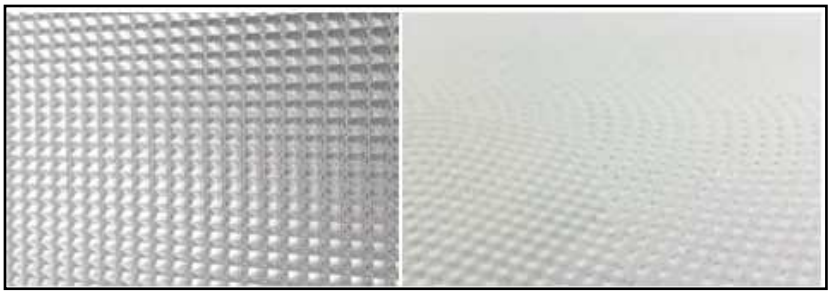

Figure 3.10: Dimensions 12” x 18” Fabricated rough walls test materials.

3.2 Test Materials

Mixing on the fly and batch mixing techniques were employed for the experiments. For mixing on the fly, tap water and proppant were the test materials. For batch mixing, tap water, proppant and friction reducer were the test materials. Two types of proppant were used: white sand and ceramic. Hybrid proppants, which are a mixture of different proppant at different percentages of volume, were also used. The characteristics of the proppant used are listed in types, and the components of the hybrid proppant are listed in Table 3.3. The sizes of the proppant were chosen based on the field practices used in hydraulic fracturing. In the field practices, 100 mesh sand is typically used in the early portion of the job to obtain enhanced distance, height, diversion, etching, and also as a propped agent. A 40/70 mesh is currently the predominant proppant used in gas shale. Ceramic proppants are utilized where higher conductivity and strength are required. A 14/40 mesh ultra-weight was provided and recommended to test by the FAST Consortium member. For these reasons, those proppant types, and sizes were chosen for this research study. Hybrid proppants were also recommended by Sahai (2012) and Alotaibi, (2015) to use to further our understanding of fracturing and proppants. The detailed original sieve distribution for the 100, 40/70 and 14/40 mesh is shown Figure 3.12.

Table 3.2: The characteristics of the different proppant sizes and types

Characteristics	40/70	100	14/40
Average Diameter (in.)	0.015	0.0074	0.038
Average Diameter (mm)	0.38	0.18	0.965
Specific Gravity (g/cm^3)	2.65	2.65	1.054
Specific Gravity (lb/ft^3)	165.43	165.43	65.5
Bulk Density (g/cm^3)	1.51	1.5	1.054
Bulk Density (lb/ft^3)	94.3	99	66.2

Figure 3.11: The left-hand side represents 100 mesh. The middle represents 40/70 mesh. The right-hand side represents 14/40 mesh.

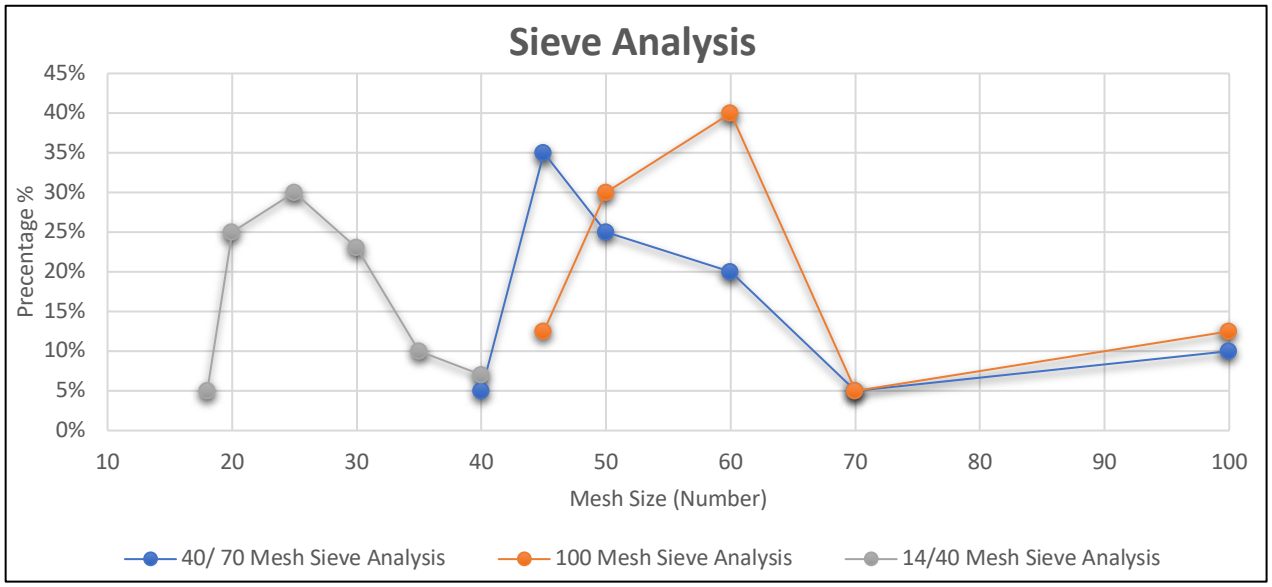

Figure 3.12: Original sieve distribution for 100, 40/70, and 14/40 mesh.

A preferred fracturing fluid in many reservoirs is slickwater, the use of which results in little to no damage to the formation. In shale formations, slickwater increases fracture complexity and reduces friction, which is in stark contrast to linear or cross-linked gels that are more viscous. This was observed by field personnel since the mid-1950s (White 1964). Slickwater has also been shown to escalate injection rates while simultaneously reducing surface-treating pressure. While

flowing in a pipeline, it disrupts the near-wall turbulence regeneration cycle and reduces the turbulent friction drag by directly interacting with a created vortex, thereby decreasing the flow of friction in the pipeline (White 1964). The types of the fracturing fluids tested in this work are listed in Table 3.4.

Table 3.3: Composition of the Hybrid Proppant

Characteristics	**100**	**14/40**	**100**	**40/70**	**40/70**	**14/40**
Percentage Per	75	25	75	25	75	25
Volume (%)	50	50	50	50	50	50
	25	75	25	75	25	75

There are many different types of friction reducers, but they all have a couple of shared properties. First, they are most commonly large polymers, where the larger the polymer chain, the more effective the material. Second, they build on non-Newtonian gel structures and their efficacy is diminished with extended agitation, meaning they are shear sensitive (White 1964). The polymer solutions utilized as friction reducers in aqueous systems (such as water, brine, and hydrochloric acid solutions) are anionic, nonionic polymers and guar. In hydrocarbon systems, such as crude oils (like kerosene or diesel fuel), synthetic polymer solutions and in-situ soap gels are more suitable. In acidizing, cationic friction reducers are employed and are also appropriate for use in hydraulic fracturing fluids. However, their cost is drastically higher than conventional anionic polymers. Guar, an uncharged polysaccharide polymer, will need higher concentrations of a greater magnitude, resulting in exponentially higher costs (Rimassa et al. 2009). The conclusion was drawn that within a tight formation, hydraulic stimulation, such as shale gas and tight gas reservoirs, synthetic anionic polymers are recommended. One theory noted that synthetic anionic polymers would not be advisable to use in highly ionic systems because the presence of cations can greatly reduce their efficiency. This has been found to be true of divalent cations, such as calcium and magnesium (White 1964). For slickwater fracturing fluids, the most widely used friction reducers currently are ionic polyacrylamide-based polymers. They are noted for: 1) their higher efficiency in fresh water to reduce friction, 2) are more shear sensitive, and 3) give the "apparent viscosity" when added to water (Kaufman et al. 2008). The ionic friction reducer used in this study was provided from Calfrac Well Services Corporation.

The concentration level is a major contributing factor that results in different levels of drag reduction. For most friction reducers, higher concentrations produce increased friction reduction. The anionic polyacrylamide friction reducer is a shear thinning fluid and it is a strong shear sensitive friction reducer (Rimassa et al. 2009). When the anionic polyacrylamide friction is applied in a tight formation reservoir simulation, very small loading is commonly used. Its viscosity generally increases to 3–4 cp, even though the shear rate has increased two orders of magnitude (Sun et al. 2013). In slickwater fracturing today it is not necessary to pump water first to fracture and then follow slickwater laden with proppant. Fracturing is now frequently done by pumping a spacer of water ahead followed by the slickwater with friction reducer and proppant. Therefore, this test was conducted by decreasing the friction reducer concentration, from 0.1 to 1 gal/1000 gal. Based on previous reviews and analysis in this research, a polyacrylamide-based anionic polymer was used. It has a molecular weight around 20 million Daltons. It also breaks down more easily resulting in minimal or no formation damage in the fracture. Since the industry has been conducting experimental work at higher concentrations than what has been previously used, this research applied that method and used a higher concentration of friction reducers at 1 gal/1000 gal and 2 gal/1000 gal.

Table 3.4: Concentration of friction reducer in the fracturing fluids used in the experiments.

Fractured Fluids	**Concentration of Friction Reducer**
Water with 0% Friction Reducer	-
Water with Friction Reducer	1 gal/1000 gal
Water with Friction Reducer	2 gal/1000 gal

3.3 Test Parameters

It was crucial to use a proppant concentration identical to the field practices for slickwater treatments to avoid high settling rates of the slurry in unconventional reservoirs. For the purposes of the experiments conducted in this work, the proppant concentration was set to 2 lb/gal (ppg) which is the higher field concentration used in slickwater treatments (Woodworth and Miskimins 2007). To compare the results of the laboratory scale hydraulic fracturing experiments to the field scale operations, it was essential to use scaling laws. Scaling laws are the application of dimensional analysis involving the energy dissipation during the fracture growth. Sample size, wellbore dimensions, and the hydro-mechanical properties of the sample are the inputs for the

scaling model. This allows output variables such as fluid viscosity, injection rate, and total proppant transport to be determined. It further enhances the design of the laboratory hydraulic fracturing test (de Pater et al. 1994). In the past, laboratory scale experiments were frequently conducted without scaling laws. As a result, parameters such as fluid viscosity and injection rates were obtained from real field operations. This contributed to low fluid viscosities and exaggerated injection rates in the laboratory. However, to monitor and analyze proppant transport in a small sample at a lab scale, fracturing fluids with higher viscosities and reduced injection rates are required. This ensures proper containment of the proppant transport within the fracture slots and enables monitoring of proppant transport mechanisms.

To conduct a scaled hydraulic fracturing experiment, a high fracturing fluid viscosity that imitates field practices was used. This was to replicate the real physical structuring that occurs in the field. The other relevant parameter in the fracturing was the injection flow rate. In laboratory experiments, when dealing with a high viscous fluid, the injection flow rate should be considerably lower than the field rates (Shah and Asadi 1997). In this study, three different fracturing fluids were used at different viscosities. In each test, injection flow rates of 1 and 2 gal/min were used to study their impacts on dune height, dune area, and proppant distribution within the four fracture groups of the SRV. To address the proppant transport concern of slickwater, operators frequently pump a massive amount of water with high pump rates, which is equivalent to 16 ft/min of slurry velocity. In this research study, the injection rate was set at 1 and 2 gal/min respectively, which was equivalent to 8 ft/min and 16 ft/min at a slurry velocity similar to slurry rates used in the field. Correct representation of the fracturing fluid velocity across the fracture face forms the basis of the scaling calculation for this research.

To obtain these values, the proppant and water flowrates needed to be controlled and set at specific values. The water was controlled using the VFD device. For mixing on the fly, the proppant flow rate was regulated by gravity through the Plexiglas disk ports. There are three disks and each disk has six ports. The mass flow rate through each of these ports was calibrated using a scale and a timer. Results are listed in Table 3.5, Table 3.6,

Table 3.7, and Table 3.8. The mass flow rate of the proppant from the disk ports allowed the correct port to be selected to achieve the desired proppant concentration in pounds per gallon (ppg).

Table 3.5: Proppant (40/70 -100) mass flow rate through the hopper disk ports

Disk Port Opening Number	Disk Port Opening Size inch	Flow Rate Pound-Mass/Minute (PPM)
1	5/16	1.25
2	21/64	1.40
3	11/32	1.59
5	23/64	1.95
6	3/8	2.30
7	25/64	3.10
8	13/32	3.36
9	27/64	3.70
10	7/16	4.20

Table 3.6: Proppant (14/40) mass flow rate through the hopper disk ports

Disk Port Opening Number	Disk Port Opening Size inch	Flow Rate Pound-Mass/Minute (PPM)
1	5/16	0.28
2	21/64	0.34
3	11/32	0.48
5	23/64	0.67
6	3/8	0.79
7	25/64	0.92
8	13/32	1.06
9	27/64	1.28
10	7/16	1.5
11	29/64	1.95
12	15/32	2.21
13	31/64	2.52
14	1/2	2.78
15	33/64	3.10
16	17/32	3.42
17	35/64	3.89
18	9/16	4.08

Table 3.7: Proppant mass flow rate through the hopper disk ports at 1 gal/min

Characteristics	**40/70**	**100**	**14/40**
Disk Port Opening Number	5	5	11
Flow Rate, Pound-Mass/Minute(PPM)	1.95	1.95	1.95

Table 3.8: Proppant mass flow rate throughthe hopper disk ports at 2 gal/min

Characteristics	40/70	100	14/40
Disk Port Opening Number	10	10	18
Flow Rate, Pound-Mass/Minute(PPM)	4.20	4.20	4.08

The fluid viscosities for the treatment design are determined from laboratory tests and are reported in service company literature. The ideal experiment for describing fluid flow in a fracture would be to shear a fluid between two plates that are moving parallel and relative to one another. The shear stress on the fluid equals the drag force on the plates divided by the area of the plates, and has units of stress or pressure (e.g., psi). The shear rate (or velocity gradient) is the relative velocity of the two plates divided by the separation distance between the plates. Shear rate has the units of sec^{-1}. Such an ideal test is not feasible for day- to -day applications and so a rotating "cup and bob" viscometer know as a "Couette" viscometer is generally used. API standard RP3912 and ISO 13503-113 describe the current testing procedures used by the industry. The viscometer uses a rotating cup and a stationary bob, with a gap between the two that simulates the fracture. As shown in

Figure 3.10, the rotational speed of the cup imparts a shear rate and the bob measures the shear stress or drag force exerted on the walls of the cup and bob. This is obtained by measuring the torque on the bob. The shear rate is the relative velocity between the stationary bob and the rotating cup divided by the separation gap. For a Fann 35 (See Figure 3.13) equipped with a R1 rotor and a B1 bob, the rotational speed of 100 RPM represents a shear rate of 170 sec-1 and a speed of 300 RPM gives a shear rate of 511 sec-1 (Harris et al. 2005).

The tests described above measure the shear stress generated by the specific increased shear rates (called a ramp). This data is then converted to a "viscosity" value by using a rheological model to describe fluid behavior. The three models which are in constant use by the oil industry

are: (1) Newtonian fluid - Newtonian fluid has a linear relation between shear rate and shear stress. Fluid viscosity is the slope of the shear rate versus shear stress data. (2) Bingham Plastic - Bingham Plastic fluids differ from a Newtonian fluid in that a non-zero shear stress called the Plastic Yield Value is required to initiate fluid flow. The slope of the shear rate/shear stress data is labeled Plastic Viscosity and this model is used for cements and many drilling muds. (3) Power Law Fluid - this is the most common fluid model used for current fracturing fluids.

For this rheological model, the shear stress/shear rate data give a linear relation on log-log scales. The slope of this log-log line is denoted by n' and is labeled the Flow Behavior Index. n'=1 implies a Newtonian fluid; n'>1 is called a shear stiffening fluid. By using three types of slickwater at various viscosities, an assessment of the impact and advantage of expanding the slurry thickness on the proppant transport can be determined. Likewise, a study can be performed on the impact of the proppant density on proppant settling while keeping the proppant shape and size the same. A comparison can be made on the three different types of proppant. Then, an assessment of the effect of secondary fractures on the proppant settling in the primary fracture can be done by comparing the settling with and without intersecting fractures.

For non-Newtonian fluids, (e.g.: Power Law fluid) the "apparent viscosity (μ_a)" is used as a shorthand way of characterizing the fluid. Thus, a fluid's apparent viscosity depends on the shear rate at which the viscosity is measured (or calculated). For a Power Law fluid with n'<1, the apparent viscosity will decrease with increasing shear rate. To find n' and K', a fluid is placed in a rheometer and sheared at a constant rate while the temperature was brought to equilibrium. Periodically the fluid n' and K' is measured by bringing the shear rate up, holding the rate for a few seconds, then increasing the rate again typically over a range of at least four shear rates. This is termed a ramp and is typically done every 30 minutes during the fluid test. Note that for each ramp four shear rates were used. The slope of the line is the n' and the intercept at a zero-shear rate is the K'. Using this information an apparent viscosity for any shear rate can be calculated with the following equation:

$$n = 0.657 \log \frac{\theta 100}{\theta 3} \tag{3.2}$$

$$k' = \frac{5.11\ \theta 3}{511^n} \tag{3.2}$$

$$\mathrm{n} = \mathrm{n}' \tag{3.3}$$

In fractures, shear is calculated from n' per Equation 3.5 (Gidley et al. 1989). The assumption here is that n' and K' are relatively shear- rate insensitive over the shear range in the fracture.

$$\gamma = (\frac{2n'+1}{3n'})\frac{6q}{hw2} \tag{3.4}$$

Then, the nominal shear rate, by Shah and Asadi, (1997) in the slot is calculated based on the flow rate and the slot dimensions as,

$$\gamma' = \frac{1.925\ Q\prime}{W'2H} \tag{3.5}$$

Thus, for a given flow rate, a range of shear rates can be obtained by simply changing the gap width of the slot. For these shear rates, the apparent viscosity of the fluid is determined by,

$$\mu_a = k'\gamma^{n'-1} = \frac{k'}{\gamma^{1-n'}} \tag{3.6}$$

A Power- Law fluid is a type of generalized Newtonian fluid for which the relationship between the shear stress and shear rate can be described as:

$$\tau_y = \gamma\mu_a \tag{3.7}$$

Where,

μ_a is apparent viscosity (cp) [$\frac{\text{Mass}}{\text{Length x Time}}$]

γ is the shear rate (sec^{-1}) [$\frac{1}{\text{Time}}$]

K' is consistency index, Ib-sec/ft^2 [$\frac{\text{Force x Time}}{\text{Area}}$]

n' is flow behavior index (dimensionless)

h is the slot height (ft) [Length]

w is the slot width (ft) [Length]

q is the injection rate (ft^3/sec) [$\frac{\text{Volume}}{\text{Time}}$]

τ_y is the shear stress (lb/ft^2) [$\frac{\text{Force}}{\text{Area}}$]

Q' is the injection rate (gal/min) [$\frac{\text{Volume}}{\text{Time}}$]

W is the fracture width (inch) [Length]

H is the fracture height (ft) [Length]

Service company literature reports viscosity at different shear rates (170 or 511 sec^{-1}). The shear rate in a fracture can be as low as 30 to 40 sec^{-1}. Smith and Montgomery (2015) stated that an identical fluid might be reported by one company to have a viscosity of 300 cp (170 sec^{-1}) and another to have 200 cp (511 sec^{-1}), but the fluid may have over 600 cp in the fracture (at 40 sec^{-1}). The widest laboratory research conducted on fracturing fluids are the steady-shear rheological measurements. To start out, the friction reducer is added to the water to produce slickwater. The property to be measured is the apparent viscosity of the fluid as a function of the shear rate, temperature, fluid composition, and time. For the fracture fluid, the proppant particles are batch-mixed with water base fluid and friction reducer. These are combined before the pumping begins. The values obtained from the equations for the subject fluids of this study are displayed in the Table 3.9, and Table 3.10, which are similar to what was used in the field.

Table 3.9: Measured parameters for shear rate the slickwater at friction reducer 1 gal/1000 gal

Q ft^3/sec	**H ft**	**W^2 ft^2**	**K'**	**n**	**ϒ sec^{-1}**	μa **cP**	τ_y **lb/ft^2**
0.00223	1	0.000277	5.36	0.395	72.70	0.401	29.21
0.00447	1	0.000277	5.36	0.395	145.40	0.264	38.42
0.00670	1	0.000277	5.36	0.395	218.43	0.206	45.13
0.00893	1	0.000277	5.36	0.395	291.13	0.174	50.57
0.01117	1	0.000277	5.36	0.395	364.05	0.152	55.25
0.0134	1	0.000277	5.36	0.395	436.85	0.136	59.37
0.0156	1	0.000277	5.36	0.395	508.25	0.124	63.04
0.0178	1	0.000277	5.36	0.395	580.95	0.114	66.47
0.0201	1	0.000277	5.36	0.395	653.73	0.106	69.64
0.0223	1	0.000277	5.36	0.395	726.35	0.099	72.60
0.0245	1	0.000277	5.36	0.395	798.73	0.094	75.39
0.0267	1	0.000277	5.36	0.395	781.4	0.089	78.03

Table 3.10: Measured parameters for shear rate the slickwater at friction reducer 2 gal/1000 gal

Q ft^3/sec	H ft	W^2 ft^2	K'	n	Υ sec^{-1}	μa cP	τ_y lb/ft^2
0.00223	1	0.000277	9.193	0.313	83.33	0.441	36.77
0.00447	1	0.000277	9.193	0.313	166.66	0.274	45.70
0.00670	1	0.000277	9.193	0.313	250.36	0.207	51.92
0.00893	1	0.000277	9.193	0.313	333.69	0.170	56.82
0.01117	1	0.000277	9.193	0.313	417.27	0.146	60.94
0.0134	1	0.000277	9.193	0.313	500.72	0.128	64.52
0.0156	1	0.000277	9.193	0.313	582.56	0.116	67.66
0.0178	1	0.000277	9.193	0.313	665.89	0.106	70.55
0.0201	1	0.000277	9.193	0.313	749.29	0.097	73.21
0.0223	1	0.000277	9.193	0.313	832.54	0.091	75.67
0.0245	1	0.000277	9.193	0.313	915.49	0.085	77.96
0.0267	1	0.000277	9.193	0.313	998.83	0.080	80.12

Table 3.11: Measured parameters for shear rate the slickwater at friction reducer 2 gal/1000 gal

Q' Gal/min	Υ' sec^{-1}
1	48.13
2	96.25
3	144.38
4	192.50
5	240.63
6	288.75
7	336.88
8	385.00
9	433.13
10	481.25
11	529.38
12	577.50

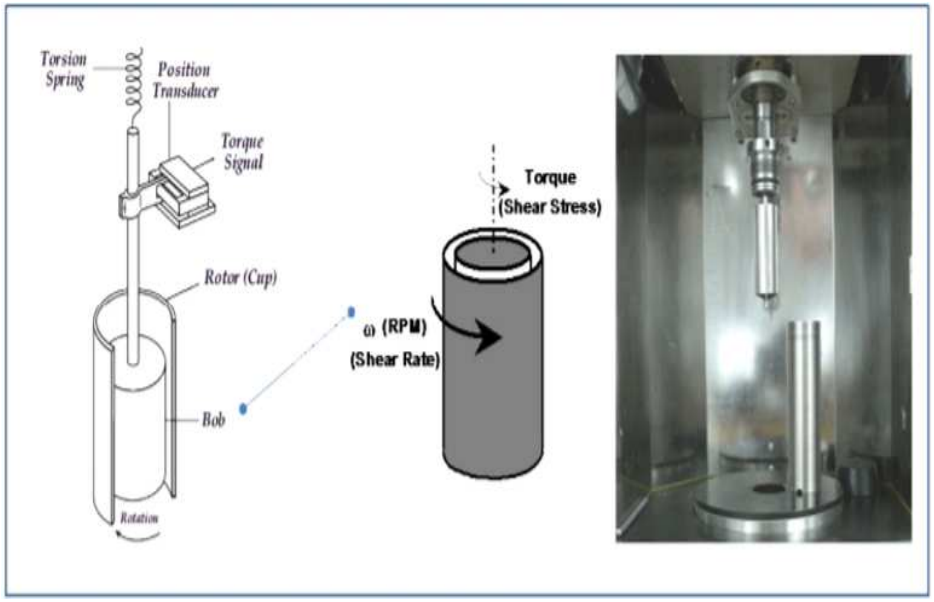

Figure 3.13: The geometry of a Collette "Cup & Bob" viscometer.

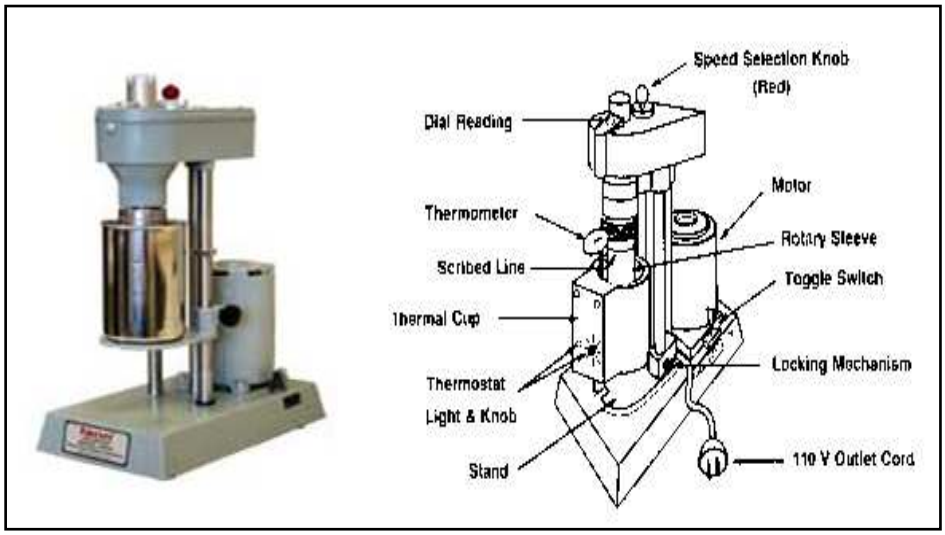

Figure 3.14: Fann Model 35 Viscometer (from Sampaio 2016).

Static pressure ports placed at selected locations in the slot were used to measure the pressure drop along the length of the slot. At periodic intervals, the data acquisition system records pressure drop, flow rate, temperature, and other pertinent data. The rheological characterization of the fluid is achieved by determining the apparent viscosity μ_a, of the test fluid. After the wall shear stress τ_y in the slot has been determined, the pressure drop can be calculated using the following Equation 3.9.

$$\tau_y = \frac{6\,W\,\Delta P}{L} \tag{3.8}$$

Table 3.12: Calculated parameters for pressure drop in the slot

Slickwater at 1G/1000 G FR		Slickwater at 2G/1000 G FR	
ty lb/ft^2	Δp psi	ty lb/ft^2	Δp psi
29.21	73.03	36.77	91.94
38.42	96.07	45.70	114.26
45.13	112.85	51.92	129.80
50.57	126.43	56.82	142.04
55.25	138.12	60.94	152.35
59.37	148.45	64.52	161.31
63.04	157.61	67.66	169.15
66.47	166.16	70.55	176.39
69.64	174.10	73.21	183.03
72.60	181.51	75.67	189.18
75.39	188.46	77.96	194.90
78.03	195.07	80.12	200.29

To compare the pressure changes in Equation 3.9, pressure transducer was installed in the system. After defining the pressure values, the same equation was used to calculate shear stress.

Table 3.13: Measured parameters for pressure drop in the slot

Slickwater at 1G/1000 G FR		**Slickwater at 2G/1000 G FR**	
ty **lb/ft^2**	Δp psi	**ty lb/ft^2**	Δp psi
0.00	0.00	0.00	0.00
0.00	0.00	0.00	0.00
0.00	0.00	0.00	0.00
0.00	0.00	0.00	0.00
0.00	0.00	0.00	0.00
0.16	0.40	0.00	0.00
0.16	0.40	0.16	0.40
0.24	0.60	0.24	0.60
0.36	0.90	0.32	0.80
0.56	1.40	0.40	1.00
0.64	1.60	0.48	1.20
0.64	1.60	0.60	1.50

After determining the pressure value for each flow rate, the results were plotted (Figure 3.15 and Figure 3.16). Using the results from these equations with the Darcy equation for linear flow, the permeability of the slots was determined to be 26735 mD. The permeability was calculated with the following:

$$k = \frac{\mathrm{QL\mu}}{0.001127\ \mathrm{A\triangle P}} \tag{3.9}$$

Where,

μ is apparent viscosity (cp) [$\frac{\mathrm{MASS}}{\mathrm{Length\ x\ Time}}$]

L is the slot length (ft) [Length]

A is the slot Area (ft^2) [Area]

Q' is the injection rate (gal/min) [$\frac{\mathrm{Volume}}{\mathrm{Time}}$]

$\triangle$ P is the pressure change (psi) [$\frac{\mathrm{Force}}{\mathrm{Area}}$]

K is the fracture permeability (md)

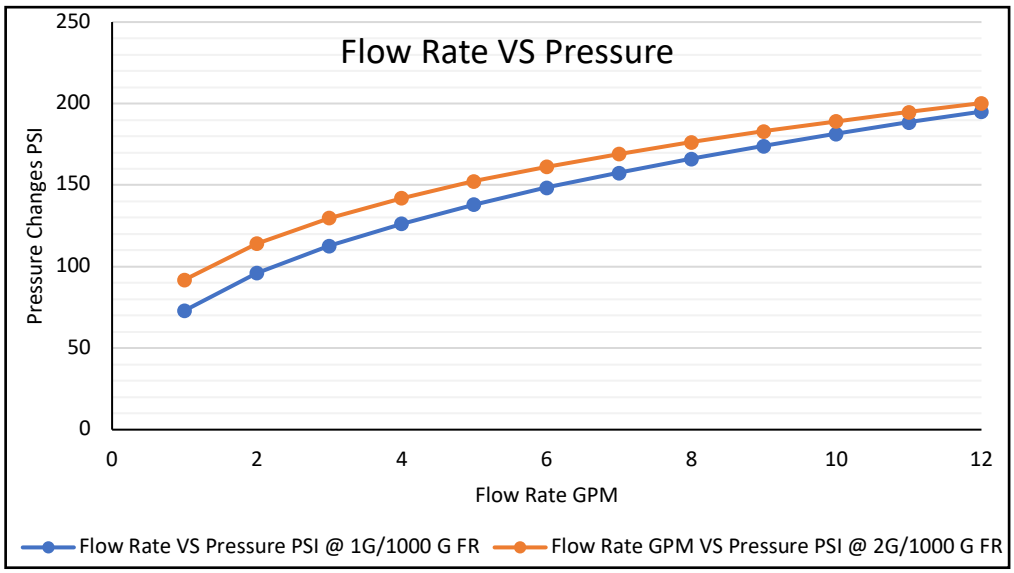

Figure 3.15: The calculated values of calculated pressure with varying flow rates using slickwater at different concentrations of friction reducers

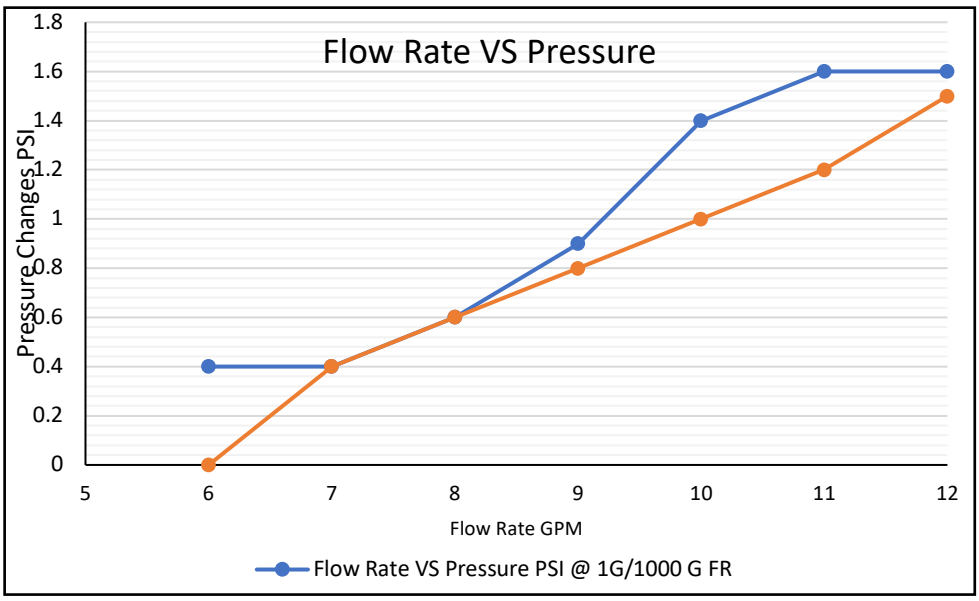

Figure 3.16: The measured values of measured pressure with varying flow rates using slickwater at different concentrations of friction reducers.

A flow regime is determined by whether the dimensionless Reynolds number fall in the plug, transitional, laminar, or turbulent regimes; here Plug flow is $N_{Re}<100$, Laminary flow is $1000>N_{Re}>2000$, Transitional flow is $2000>N_{Re}>4000$, and Turbulent flow is $4000>N_{Re}$. At low values of N_{Re}, the flow is dominated by viscous forces and the flow is laminar. Laminar flow is smooth, streamlined, and good for mixing. At large values of N_{Re}, turbulent flow occurs. In turbulent flow there are irregular and unpredictable motions or swirls called eddies. The transition from laminar to turbulent flow occurs at a critical Reynolds number between 2000-4000. The critical Reynolds number for flow in a rectangular duct ranges between 1800 at aspect ratio near 1.5 to 2800 at infinite aspect ratio, corresponding to flow between parallel plates (Hanks and Ruo, 1966). The characteristic length scale for flow through a slot is the hydraulic diameter (D_h), equal to two times the cross-sectional area divided by the perimeter.

For an infinite aspect ratio (flow between parallel plates), the hydraulic diameter is double the width. For flow in a wide-open channel such as a river, the characteristic length scale is the depth of the channel. During hydraulic fracturing, turbulent flow is likely near the wellbore because of the high velocity created by flow convergence. It is known that not all fractures are propagated during a pumping operation. Consequently, the injection rate entering a given fracture can be as large as 40 barrels per minute. Such a large fluid injection rate questions the classical hypothesis of laminar flow in a propagating hydraulic fracture. Using turbulent flow in part of the

fracture may cause a wrong estimation of fracture length, width, and pressure with time. The turbulent flow will lead to pressure loss, such that the pressure at the tip of fracture may not be high enough to propagate the fracture. Based on this, it is crucial to simulate field practice to produce laminar flow inside the fractures. Further from the well, the occurrence of turbulent flow depends on job-specific parameters such as: injection rate, net pressure, fluid viscosity, the number of flowing fractures, and fracture height. For example, if fluid is flowing at 0.132 m^3/s (50 bpm) into one wing of a bi-wing fracture, with a viscosity of 0.3 cp, it can be estimated (using the PKN fracture geometry assumption) that the critical Reynolds number will be reached as long as the height is less than 314 meters. If the fluid viscosity is 10 cp, turbulent flow will occur if the height is less than 10 meters. Aperture is highest along the centerline of the fracture, tapering to zero at the top and bottom, and so turbulent flow is most likely along the center of the fracture. The onset of turbulent flow is associated with non-Darcy pressure drop (Fourar et al. 1993). Fluid Reynolds number reflects the relative importance of inertial versus viscous force. The fluid Reynolds number, N_{Ref}, for flow in a circular pipe, is defined in the calculation as:

$$N_{Ref} = \frac{\rho V d}{v} \tag{3.10}$$

Where the flow velocity ($m\ s^{-1}$), d is the diameter of circular pipe (m), and v is the kinematic viscosity ($m^2\ s^{-1}$). For flow in a cross-section other than the circular shape, d is substituted by the hydraulic radius (R) (Shah and Asadi 1997). In a confined flow condition with a rectangular shape of cross-section, R is:

$$R = \frac{bh}{2(b+h)} \tag{3.11}$$

Where b is the fracture aperture (m) and h is the water depth (m), equal to the height of fracture here. Thus, the Reynolds number for flow in fractures becomes:

$$N_{Ref} = \frac{\rho V b h}{2v(b+h)} \tag{3.12}$$

The equation can be simplified to the following:

$$N_{Ref} = \frac{\rho Q}{2h\mu} \tag{3.13}$$

Where,

N_{Ref}= Reynolds number for fluid (Dimensionless)

ρ = density of the fluid (kg/m^3) [$\frac{\text{MASS}}{\text{Volume}}$]

d = diameter of the fracture width (m) [Length]

H = height of the fracture (m) [Length]

μ = viscosity (kg/m. sec) [$\frac{\text{MASS}}{\text{Length x Time}}$]

Q = fluid volumetric flow rate, m^3/sec [$\frac{\text{Volume}}{\text{Time}}$]

After the injection rates are determined, the value of the tested slurry's velocity used in this research is referred to as the initial slurry velocity. This is where the proppant settling has yet to occur. It is calculated by dividing the volumetric flow rate by the fracture slot cross sectional area. Friction factor was included to get accurate results. These results mimic field conditions using the Moody chart (1944). The results are as shown in Table 3.14 and 3.15.

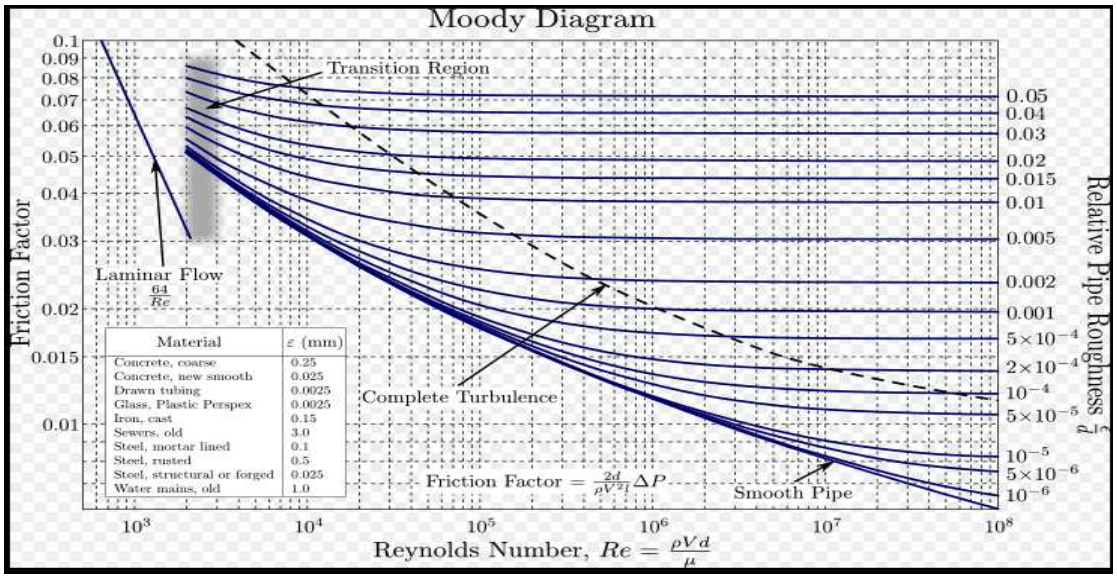

Figure 3.17: Moody diagram showing the Darcy-Weisbach friction factor plotted against the Reynolds number, Re for various relative roughness, (Moody 1944).

Due to the limitation of the model, the maximum flow rate that the system can produce is 12 gal/min. The three types of fluid systems are water, slickwater at 1 gal/1000 gal of friction reducer, and slickwater at 2 gal/1000 gal of friction reducer.

Table 3.14: Measured parameters for Reynold number for fluid in the slot

		Water System	Slickwater at 1G/1000 G FR	Slickwater at 2G/1000 G FR
Q Gal/min	**V ft/min**	N_{Ref}	N_{Ref}	N_{Ref}
1	8.02	103.961	12.19305	12.21851
2	16.04	207.923	24.38611	24.43703
3	24.06	311.884	36.57916	36.65554
4	32.08	415.846	48.77221	48.87406
5	40.1	519.807	60.96527	61.09257
6	48.12	623.769	73.15832	73.31108
7	56.15	727.73	85.35137	85.5296
8	64.17	831.692	97.54443	97.74811
9	72.19	935.653	109.7375	109.9666
10	80.21	1054.47	123.6724	123.9306
11	88.23	1143.58	134.1236	134.4037
12	96.25	1249.19	146.5102	146.8161

Table 3.15: Measured parameters for friction factor in the slot

		Water System	Slickwater at 1G/1000 G FR	Slickwater at 2G/1000 G FR
Q Gal/min	**V ft/min**	F_f	F_f	F_f
1	8.02	0.62	5.249	5.238
2	16.04	0.31	2.624	2.619
3	24.06	0.207	1.75	1.746
4	32.08	0.155	1.312	1.309
5	40.1	0.124	1.05	1.048
6	48.12	0.103	0.875	0.873
7	56.15	0.089	0.75	0.748
8	64.17	0.077	0.656	0.655
9	72.19	0.069	0.583	0.582
10	80.21	0.061	0.517	0.516
11	88.23	0.056	0.477	0.476
12	96.25	0.052	0.437	0.436

3.4 Experimental Procedure

As mentioned above, there were two types of mixing procedures used in this work including mixing on the fly and batch mixing. Mixing on the fly began with filling the tank with water and then the proppant was deposited into the proppant hopper. The VFD, flow meter and pump were turned on, with the mixer speed beginning at 120 RPM to proportionally mix the water and proppant. Underneath each group of fractures, a bucket was placed to collect the slurry throughout the experiment. Prior to pumping the slurry, clean water was pumped throughout the system to certify that there were no leaks in the system. The proppant flow control disk was set at the chosen port and the hopper vibrator was turned on allowing the proppant to discharge at the designed mixing rate in with water and forming the slurry. The VFD device started the pumping of the slurry at a set flow rate. The slurry then pumps into the fracture slots and data acquisition begins. The proppant flow and dune heights in the fractures were captured using a camera pointed at the system. Data collection occurs when the settling proppant developed a dune that kept increasing in height with time until reaching a constant value where all injected proppant is transported further inside. This height is called the equilibrium dune height. Upon completion of the experiment, the 120 lbs of proppant used in the experiment was collected from the four buckets. The proppant was dried in the oven, sieved, and put into the original container to be reused.

In batch mixing, the tank was filled with water. A desired value of friction reducer was left to mix for 20 minutes. After 20 minutes, a sample was taken for a viscosity measurement using the viscometer. Upon reaching the optimum viscosity value, proppant was added directly to the mixing tank in small increments to ensure proper mixture with no buildup of sand at the bottom of the tank. Similar to the mixing on the fly procedure, the slurry was pumped into the system and data was captured using a camera until the equilibrium height in the fracture slots was reached. Upon experiment completion, the 120 lbs. of proppant were collected from the buckets, dried in the oven, sieved and put into the original container to be reused.

3.5 Experimental Data Verification and Error Analysis

Reproduction of experimental data is the most crucial aspect of any study, establishing the reliability of the data and it's resulting conclusions. The design stage of the apparatus (Illustrated in Section 3.1) accounted for its high precision level. A methodical implementation of the

procedure and meticulous monitoring of the system during the experiment was critical to ensure the accuracy of the produced data. This section examines any uncertainty or error margins of the obtained results.

The first uncertainty examined was the pressure measurements. According to the manual of the pressure sensor used, there was a total error band of 2%. Throughout the experiment, the highest pressure used was 1.6 psi. This was the highest pressure obtained which was a very small amount that would have a negligible or minimal effect.

The second element of uncertainty was the injection rates. The injection rate was set at 1 gal/min and 2 gal/min based on the flow meter. Along the flow path to the fracture network, the flow was divided in two tubes with one each going to the top and bottom of the perforations. When the slurry reaches the fracture network the results could not be effectively measured. In addition, the fluid velocity was constant at the earliest stage of pumping until it reached the fractures. This was due to the system's limitation which cannot measure the pressure and velocity accurately for each sub-fracture group and main fracture.

The third uncertainty examined was the proppant concentration as mixing on the fly and batch mixing left concentrations of 2 to 10 pounds of sand on the bottom of the mixing tank, since the concentration was assumed to be constant at 2 ppg, it found that the effective concentration of sand into the fracture was 8.33% less, resulting in 130 lbs. of sand in the fracture network. This was due to settling in the mixing tank.

The fourth uncertainty examined was the slurry volume. A controlled slurry volume of 60 gallons was used in the batch mixing. It was pumped to the fracture network until the equilibrium dune height was achieved and used as benchmark for the water system. In comparison using the other two fluid systems, which were slickwater with different concentrations of friction reducer, were also set at 60 gallons. This altered the results as the slickwater did not reach the equilibrium dune height expected.

The fifth uncertainty was the roughness of the wall. The pattern of the grooves added to the Plexiglas to attain the desired roughness was provided from the company manufacturer. The roughness was achieved by using a computerized v-shaped drill bit machine that drills at very low depths on the Plexiglas sheet surfaces following a programmed pattern of curves. There was no actual value for roughness to add for the calculation, which would cause the results to be altered.

The sixth and final uncertainty was the physical measurements for the dune height. The recorded video was played back to make sure the measurements were accurate. The measurements were taken every five minutes, which gave error results from 2% to 5%.

After defining and reducing the error of margin in the model, the results were analyzed. The first method of analysis of the obtained results trended in terms of the proppant dune height in the main fracture with sensitivity to the changing of the experimental parameters. The R^2 values trended to a wide range of variables and values, most of which were above 98%. This was an indication of a highly reliable system with extremely accurate results. In the sub-fracture groups, the data also resulted in trends of the terms of proppant dune area with sensitivity to the changing of the experimental parameters. The R^2 values of the data trended mostly above 95% that indicated a reliable system with highly accurate results. In addition, the logical result trends acquired were easily explained with the laws and properties of physics as discussed in Section 4.5.

3.6 Lab Data Collection and Analysis

Before finishing the experiment, a video was recorded to capture the proppant transport, settling rates, and the dune heights. The physical measurements were taken every five minutes. In view of the outcomes, relationships had been created that enhanced the hydraulic fracturing design and provided more insight about the anticipated propped height inside induced fractures.

The first impact was to evaluate the proppant dune development when both perforations were opened using three different fluids, two proppant types, three proppant sizes, nine hybrid proppants, and two injection rates to evaluate transport behaviors. The following evaluations were examined: 1) dune height, 2) the propped area, 3) conductivity, 4) proppant distribution and 5) proppant transport behavior. This study analyzed the height and lateral distance of the formed dune as essential aspects of slickwater hydraulic fracture conductivity stimulation and design optimization. The equilibrium dune height (EDH) was measured using measuring tapes, which measure to 1/16th of an inch attached to the fracture slot sides. The equilibrium dune height for the water system was used to benchmark between various fluid systems. After measuring dune heights from different fluid viscosities, injection rates, proppant types and sizes, the dune area propped fracture (trapezoid) areas were measured by:

$$Area = \left(\frac{(B_1+B_2)}{2}\right) \times H \quad (3.14)$$

Where B_1 and B_2 are the base of the dune (top and bottom) sides and H is the height of the dune. The propped area of the sub-divided dunes of the primary fracture were analyzed by calculating the ratio of each sub-division using the proppant dune area to the total dune area of the primary fracture. The proppant transport behaviors were analyzed by evaluating the particle motions, proppant transport mechanisms, proppant density, proppant size, injection rate and fluid viscosity in the three different fluid systems. Finally, sand samples were removed from different sections of the slot to study the size segregation. Sieves were arranged in order of decreasing size from top to bottom to determine particle size distribution.

For the second impact, there were two perforation locations heights seen in Figure 3.18. One objective was to simulate the proppant transport using different sizes and density of proppant and at different perforation locations: (1) simulation of the base of the wellbore; and (2) simulation of the highest point of the wellbore. Note that both exercises were done with water and not slickwater. The key finding from this analysis was related to the volume of proppant settled, proppant transport mechanisms, dune shape, slurry density, and flow behavior.

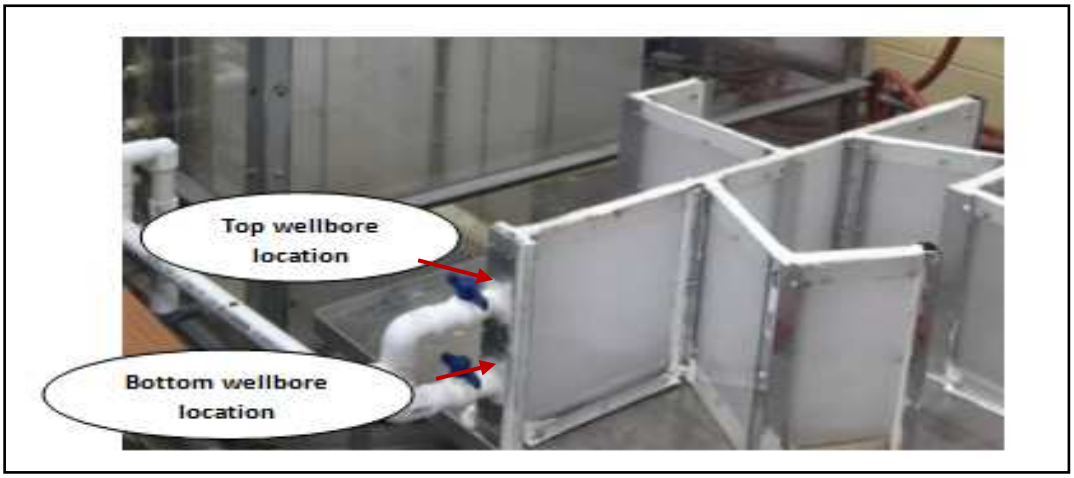

Figure 3.18: Wellbore locations.

3.7 Experimental Workflow

The laboratory work is designed to study and understand the objectives listed in Section 1.2. Figure 3.19 shows all experiments which are necessary to investigate the first impact in Section 4.1- 4.4. Figure 3.20 shows all experiments for the second impact in Section 4.6.

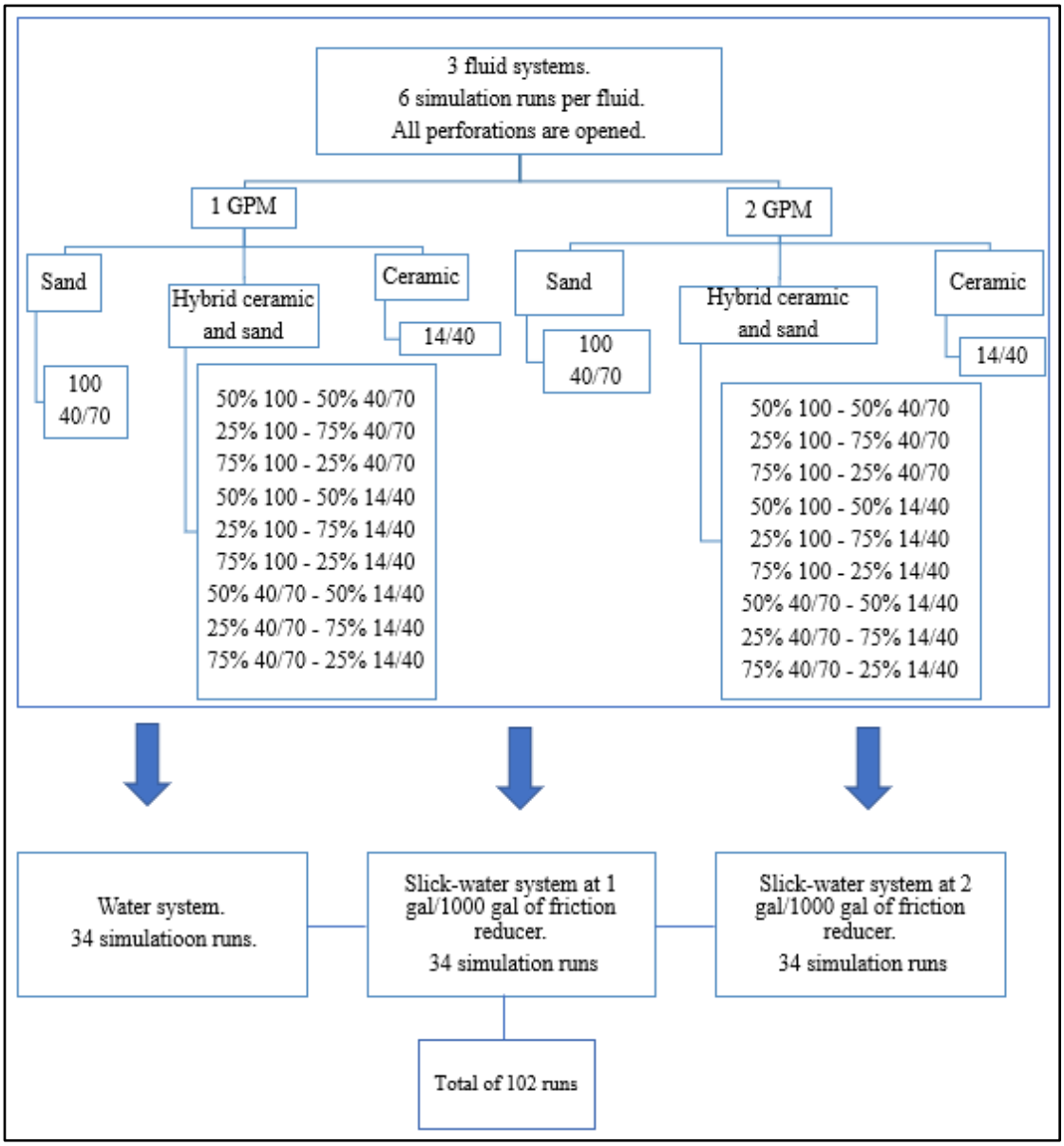

Figure 3.19: First impact workflow.

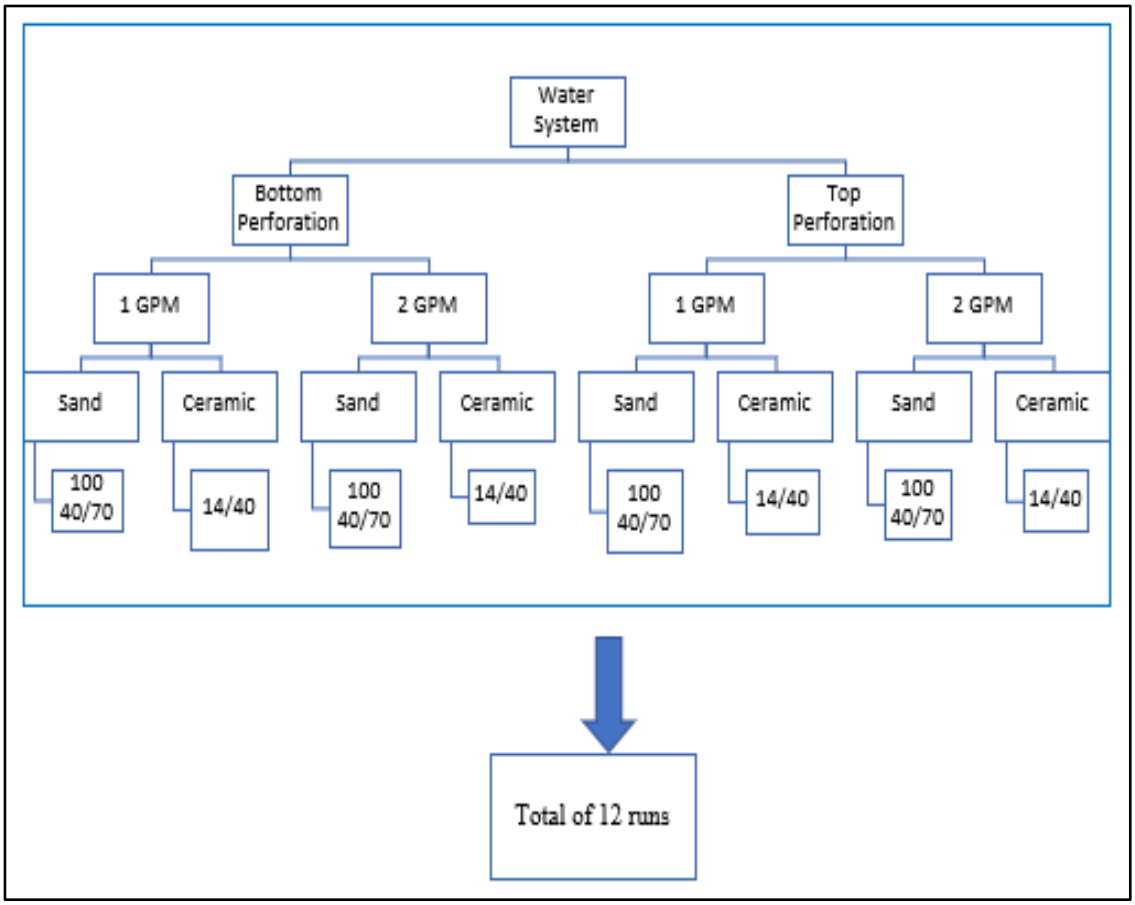

Figure 3.20: Second impact workflow.

CHAPTER 4

EXPERIMENTAL RESULTS

This chapter presents the experimental results that performed using the apparatus described in Chapter 3. Section 4.1 presents experimental results of proppant dune development related to dune height, dune area, and proppant distribution. Section 4.2 evaluates the effects of proppant size and its density, fluid properties, and injection rates on slickwater proppant transport in the main fracture. Section 4.3 extends the discussion to include proppant transport in sub-fracture groups, while Section 4.4 evaluates hybrid proppant mixtures. Section 4.5 shows the experimental data repeatability and error analysis. The results of Section 4.1 to Section 4.4 are synthesized in Section 4.6 for proppant transport mechanisms as a function of perforation location height.

4.1 Slickwater Proppant Dune Development

Observations obtained through this research are: 1) water in and of itself has no viscosity to support and move proppants successfully into fractures and sub-fractures, thus transportability is only through velocity with a large amount of settling occurring; and 2) slickwater with increased viscosity and injection rates reduces settlement and enhances transport capacity in the sub-fracture groups. Displayed in Tables 4.1 – 4.3 are results which show the percentages of the main fracture height that was occupied by the equilibrium proppant dune height (Section 3.4) for two flow rates, two proppant sizes, and three fluid systems.

The proppant dune in the main fracture was observed at two different times: (1) the time at which the dune started developing and (2) the time at which the dune achieved equilibrium height. The experimental results show that the three different fluid systems impact the proppant transport mechanism, dune shape, and the distribution of the proppant inside the main fracture. In the following sub-sections there are measurements of the dune height and length at 2 ppg for 40/70 and 100 mesh. The fluid viscosities of water, slickwater at 1 gal/1000 gal of friction reducer, and slickwater at 2 gal/1000 gal of friction reducer were used to compare the dune length and height in the primary fracture. The subject flow velocities in the fracture were 8 ft/min and 16 ft/min, which were continued until the slurry reached the velocity where it slowed and could no longer be measured. The equilibrium dune height for the water system was used as a benchmark between

various fluid systems. Section 4.1.1 discusses the equilibrium dune height. Section 4.1.2 describes the area. Section 4.1.3 evaluates the transport mechanisms.

4.1.1 Proppant Dune Height

The equilibrium dune height was achieved when the dune maintained a steady state condition and there was no more settling of the proppant. In the water system, the settled proppant achieved equilibrium with a flow rate of 2 gal/min in 25 minutes. With a flow rate of 1 gal/min, equilibrium occurred at 35 minutes. The high dune fill-up percentage of the primary fracture slot showed significant proppant settling and low proppant transport capacity in the water system. When the dune attained equilibrium height in the main slot, the injected proppant was transported inside the sub-fracture groups. Grains moving over the dune were transported via saltation and suspension. The slurry velocity increased because of the decreased flow area which moved smaller grains via suspension. At a low flow rate, increased fluid viscosity with the friction- reduced water was strong enough to affect the proppant dune height. In terms of proppant size, 100 mesh transports better than 40/70 mesh as shown in percentages in Table 4.1– 4.3 using the same fluid, slurry concentration, and injection rate.

Table 4.1: Proppant dune height to fracture height ratio in the main fracture in the water system

Proppant Size	Flow rate (Gal/min)	Dune Height (In.)	Proppant Dune Height to Fracture Height Ratio (%)
100 mesh	1	10.3	85.83
100 mesh	2	9.2	76.66
40/70 mesh	1	11.4	95
40/70 mesh	2	10.5	87.5

Table 4.2: Proppant dune height to fracture height ratio in the main fracture slickwater at 1 gal/1000 gal of friction reducer

Proppant Size	Flow rate (Gal/min)	Dune Height (In.)	Proppant Dune Height to Fracture Height Ratio (%)
100 mesh	1	7.3	60.8
100 mesh	2	6.8	56.6
40/70 mesh	1	8.5	70.83
40/70 mesh	2	7.4	61.67

Table 4.3: Proppant dune height to fracture height ratio in the main fracture slickwater at 2 gal/1000 gal of friction reducer

Proppant Size	Flow rate (Gal/min)	Dune Height (In.)	Proppant Dune Height to Fracture Height Ratio (%)
100 mesh	1	5.6	46.66
100 mesh	2	4.3	35.83
40/70 mesh	1	6.8	56.66
40/70 mesh	2	5.7	47.5

4.1.2 Proppant Dune Area

Estimating the propped fracture area is essential for hydraulic fracture conductivity measurement and design. The dune heights measured from the different fluid types and proppant sizes are used to estimate the developed dune area or propped fracture area (Section 3.6). In all cases, the lab results show that the proppant filled up the lateral distance. In the water system, the majority of the proppant settled in the primary fracture and the remaining entered the sub-fractures. The lab results showed in the water system that 40/70 mesh in the main fracture has a dune height higher by 1.1 inch (13.5%) at 1 gal/min and 1.3 inch (16.2%) at 2 gal/min than the 100 mesh. The lab results with slickwater at different concentrations of friction reducer resulted in less proppant settling in the primary fracture with more proppant traveling into the sub-fracture groups. For example, the proppant dune area for the water system at 1 gal/min for 100 mesh is 263.4 $inch^2$; using slickwater at 1 gal/1000 gal of friction reducer, the proppant dune area decreased to 148.8 $inch^2$, the result of reduction is around 43.5%. Tables 4.4 – 4.6 show the calculated area for the three different fluid systems, two flow rates, and two proppant sizes. The results are also displayed in Figures 4.1– 4.4 which show the percentages and shapes of dune area for the two flow rates, two proppant sizes, and three fluid systems.

Table 4.4: Calculated proppant dune area for water system

Characteristics	100 Mesh				40/70 Mesh			
	A	B	C	Total	A	B	C	Total
Area (in^2) at 1 gal/min	123.6	97.8	42	263.4	136.8	112.2	55.8	304.8
Area (in^2) at 2 gal/min	110.4	82.8	33.6	226.8	126	98.4	46.2	270.6

Table 4.5: Calculated area for slickwater at 1 gal/1000 gal of friction reducer

Characteristics	100 Mesh				40/70 Mesh			
	A	B	C	Total	A	B	C	Total
Area (in2) at 1 gal/min	67.2	60	21.6	148.8	85.8	76.2	33.3	195
Area (in2) at 2 gal/min	59.4	56.4	20.1	135.9	73.8	67.2	28.2	169.2

Table 4.6: Calculated area for slickwater at 2 gal/1000 gal of friction reducer

Characteristics	100 Mesh				40/70 Mesh			
	A	B	C	Total	A	B	C	Total
Area (in^2) at 1 gal/min	52.8	46.2	15.6	114.6	66.6	60.0	25.8	152.4
Area (in^2) at 2 gal/min	43.2	35.4	10.8	89.4	52.8	48.6	19.2	120.6

The propped area of the sub-divided dunes of the primary fracture was analyzed by calculating the ratio of each sub-division's dune area to the total dune area of the primary fracture. The water system has the largest dune propped height in sub-division A (main slot). For example, the sub-division's dune area for section A for the water system at 1 gal/min for 100 mesh is 123.6 $inch^2$, using slickwater at 1 gal/1000 gal of friction reducer, the proppant dune area decreased to 67.2 $inch^2$, a reduction of around 45.6%. Increasing the flow rate also resulted in a reduction of the propped fracture area. For example, the proppant dune area for the water system at 1 gal/min for 100 mesh is 263.4 $inch^2$ and at 2 gal/min is 226.8 $inch^2$, a reduction of 14%. Increasing the fluid viscosity decreased the propped area in section A and increased the propped area in sections B and C of the main fracture. Although section C had the longest propped length, its propped area to the total dune ratio was small. This showed that long propped length does not lead to high propped area. The results showed 40/70 mesh settled at the beginning of the primary fracture and 100 mesh traveled further into the sub-fracture groups. In the water system, the highest dune was at the beginning of the primary fracture in section A, while in the slickwater system, the highest dune was in section B, the middle of the main fracture. The above stated result was attributed to the fluid viscosity and carrying capacity of slickwater. Slickwater distributed the proppants in the primary fracture and transported them into the sub-fractures. Slickwater at 1 gal/1000 gal of friction reducer and slickwater at 2 gal/1000 gal of friction reducer had similar dune shapes and less proppant inside the primary fracture.

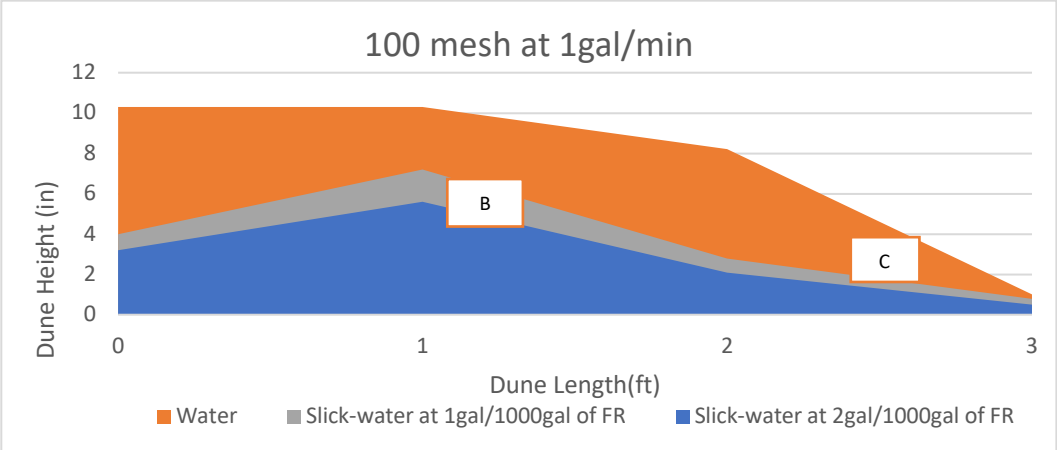

Figure 4.1: Dune area of 100 mesh at 1 gal/min using water system, slickwater at 1 gal/1000 gal and 2 gal/1000 gal of friction reducer.

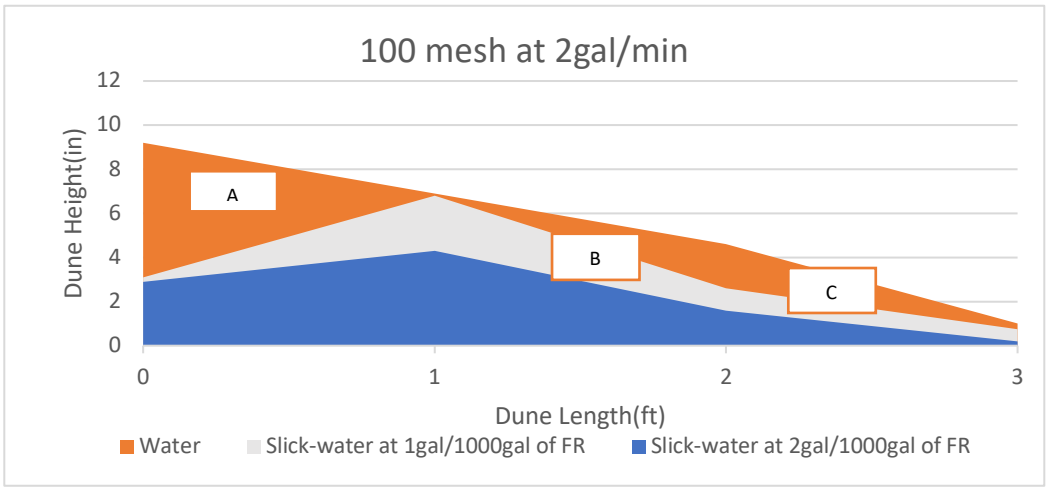

Figure 4.2: Dune area of 100 mesh at 2 gal/min using water system, slickwater at 1 gal/1000 gal and 2 gal/1000 gal of friction reducer.

For slickwater at 1 gal/ 1000 gal of friction reducer, the reductions in the propped area were 8.33% for 100 mesh, and 3.13% for 40/70 mesh. For slickwater at 2 gal/ 1000 gal of friction reducer, the reductions of propped area were 2.32% for 100 mesh and 11% for 40/70 mesh.

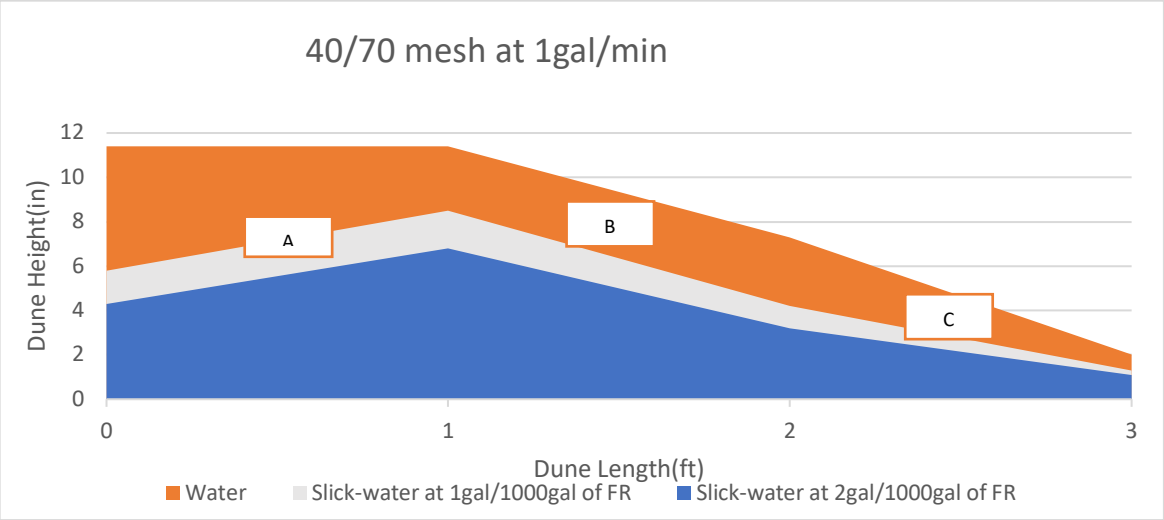

Figure 4.3: Dune area of 40/70 mesh at 1 gal/min using water system, slickwater at 1 gal/1000 gal and 2 gal/1000 gal of friction reducer.

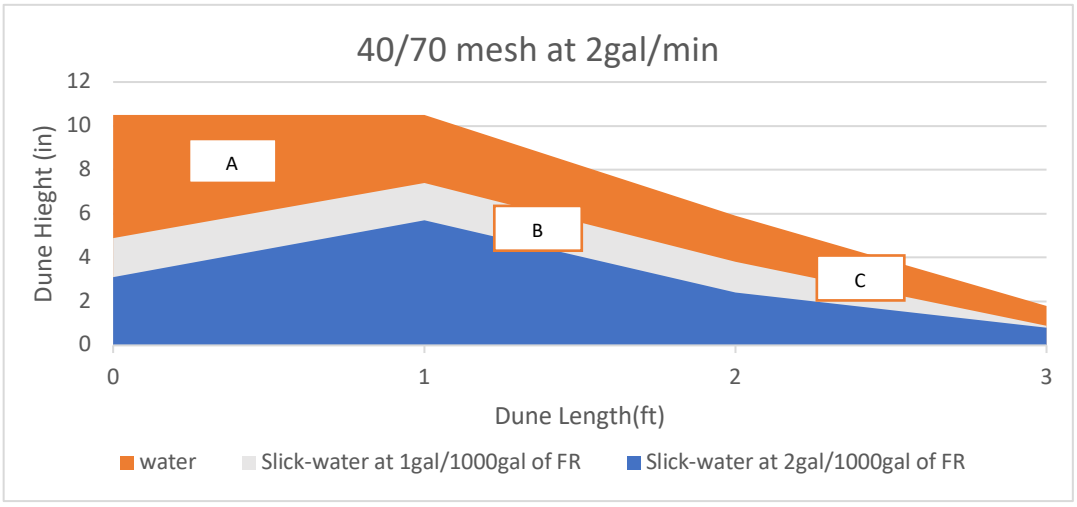

Figure 4.4: Dune area of 40/70 mesh at 2 gal/min using water system, slickwater at 1 gal/1000 gal and 2 gal/1000 gal of friction reducer.

4.1.3 Proppant Transport Behavior

The lab results showed that larger particles settled near the wellbore in the primary fracture when using the water system. While using slickwater, larger particles were transported to the middle of the primary fracture. Proppant in the fracture travels as a suspended load and/or bed load depending on the characteristics of the particle, velocity profile, bed-shear stress and shear velocity. In all experiments, the proppant moved in three ways: traction, saltation, and suspension.

Increased viscosity of the fluids improved the transportation of the proppant. Slickwater is more viscous than water and lifted the particles into suspension at the two concentrations of friction reducer. The increased viscosity of slickwater increased the shear velocity to the point at which it exceeded the settling velocity of the particle and transported more proppant. In regard to the 14/40 mesh, there was no settlement during the experiment with water. The proppants were collected at the end of each experiment from the four fractures groups and analyzed to get weight percentages of the proppant that entered each fracture group. This resulted in the finding that the water viscosity yielded minimal proppant in the sub-fracture groups as shown in Tables 4.7-4.9. Doubling the flow rates increased the proppant in all sub-fracture groups for the three fluid types.

Table 4.7: Proppant weight percentage of 40/70 mesh in water system at 1 gal/min, and 2 gal/min for main slot

Velocities	**100 Mesh**				**40/70 Mesh**			
	Main	**A**	**B**	**C**	**Main**	**A**	**B**	**C**
1 gal/min	71%	5.50%	19%	4.50%	80%	3.50%	15%	1.50%
2 gal/min	64%	8.00%	21%	7.00%	73%	6.20%	18%	2.80%

Table 4.8: Proppant weight percentage of 40/70 mesh in slickwater at 1 gal/1000 gal of friction reducer at 1 gal/min, and 2 gal/min main slot

Velocities	**100 Mesh**				**40/70 Mesh**			
	Main	**A**	**B**	**C**	**Main**	**A**	**B**	**C**
1 gal/min	50%	15%	25%	10%	66%	8.00%	20%	6.00%
2 gal/min	42%	18%	28%	12%	55%	14%	25%	10%

Table 4.9: Proppant weight percentage of 40/70 mesh in slickwater at 2 gal/1000 gal of friction reducer at 1 gal/min, and 2 gal/min main slot

Velocities	**100 Mesh**				**40/70 Mesh**			
	Main	**A**	**B**	**C**	**Main**	**A**	**B**	**C**
1 gal/min	38%	17%	30%	15%	53%	14%	23%	10%
2 gal/min	22%	23%	34%	21%	37%	20%	30%	13%

One of the purposes of this study was to investigate whether slickwater at different concentrations of friction reducer has the ability to transport proppants of all sizes to the sub-fracture groups. To begin, a simple base system of water was used so comparisons between water

and slickwater could be made. The sieve analysis for the main fracture showed that doubling the flow rate for all studied mesh sizes results in the reduction of the larger sizes of proppant settling in the main fracture. Tables 4.10 and 4.11 show the percentages for the main fracture using different proppant sizes. Using slickwater at 1 gal/1000 gal of friction reducer, the sieve analysis for the main fracture compared to the water system showed that the 40/70 and 100 mesh resulted in the reduction of settled larger proppant due to the addition of viscosity as shown in Table 4.12. Doubling the flow rate for 40/70 and 100 mesh, results in the reduction of the larger sizes of proppant settled in the main fracture as shown in Table 4.13. The same comparison for slickwater at 2 gal/1000 gal of friction reducer is shown in Tables 4.14 and 4.15.

Table 4.10: Sieve analysis for main fracture using water system for 40/70 mesh and 100 mesh.

Size	Sieve # 40	Sieve # 45	Sieve # 50	Sieve # 60	Sieve # 70	Sieve # 100
40/70	4.0%	12.0%	18.0%	19.0%	27.0%	20.0%
100	-	28.0%	35.0%	6.0%	20.0%	11.0%

Table 4.11: Sieve analysis for main fracture using water system for 14/40 mesh.

Size	Sieve # 18	Sieve # 20	Sieve # 25	Sieve # 30	Sieve # 35
14/40	25.0%	7.0%	10.0%	20.00%	38.0%

Table 4.12: Sieve analysis for main fracture using slickwater system with 1 gal/1000 gal of friction reducer for 40/70 mesh and 100 mesh at 1 gal/min.

Size	Sieve # 40	Sieve # 45	Sieve # 50	Sieve # 60	Sieve # 70	Sieve # 100
40/70	2.5%	9.0%	22.0%	21.5%	29.0%	16.0%
100	-	25.0%	32.0%	8.0%	22.5%	12.5%

Table 4.13: Sieve analysis for main fracture using slickwater system with 1 gal/1000 gal of friction reducer for 40/70 mesh and 100 mesh at 2 gal/min.

Size	Sieve # 40	Sieve # 45	Sieve # 50	Sieve # 60	Sieve # 70	Sieve # 100
40/70	1.75%	7.0%	18.25%	23.0%	31.0%	19.0%
100	-	23.0%	29.0%	11.0%	24.0%	13.0%

Table 4.14: Sieve analysis for main fracture using slickwater system with 2 gal/1000 gal of friction reducer for 40/70 mesh and 100 mesh at 1 gal/min.

Size	Sieve # 40	Sieve # 45	Sieve # 50	Sieve # 60	Sieve # 70	Sieve # 100
40/70	2.0%	8.5%	20.0%	23.0%	32.0%	14.5%
100	-	22.0%	30.0%	12.0%	25.0%	11.0%

Table 4.15: Sieve analysis for main fracture using slickwater system with 2 gal/1000 gal of friction reducer for 40/70 mesh and 100 mesh at 2 gal/min.

Size	Sieve # 40	Sieve # 45	Sieve # 50	Sieve # 60	Sieve # 70	Sieve # 100
40/70	1.25%	7.0%	22.75%	25.0%	34.0%	10.0%
100	-	19.0%	31.5%	15.0%	26.5%	8.0%

4.2 The Effect of Key Parameters on Slickwater Proppant Transport

Slickwater proppant transport relies on factors such as the slurry injection rates, proppant diameter, carrying fluid density, and viscosity. These factors and their impacts on slickwater hydraulic fracturing are described in Sections 4.2.1 - 4.2.4.

4.2.1 Proppant Diameter

The diameter of the proppant affects the settling rate and transportability of the proppant in slickwater. Heavier proppants are harder to lift, so they settle readily in the main slot. The larger the diameter of the proppant results in higher proppant ability to interact with the walls of the fracture. Smaller proppant sizes are easier to move because of their smaller grain weights. A water flow rate of 1 gal/min at 2 ppg showed that the dune height increased from 86.85% to 95% when the average median diameter of the proppant was doubled from 0.0074 inch (100 mesh) to 0.015 inch (40/70 mesh). This shows that doubling the proppant diameter increases settling and hinders the slickwater proppant transport. Increasing the velocity from 1 gal/min to 2 gal/min produced a decrease of 14% equilibrium dune height between 100 mesh and 40/70 mesh.

A flow rate of 1 gal/min using 1 gal/1000 gal of friction reducer at 2 ppg showed that the dune height increased from 60.8% to 70.83% when the average median diameter of proppants was doubled from 0.0074 inch (100 mesh) to 0.015 inch (40/70 mesh). Increasing the velocity from 1 gal/min to 2 gal/min showed a change of 8.95% dune height between 100 mesh and 40/70 mesh.

A flow rate of 1 gal/min using 2 gal/1000 gal of friction reducer at 2 ppg showed that the dune height increased from 46.66% to 56.66% when the average diameter of the proppant was increased from 0.0074 inch (100 mesh) to 0.015 inch (40/70 mesh). Increasing the velocity from 1 gal/min to 2 gal/min shows a change of 32.6% of the dune height between the 100 mesh and the 40/70 mesh. Figure 4.5 provides a summary of the dune height developments for the various tested systems.

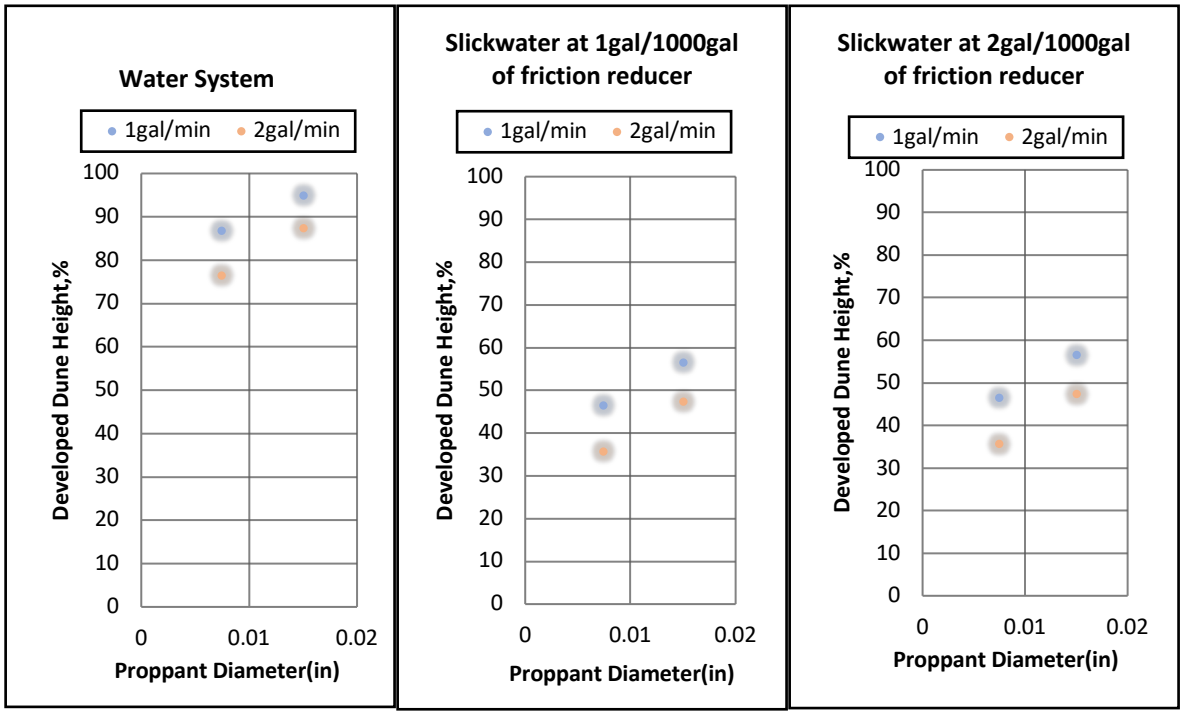

Figure 4.5: Dune height development versus proppant diameter for the water system, for slickwater at 1 gal/1000 gal of friction reducer, and for slickwater at 2 gal/1000 gal of friction reducer.

4.2.2 Carrying Fluid Densities

The density of the carrying fluid is a very crucial factor in the proppant transport process. The density helps determine the buoyancy forces that are acting on the proppant (Equation 3.11). The gravity pulls the proppant down, while the buoyancy works to keep the proppant suspended in the fluid. If buoyancy is equal to gravity, then the particle stays in suspended motion. In this study, water and slickwater at different concentrations of friction reducer were used. The density of water, slickwater at 1 gal/1000 gal of friction reducer, and at 2 gal/1000 gal of friction reducer

are 8.35 lb/gal, 11.8 lb/gal, and 14.8 lb/gal, respectively. Figure 4.6 shows that as the density of the fluid increases, the dune height reduces, and the proppant is transported further.

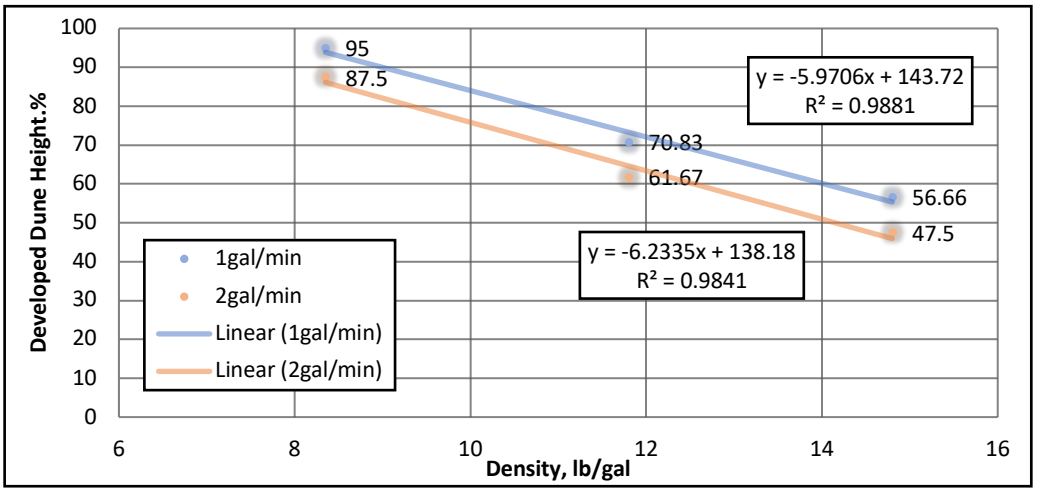

Figure 4.6: Linear relation between density of the fluids and the developed dune height for 40/70 mesh.

4.2.3 Injection Rate

Increasing the injection rate increases the transport of proppant and decreases proppant settling. In this section, the effect of slurry velocity on the developed dune height and length is evaluated over two injection rates. The injection rate relates to the velocity at which the slurry is pumped into the fracture. The developed dune height is used to quantify the erosional effect of increasing the velocity and the settling effect with reduced velocity.

4.2.3.1 40/70 Mesh

The slurry rate was increased from 1 gal/min to 2 gal/min to study the effect on the dune area using three different fluids. For 40/70 mesh, increasing the flow rate from 1 gal/min to 2 gal/min decreased the dune height from 95% to 87.5% in the water system, 70.83% to 61.67% in slickwater at 1 gal/1000 gal, and 56.66% to 47.5% in slickwater at 2 gal/1000 gal of friction reducer, respectively. The increase in the flow rate is 50% and reflects 7.89%, 12.93%, and 16.17% decreases in dune height of the three systems, respectively. Using water, the equilibrium dune height is still quite high after the rate was doubled showing the high settling tendency of 40/70 mesh in water. See Figure 4.7and Figure 4.8 for results of this analysis.

Figure 4.7 shows the power law equation for 40/70 mesh at two flow rates for all three fluid systems. The higher friction experienced by the bed allow for a linear change in the velocities with an increase in slurry velocity. The slurry velocity loses power to reduce the dune height at high velocity and creates a non-linear trend with a developed dune height. Another observation is that slurry transport power increases with increased fluid viscosity, which can be seen by comparing the linear equation slopes at different fluids. Figure 4.7 shows that 40/70 mesh has a slope of -0.119 using water and increases in the negative direction to -0.2 and -0.254 for slickwater at 1 gal/1000 gal and 2 gal/1000 gal of friction reducer, respectively. This negative increase indicates an increasing transport power with more viscosity.

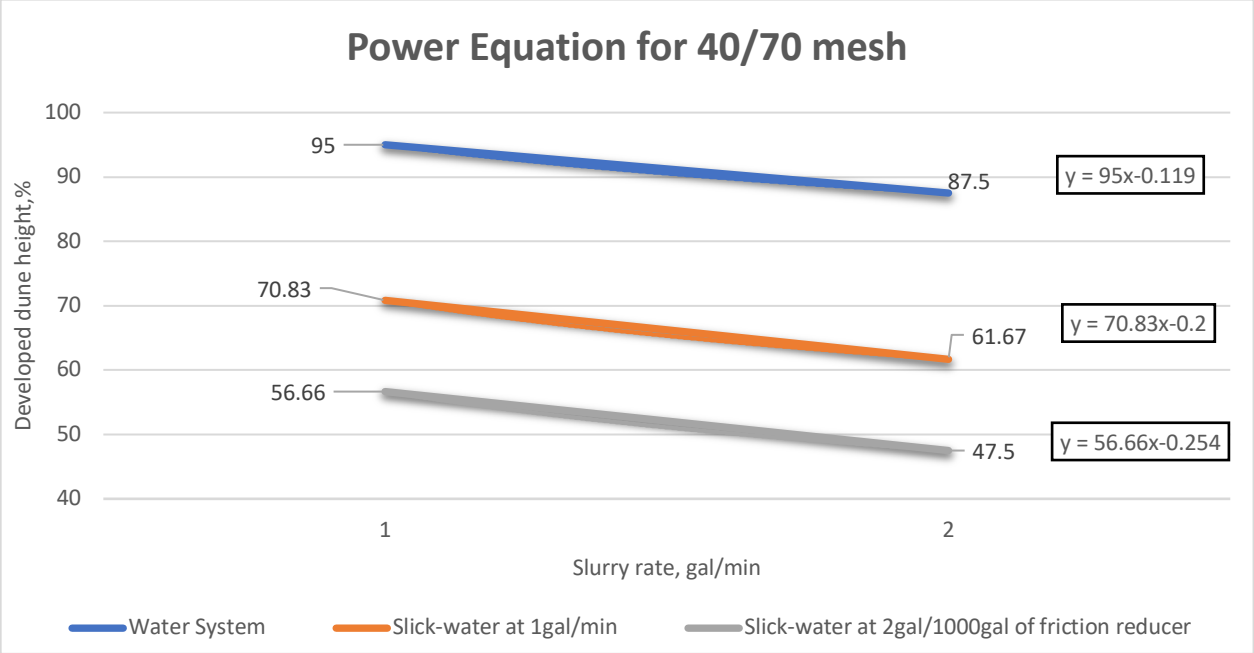

Figure 4.7: Power law equation for 40/70 mesh in the three different fluid systems.

4.2.3.2 100 Mesh

The effect of flow rate on the proppant transport and proppant dune height was evaluated using 100 mesh as shown in Figure 4.8. The average diameter of 100 mesh is 49.3% less than the diameter of 40/70 mesh. For 100 mesh, increasing the velocity from 1 gal/min to 2 gal/min decreased the dune height from 86.85% to 76.66% in the water system, 60.8% to 56.6% in slickwater at 1 gal/1000 gal, and 46.66% to 35.83% in slickwater at 2 gal/1000 gal of friction

reducer, respectively. The increase in the velocity is 50% and reflects 11.73%, 6.91%, and 23.2% decreases in dune height of the three systems, respectively. The linear relationship between velocity and dune height shows that 100 mesh sand did not lose erosional power with increased velocity. In Figure 4.8the slope decreases from -10.19 to -4.2 and then increased to -10.83.

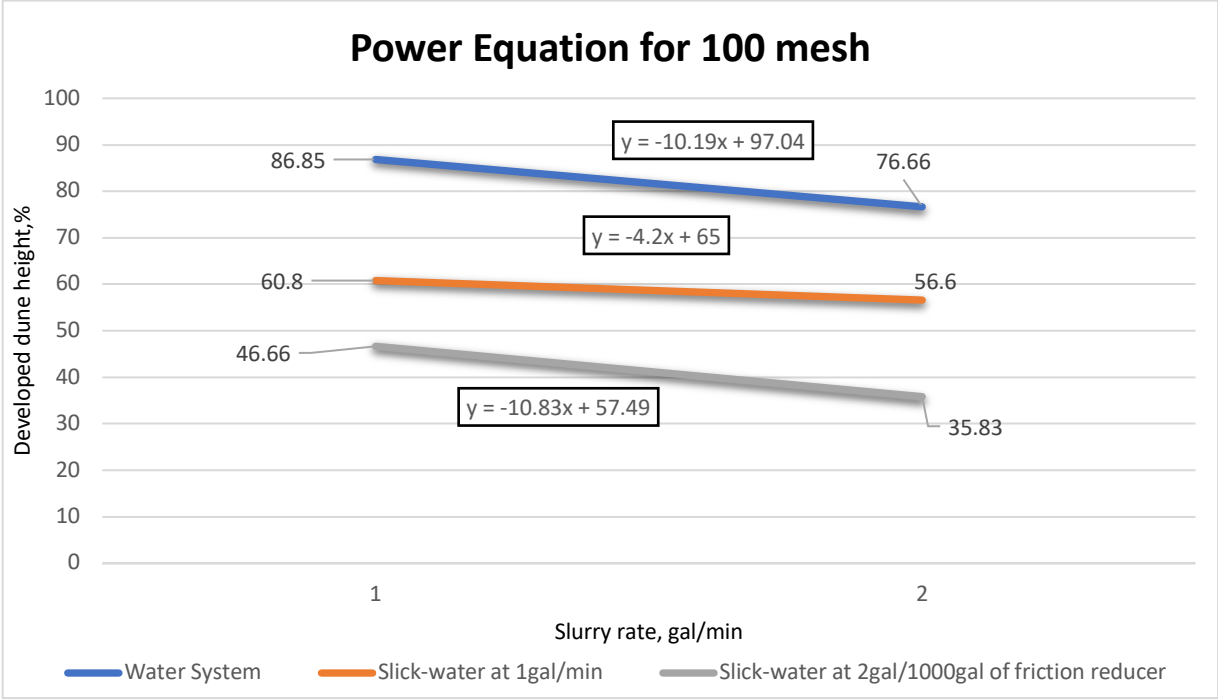

Figure 4.8: Power law equation for 100 mesh using the three fluid systems.

4.2.4 Fluid Viscosity

Viscous fluid has higher drag forces that can suspend proppant and therefore results in more proppant transport. Table 4.16 shows that apparent viscosity slickwater reduces with increases in flow rate. These values were calculated using the formula for apparent viscosity shown in Equations 3.6 and 3.7.

Table 4.16: The viscosity of the various carry fluids

Flowrate	**Water System**	**Slickwater at 1 gal/1000 gal**	**Slickwater at 2 gal/1000 gal**
1 gal/min	0.0091 cp	0.401cp	0.441 cp
2 gal/min	0.0091 cp	0.265 cp	0.274 cp

4.2.4.1 40/70 Mesh

The fluid viscosity effect was first evaluated using 40/70 mesh. The developed dune heights in water for 1 gal/min with 40/70 mesh, slickwater at 1 gal/1000 gal, and 2 gal/1000 gal of friction reducer are 95%, 70.83%, and 56.66%, respectively. These results showed a change of 20% when the amount of friction reducer is doubled. At 2 gal/min, the heights were 87.50%, 61.67%, and 47.5% lower, respectively. The results reflected a change of 22.98% when the amount of friction reducer is doubled. It is observed that at 2 gal/min, the reduction in proppant dune height is 3% higher than at 1 gal/min, which enhanced the transportability of proppant into the sub-fracture groups.

In Figure 4.9, the relationship between the dune height and viscosity is displayed. The plotted data show a linear relationship between the dune height and viscosity for the three different fluid systems at two different flow rates. The 40/70 mesh does not lose its erosional power with increasing viscosity. The friction effect by the fracture walls is reduced by the viscosity of slickwater and allows for more proppant transport. The coefficients of determination R^2 are more than 0.97. The slopes are negatively increased (-19.17 and -20**)** with an increase in the flow rate that indicates a higher transport mechanism.

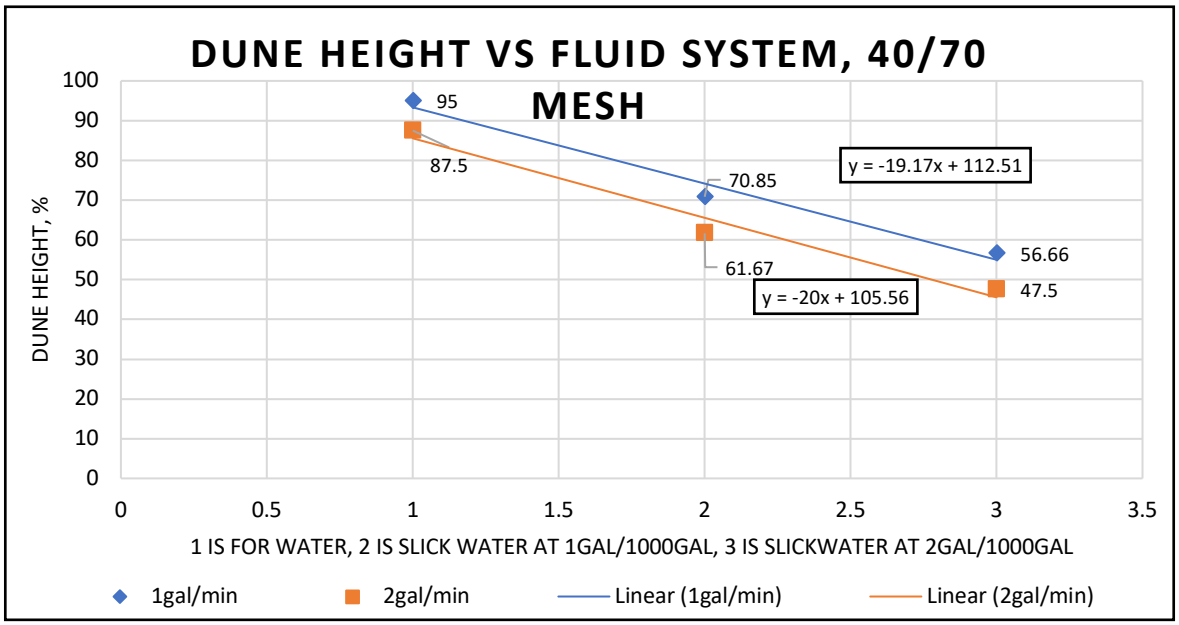

Figure 4.9: Linear Equation for 40/70 mesh using the three fluid systems at the two flow rates.

4.2.4.2 100 Mesh

The fluid viscosity effect was also evaluated using 100 mesh. The developed dune height in water for 1 gal/min with 100 mesh, slickwater at 1 gal/1000 gal, and 2 gal/1000 gal of friction reducer were 86.85%, 60.8%, and 46.66%, respectively. This reflected a change of 23% when the amount of friction reducer was doubled. At 2 gal/min the heights were 76.66%, 56.6%, and 35.83%, respectively: this reflected a change of 36% when the amount of friction reducer was doubled. It is observed that at 2 gal/min, the reduction in proppant dune height was 13% higher than at 1 gal/min.

In Figure 4.10, the relationship between the dune height and the viscosity is shown. The plotted data shows a linear relationship between the dune height and viscosity for three different fluid systems at two different flow rates. The 100 mesh did not lose its erosional power with increased viscosity. With an increased flow rate, the slopes were negatively increased (-20.10 and -20.42), and a higher transport mechanism is shown.

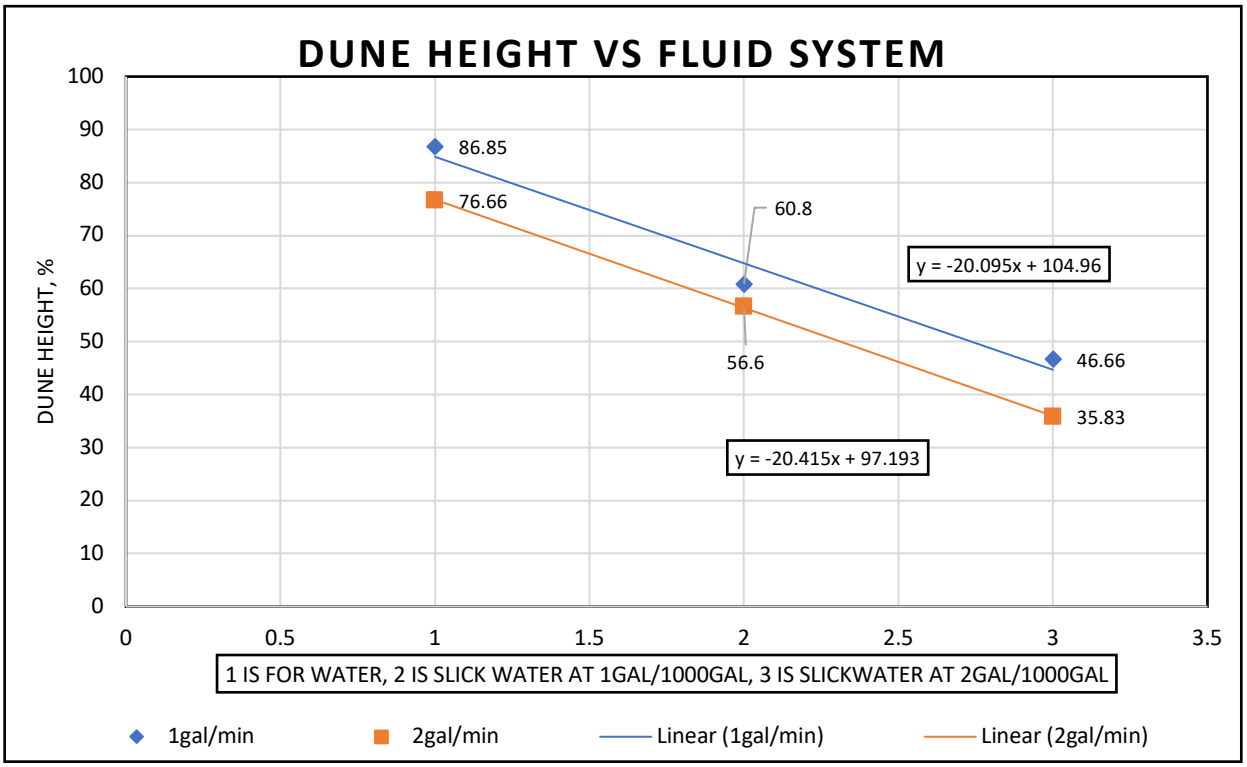

Figure 4.10: Linear equation for 100 mesh using the three fluid systems at the two flow rates.

4.3 Slickwater Proppant Transport in Secondary, Tertiary, and Quaternary Fractures

In this section, the developed dune areas and proppant reach times in the fracture networks are assessed and compared. This evaluation provides quantitative assessments of slickwater proppant transport in subsidiary fractures. The fracture network propped heights are evaluated to understand the sub-fractures proppant transport relative to the main fracture.

4.3.1 Developed Dune Height

The effects of key parameters such as proppant average diameter, slurry rates, and fluid viscosity on the sub-fractures were studied and are discussed in Sections 4.2.1- 4.2.4. Sections 4.3.1.1 - 4.3.1.3 show the impacts of these parameters on proppant dune formation in the subsidiary fractures.

4.3.1.1 Sub-fracture A

Sub-fracture A is placed at a 90-degree angle to the main fracture and is located 1.5 ft from the slot entry as shown in Figure 3.8. It is 0.1 inch-wide, 1.5 ft long and 1 ft high. 100 mesh and 40/70 mesh at 1 gal/min were used for the three different viscosity systems. The highest dune was produced when using slickwater with friction reducer at 2 gal/1000 gal and occurred at the beginning of the fracture with a 6 inch propped height for 100 mesh and a 4 inch propped height for 40/70 mesh. When 100 mesh was used, the amount of proppant at the end of the fracture increased with slickwater from 1 inch to 4.5 inch, see Figure 4.11. When running experiments with 40/70 mesh, there was a significant difference between the amount of the proppant settled at the beginning and at the end of the fractures from 0.3 inch to 2 inch. This was because 40/70 mesh had a bigger diameter and the proppant was less readily transported then when the 100 mesh was used. Figures 4.11 and 4.12 show more dune development using the flow rate of 2 gals/min. Also, using slickwater at 1 gal/1000 gal of friction reducer, showed that twice the amount was transported than by water only. For sub-fracture group A at 2 gal/min, the sand dune is 5.5 inches at the beginning of the fracture for 40/70 mesh, while 100 mesh is 9 inches. This shows that 100 mesh at 2 gal/min is found to have the best distribution of proppant for the tested systems.

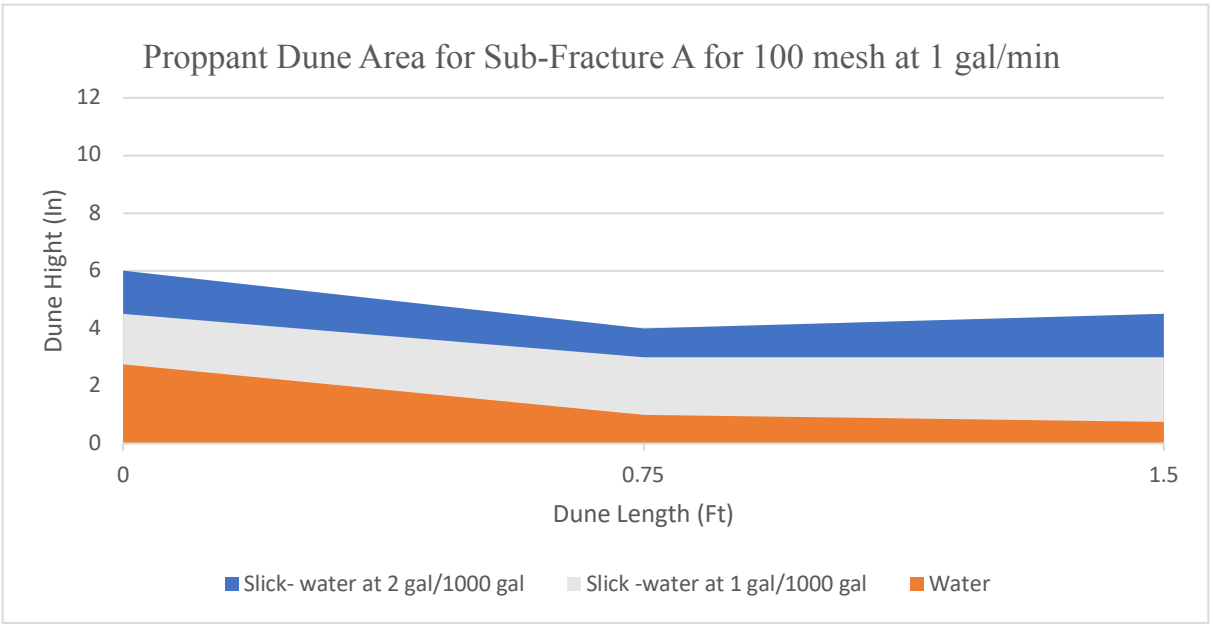

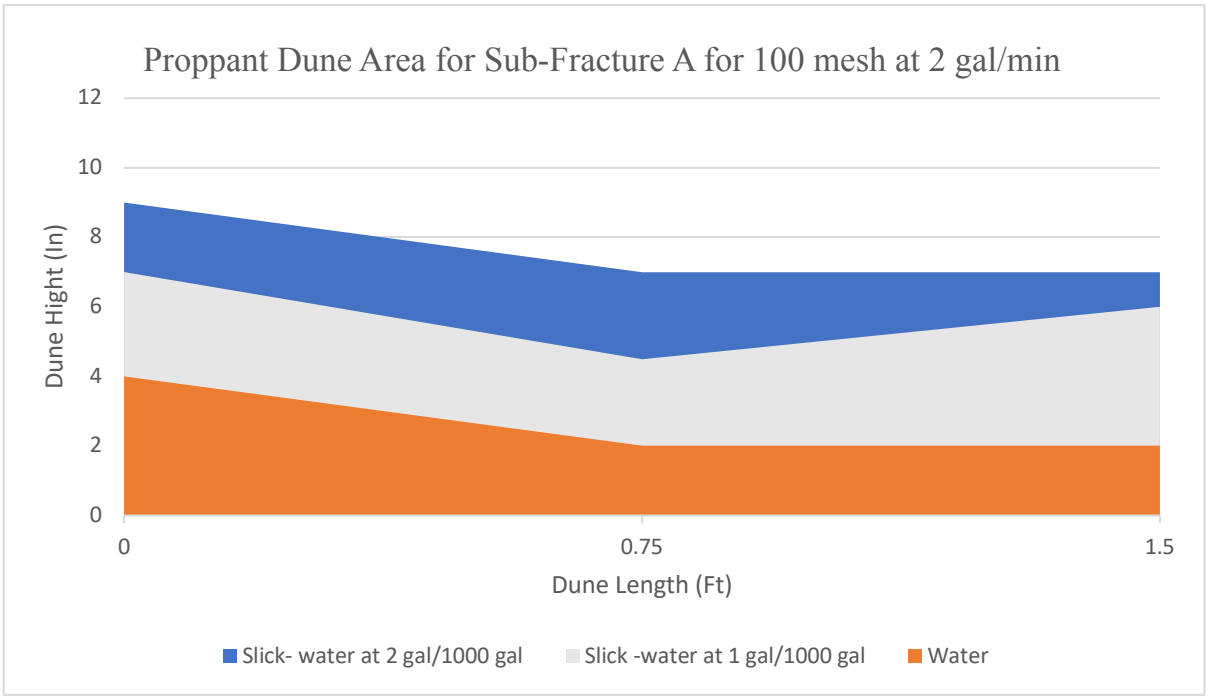

Figure 4.11: The top figure is the proppant dune area of sub-fracture A for 100 mesh at 1 gal/min in 2D. The bottom figure is the proppant dune area of sub-fracture A for 100 mesh at 2 gal/min in 2D.

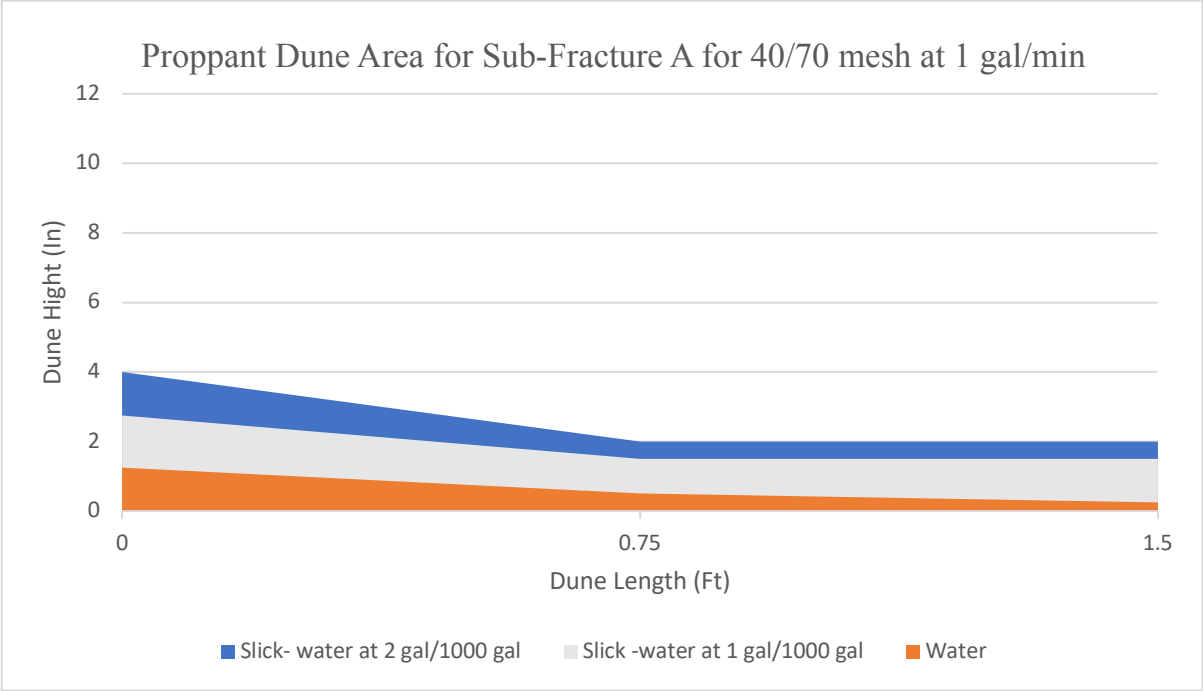

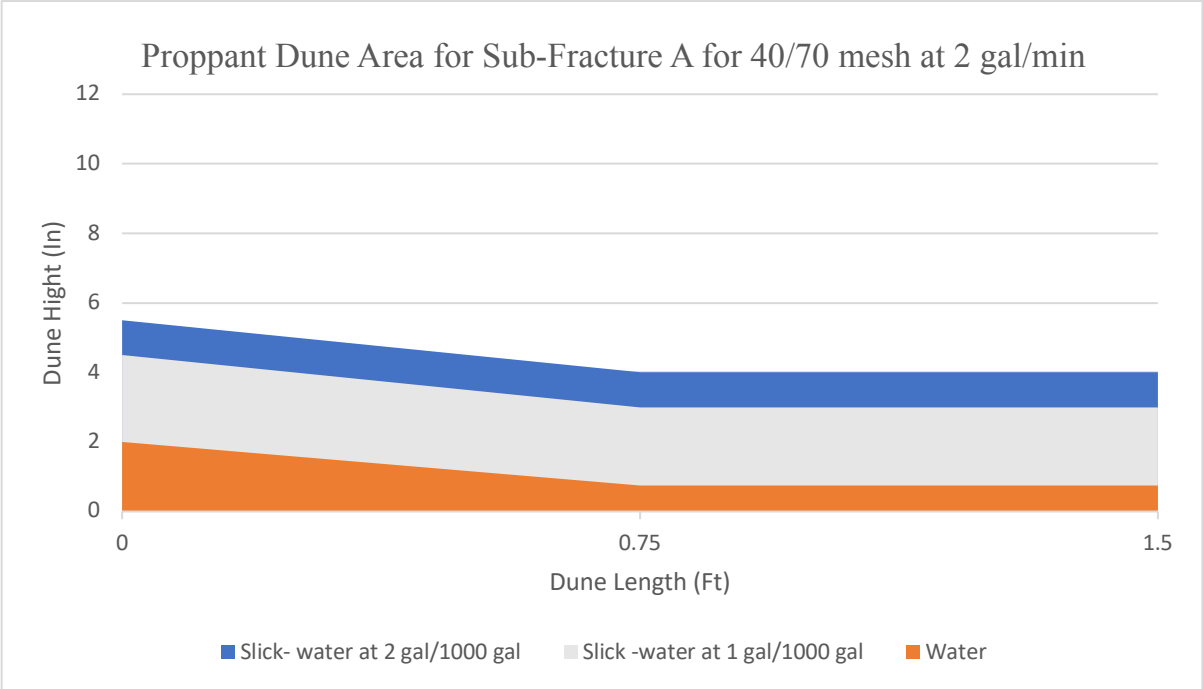

Figure 4.12: The top figure is the proppant dune area of sub-fracture A for 40/70 mesh at 1 gal/min in 2D. The bottom figure is the proppant dune area of sub-fracture A for 40/70 mesh at 2 gal/min in 2D.

One of the main purposes of this study was to investigate whether slickwater at different concentrations of friction reducer has the ability to transport all proppants both large and small to the sub-fracture groups. Using the water system, sieve analyses for the sub-fracture group A showed that doubling the flow rate for 40/70, 100 and 14/40 mesh resulted in a reduction of the larger sizes of proppant settled in the sub-fracture group A. Tables 4.17 and 4.18 show the resulting percentages for the sub-fracture group A using different proppant sizes. Using slickwater at 1 gal/1000 gal of friction reducer, the sieve analysis for the sub-fracture group A compared to the water system showed that using the 40/70 and 100 mesh resulted in incremental transport of the settled larger proppant in the sub-fracture group A, as shown in Table 4.19. Doubling the flow rate for 40/70 and 100 mesh resulted in the increments of the larger sizes of proppant settled in the sub-fracture group A as shown in Table 4.20. The same analysis was used for slickwater at 2 gal/1000 gal of friction reducer as shown in Tables 4.21 and 4.22.

Table 4.17: Sieve analysis for sub-fracture group A using water system for 40/70 mesh and 100 mesh

Size	**Sieve # 40**	**Sieve # 45**	**Sieve # 50**	**Sieve # 60**	**Sieve # 70**	**Sieve # 100**
40/70	10.0%	15.0%	15.00%	20.0%	26.0%	14.00%
100	-	18.0%	29.00%	17.0%	12.00%	24.0%

Table 4.18: Sieve analysis for sub-fracture group A using water system for 14/40 mesh

Size	**Sieve # 18**	**Sieve # 20**	**Sieve # 25**	**Sieve # 30**	**Sieve # 35**
14/40	14%	24%	18.0%	30.0%	14.0%

Table 4.19: Sieve analysis for sub-fracture group A using slickwater system with 1 gal/1000 gal of friction reducer for 40/70 mesh and 100 mesh at 1 gal/min

Size	**Sieve # 40**	**Sieve # 45**	**Sieve # 50**	**Sieve # 60**	**Sieve # 70**	**Sieve # 100**
40/70	13.0%	7.0%	20.0%	23.0%	27.0%	10.0%
100	-	20.0%	31.5%	19.5%	13.0%	16.0%

Table 4.20: Sieve analysis for sub-fracture group A using slickwater system with 1 gal/1000 gal of friction reducer for 40/70 mesh and 100 mesh at 2 gal/min

Size	Sieve # 40	Sieve # 45	Sieve # 50	Sieve # 60	Sieve # 70	Sieve # 100
40/70	14.0%	8.5%	21.5%	24.0%	28.0%	4.0%
100	-	23.0%	33.0%	20.0%	14.0%	10.0%

Table 4.21: Sieve analysis for sub-fracture group A using slickwater system with 2 gal/1000 gal of friction reducer for 40/70 mesh and 100 mesh at 1 gal/min

Size	Sieve # 40	Sieve # 45	Sieve # 50	Sieve # 60	Sieve # 70	Sieve # 100
40/70	15.0%	8.0%	22.0%	24.5%	28.5%	2.0%
100	-	22.0%	33.0%	21.0%	15.0%	9.0%

Table 4.22: Sieve analysis for sub-fracture group A using slickwater system with 2 gal/1000 gal of friction reducer for 40/70 mesh and 100 mesh at 2 gal/min

Size	Sieve # 40	Sieve # 45	Sieve # 50	Sieve # 60	Sieve # 70	Sieve # 100
40/70	17.0%	9.0%	23.0%	25.0%	24.25%	1.75%
100	-	23.0%	35.0%	23.5%	13.5%	5.0%

4.3.1.2 Sub-fracture B

Sub-fracture B is placed at an angle of 60 degrees from the main fracture and is located 1 ft from the main slot entry as shown in Figure 3.8. It is 1.25 ft long, 0.1 inch-wide and 1 ft high. Comparing sub-fractures A and B from the results of the 100 mesh at 1 gal/min, B has a higher amount of proppant than A. This is because B is angled in the direction of the flow of the slurry and A is orthogonal to the flow velocity vector. Also, when using 100 mesh at 2 gal/min, there was a negligible difference (0.3 inches) between the proppant deposited by slickwater at 1 gal/1000 gal and the proppant deposited by slickwater at 2 gal/1000 gal (see Figure 4.13). With 40/70 mesh in the water system, a small amount of sand was deposited at the middle of the fracture at 1 gal/min (0.2 inch) but increased to 3 inch at 2 gal/min as seen in Figures 4.16 and 4.17. The proppant dune shapes of the sands in sub-fractures A and B are similar but B has a larger propped area.

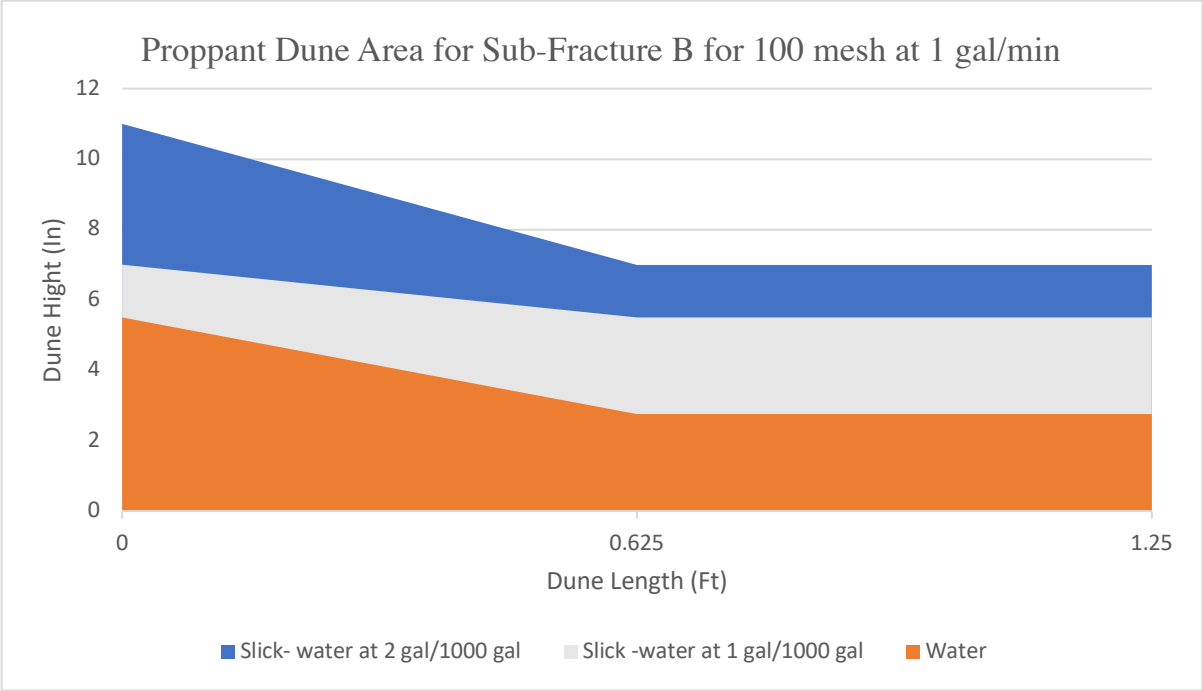

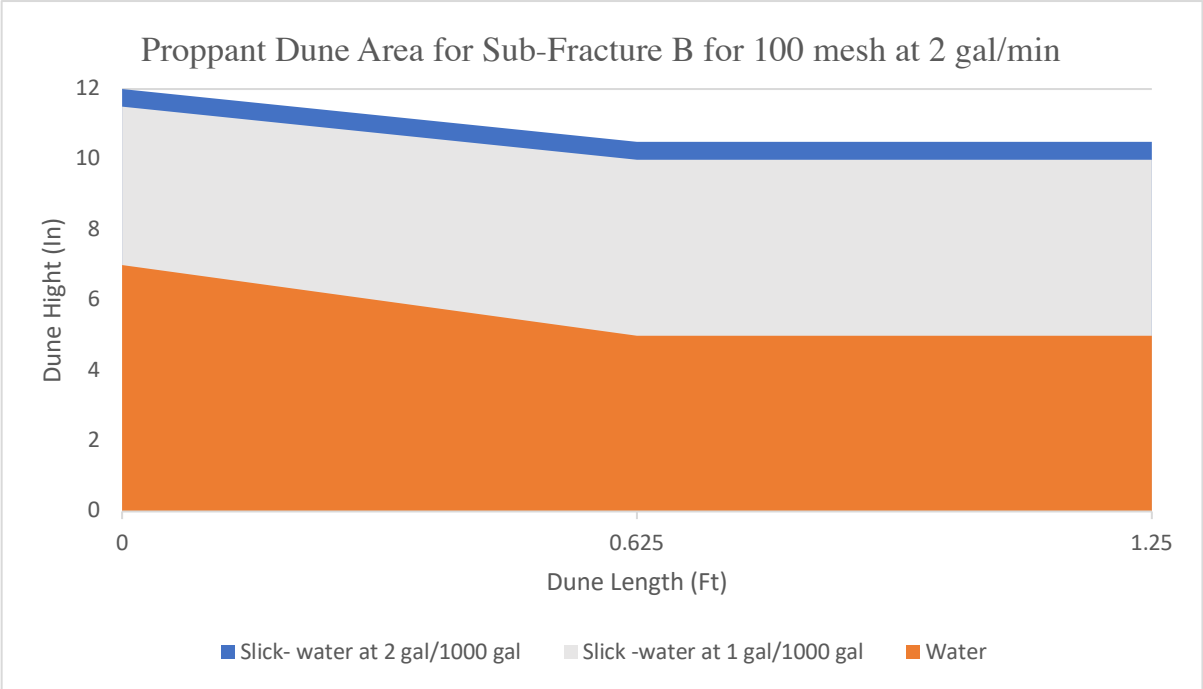

Figure 4.13: The top figure is the proppant dune area of sub-fracture B for 100 mesh at 1 gal/min in 2D. The bottom figure is the proppant dune area of sub-fracture B for 100 mesh at 2 gal/min in 2D.

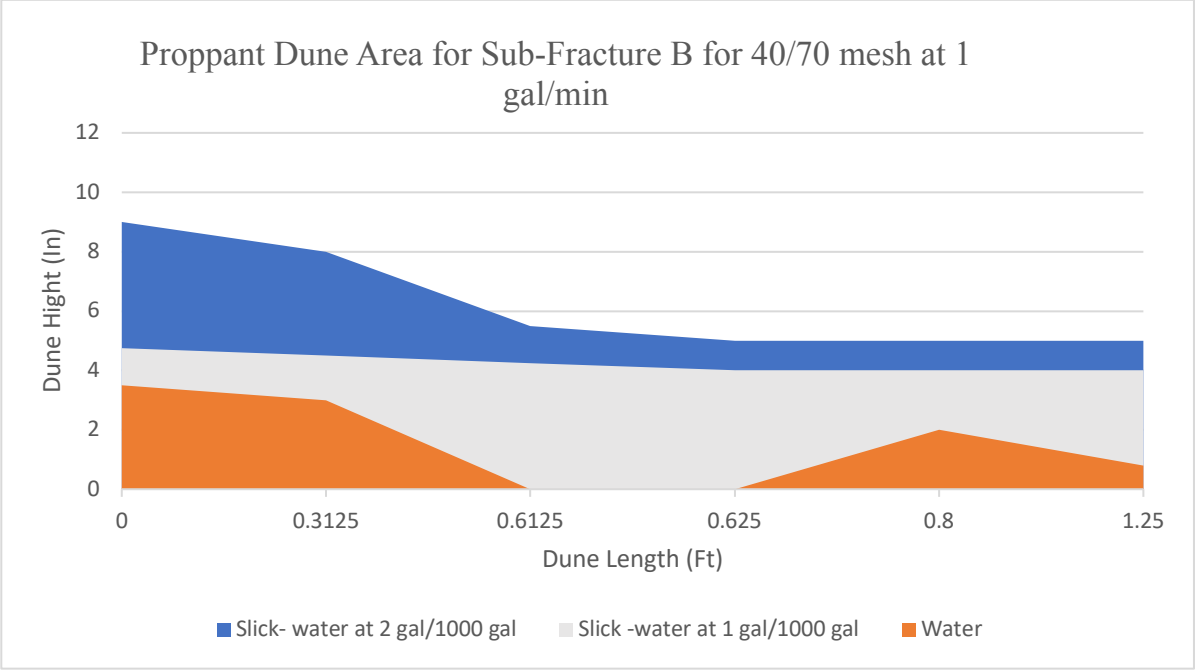

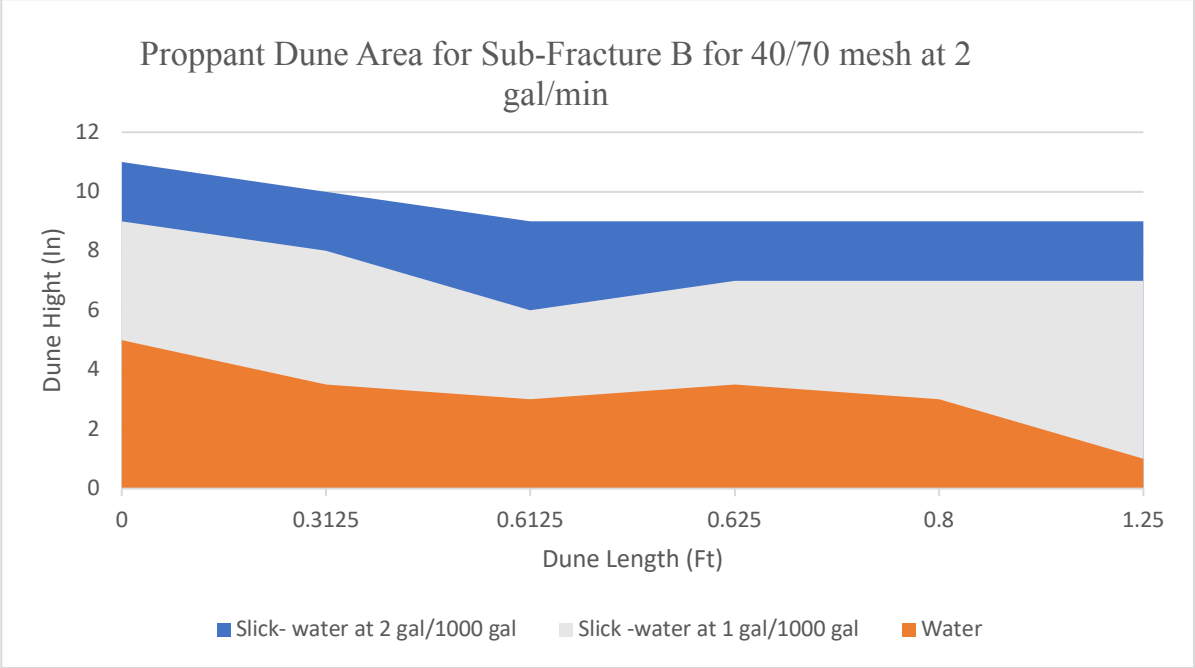

Figure 4.14: The top figure is the proppant dune area of sub-fracture B for 40/70 mesh at 1 gal/min in 2D. The bottom figure is the proppant dune area of sub-fracture B for 40/70 mesh at 2 gal/min in 2D.

Using the water system, sieve analyses for the sub-fracture group B showed that doubling the flow rate for 40/70, 100 and 14/40 mesh resulted in the reduction of the larger sizes of proppant settled in the sub-fracture group B. Tables 4.23 and 4.24 shows the percentage changes for the sub-fracture group B using different proppant sizes. Using slickwater at 1 gal/1000 gal of friction reducer, the sieve analyses for the sub-fracture group B compared to the water system showed that using the 40/70 and 100 mesh resulted in the increments of the settled larger proppant due to the viscosity increment as shown in Table 4.25. Doubling the flow rate for 40/70 and 100 mesh resulted in increments of the larger sizes of proppant settled in the sub-fracture group B as shown in Table 4.26. The same analysis was used for slickwater at 2 gal/1000 gal of friction reducer as shown in Tables 4.27 and 4.28.

Table 4.23: Sieve analysis for sub-fracture group B using water system for 40/70 mesh and 100 mesh

Size	Sieve # 40	Sieve # 45	Sieve # 50	Sieve # 60	Sieve # 70	Sieve # 100
40/70	13.0%	18.0%	11.0%	25.0%	16.0%	17.0%
100	-	12.0%	23.0%	24.0%	18.0%	23.0%

Table 4.24: Sieve analysis for sub-fracture group B using water system for 14/40 mesh

Size	Sieve # 18	Sieve # 20	Sieve # 25	Sieve # 30	Sieve # 35
14/40	15.0%	18.0%	19.0%	21.0%	27.0%

Table 4.25: Sieve analysis for sub-fracture group B using slickwater system with 1 gal/1000 gal of friction reducer for 40/70 mesh and 100 mesh at 1 gal/min

Size	Sieve # 40	Sieve # 45	Sieve # 50	Sieve # 60	Sieve # 70	Sieve # 100
40/70	15.0%	20.5%	13.5%	26.0%	13.0%	12.0%
100	-	14.0%	25.0%	26.0%	16.0%	19.0%

Table 4.26: Sieve analysis for sub-fracture group B using slickwater system with 1 gal/1000 gal of friction reducer for 40/70 mesh and 100 mesh at 2 gal/min

Size	Sieve # 40	Sieve # 45	Sieve # 50	Sieve # 60	Sieve # 70	Sieve # 100
40/70	17.0%	21.5%	14.5%	27.0%	11.0%	9.0%
100	-	17.0%	27.0%	27.5%	13.5%	15.0%

Table 4.27: Sieve analysis for sub-fracture group B using slickwater system with 2 gal/1000 gal of friction reducer for 40/70 mesh and 100 mesh at 1 gal/min

Size	Sieve # 40	Sieve # 45	Sieve # 50	Sieve # 60	Sieve # 70	Sieve # 100
40/70	17.0%	23.0%	16.0%	29.0%	9.0%	6.0%
100	-	16.0%	27.0%	28.0%	15.5%	13.5%

Table 4.28: Sieve analysis for sub-fracture group B using slickwater system with 2 gal/1000 gal of friction reducer for 40/70 mesh and 100 mesh at 2 gal/min

Size	Sieve # 40	Sieve # 45	Sieve # 50	Sieve # 60	Sieve # 70	Sieve # 100
40/70	19.0%	26.0%	19.0%	30.0%	4.0%	2.0%
100	-	19.0%	29.5%	31.5%	12.5%	7.5%

4.3.1.3 Sub-fracture C

Sub-fracture C is attached to the main fracture at an angle of 120 degrees and is the furthest from the main slot entry (see Figure 3.8). It is 0.1 inch wide, 1ft high and 1.75 ft long. In terms of proppant dune area, the sub-fracture C had the lowest height of the settled proppant. This is due to its distance from the entrance of the main fracture. The proppant dune in the main fracture accumulated proppant until some of the proppant fell into the sub-fracture C due to gravity. Also, due to the reduction of the flow area, the proppant transported via saltation and suspension. Increasing the viscosity of the carrying fluid and the treatment flow rate improved the proppant dune area in sub-fracture C. Results from the experiments are displayed in Figures 4.15 and 4.16.

Using the water system, sieve analyses for the sub-fracture group C showed that doubling the flow rate for 40/70, 100 and 14/40 mesh resulted in the reduction of the larger sizes of proppant settled in the sub-fracture group C. Tables 4.29 and 4.30 shows the percentage changes for the sub-fracture group C using different proppant sizes. Using slickwater at 1 gal/1000 gal of friction reducer, the sieve analysis for the sub-fracture group C compared to the water system showed that using the 40/70 and 100 mesh resulted in the incremental settlement of larger proppant because of the viscosity increment as shown in Table 4.31. Doubling the flow rate for 40/70 and 100 mesh resulted in increments of larger sizes of proppants settling in the sub-fracture group C as shown in Table 4.32. The same analysis was used for slickwater at 2 gal/1000 gal of friction reducer as shown in Tables 4.33 and 4.34.

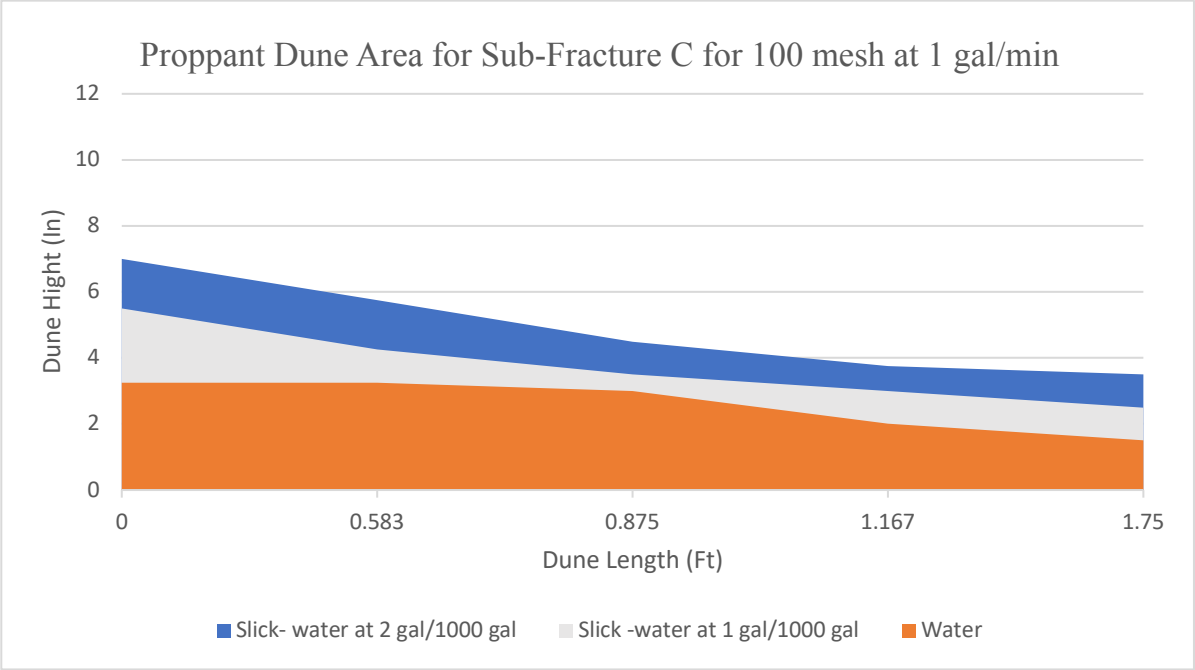

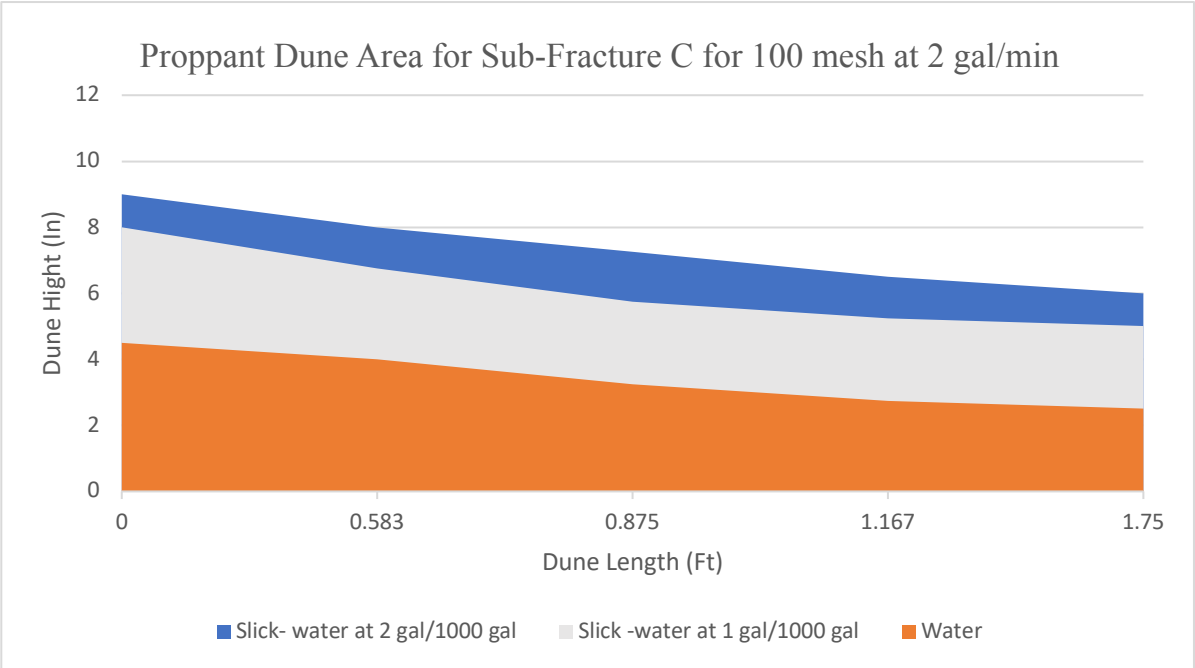

Figure 4.15: The top figure is the proppant dune area of sub-fracture C for 100 mesh at 1 gal/min in 2D. The bottom figure is the proppant dune area of sub-fracture C for 100 mesh at 2 gal/min in 2D.

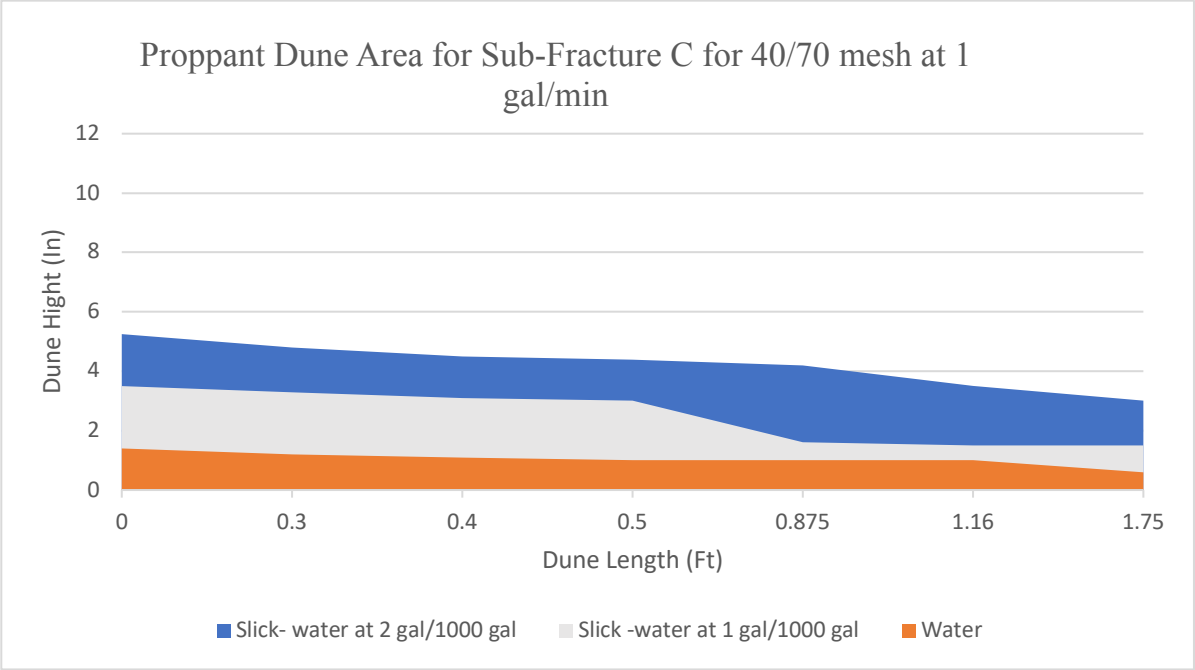

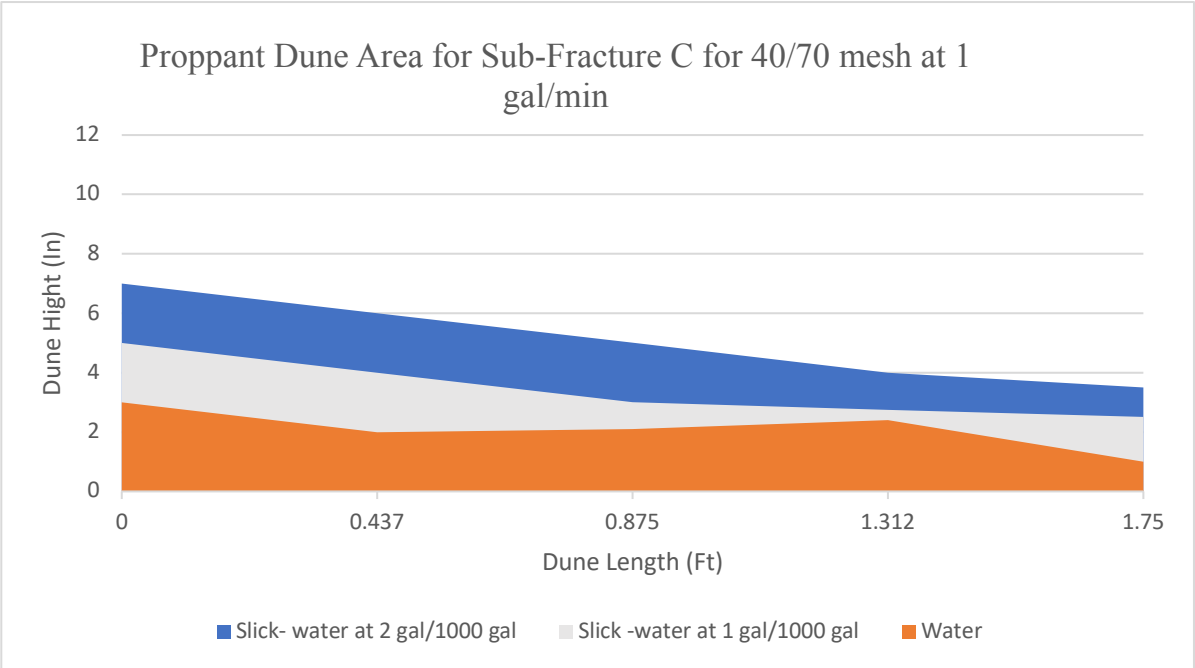

Figure 4.16: The top figure is the proppant dune area of sub-fracture C for 40/70 mesh at 1 gal/min in 2D. The bottom figure is the proppant dune area of sub-fracture C for 40/70 mesh at 2 gal/min in 2D.

Table 4.29: Sieve analysis for sub-fracture group C using water system for 40/70 mesh and 100 mesh

Size	Sieve # 40	Sieve # 45	Sieve # 50	Sieve # 60	Sieve # 70	Sieve # 100
40/70	5.0%	7.0%	15.0%	11.0%	25.0%	37.0%
100	-	8.0%	16.0%	17.0%	21.0%	38.0%

Table 4.30: Sieve analysis for sub-fracture group C using water system for 14/40 mesh

Size	Sieve # 18	Sieve # 20	Sieve # 25	Sieve # 30	Sieve # 35
14/40	5.0%	8.0%	22.0%	30.0%	35.0%

Table 4.31: Sieve analysis for sub-fracture group C using slickwater system with 1 gal/1000 gal of friction reducer for 40/70 mesh and 100 mesh at 1 gal/min

Size	Sieve # 40	Sieve # 45	Sieve # 50	Sieve # 60	Sieve # 70	Sieve # 100
40/70	6.0%	8.0%	17.0%	15.0%	22.0%	32.0%
100	-	10.0%	18.5%	18.5%	19.0%	34.0%

Table 4.32: Sieve analysis for sub-fracture group C using slickwater system with 1 gal/1000 gal of friction reducer for 40/70 mesh and 100 mesh at 2 gal/min

Size	Sieve # 40	Sieve # 45	Sieve # 50	Sieve # 60	Sieve # 70	Sieve # 100
40/70	7.5%	9.0%	18.5%	16.0%	20.0%	29.0%
100	-	11.0%	19.0%	20.0%	17.0%	33.0%

Table 4.33: Sieve analysis for sub-fracture group C using slickwater system with 2 gal/1000 gal of friction reducer for 40/70 mesh and 100 mesh at 1 gal/min

Size	Sieve # 40	Sieve # 45	Sieve # 50	Sieve # 60	Sieve # 70	Sieve # 100
40/70	8.5%	10.0 %	18.5%	17.0%	21.0%	25.0%
100	-	11.5%	19.5%	20.0%	17.0%	32.0%

Table 4.34: Sieve analysis for sub-fracture group C using slickwater system with 2 gal/1000 gal of friction reducer for 40/70 mesh and 100 mesh at 2 gal/min

Size	Sieve # 40	Sieve # 45	Sieve # 50	Sieve # 60	Sieve # 70	Sieve # 100
40/70	9.0%	11.0%	20.0%	19.0%	19.0%	22.0%
100	-	13.0 %	21.0%	22.0%	15.0%	29.0%

4.3.2 Proppant Reach Times

In this section, the proppant reach times in the sub-fractures are analyzed. The reach time is the time when the proppant first enters the sub-fractures from the wellbore, these times were captured and measured by video recording. After 0.9 minutes, the proppant started traveling into sub-fracture B-A', and after 1.0 minutes, proppant started into A-A' (see Figure 4.17). After 2.0 minutes, the proppant entered B-B' and C-A'. At 4.0 minutes, the proppant entered A-B and C-B'. At 5.7 minutes, C-C' received proppant. From the above results, sub-fracture B is the first to receive proppant. This appears to be because of its proximity to the wellbore location and its orientation to the slurry flow velocity vector. It is important to note that with the water system at 1 gal/min, the first proppant to get to the sub-fractures moved via rolling and saltation. The longest reach times were C-A', C-B', and C-C'. With tertiary and quaternary fractures, it was harder for proppant to enter into them because the proppant had to turn another corner and enter them with a slower slurry velocity. At 1 gal/min, the tertiary and quaternary sub-fracture did not receive any proppant until after the secondary sub-fracture filled up.

With slickwater at 2 gal/min, the slurry entered sub-fracture systems A and C much faster. The last sub-fracture to receive the proppant was the closest to the wellbore. The high flow rate and viscosity helped transport the proppant into the secondary and tertiary sub-fractures regardless of their angles. At 2 gal/min, more proppants were transported by suspension; the particles also traveled into the sub-fractures easily after turning the corners because of increased velocity. See Figure 4.18 for the proppant reach times.

4.4 Hybrid Proppant Results

In this section, twenty-seven experiments are discussed, using three different percentages of the hybrid proppant and three different fluid systems (see Table 4.35). In the hybrid combinations of the sands and the ultra-weight 14/40 there were always blocking issues in the fracture groups (A, B, and C) especially with the higher percentage of larger size "median average diameters" (0.0150 inch for 40/70 mesh, 0.0074 inch for 100 mesh and 0.0380 inch for 14/40 mesh) and higher densities (2.65 cc for 100 and 40/70 mesh, 1.054 cc for 14/40 mesh) of the proppants. In hybrid proppant testing, the different sizes provided an average of 40% more coverage of slots of different widths while different densities provided an average of 70% vertical

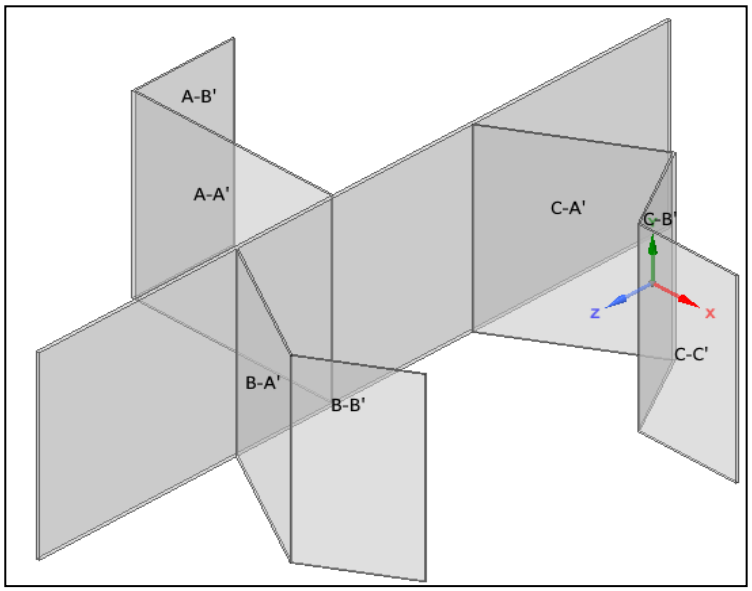

Figure 4.17: The complex fracture system with the labeled sub-fractures.

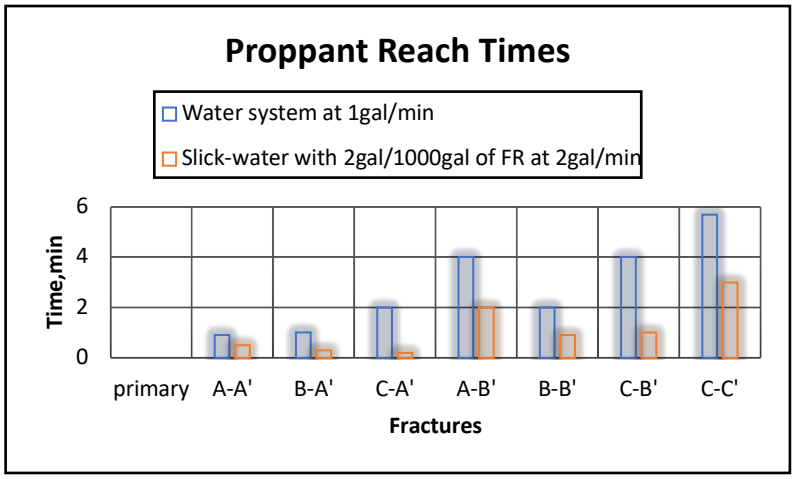

Figure 4.18: The reach time it took for every fracture to get proppant at the lowest and highest velocity and viscosity.

propped area in each slot compared to a single proppant size slurry.

Three of these combinations resulted in less blocking issues using water system, where the hybrid proppants puddled at inner pathways inside the fracture which caused blockages and reduced the rate of flow in Figure 4.19. The combinations of hybrid mix that produced less blockages were 75% of 14/40 ULW with either 100 mesh or 40/70 mesh and when 75% of 100 mesh mixed with 25% of 40/70 mesh. Also, it was observed and not measured that when the viscosity of the fluid system was increased, there were significantly reduced blocking issues.

Table 4.35: The different combinations of the hybrid proppant.

Mixture 1		Mixture 2		Mixture 3	
100	**ULW 14/40**	**100**	**40/70**	**40/70**	**ULW 14/40**
percentage per weight % (lbs/mix)					
75	25	75	25	75	25
50	50	50	50	50	50
25	75	25	75	25	75

Figure 4.19: Using the water system, the blocking issue was very prominent because of the low viscosity, and the proppant particles stick to the wall of the fracture.

In all of the experiments discussed in Sections 4.1- 4.4, the proppant moved in three ways: traction, saltation, and suspension. Increasing the viscosity of the fluids improved the transportation of the proppants into the sub-fracture groups as summarized in the following results:

1. Higher fluid viscosity yielded better transportability of the proppant into the sub-fracture groups from with an increase of dune height 20% to 36%.
2. Higher fluid viscosity transported larger proppant to the sub-fracture groups and provided more even proppant distributions between main and sub-fractures.
3. Ultra-lightweight proppant showed no settlement at all in the fracture network, even when used in the water system.

4. 100 mesh sand, showed better transport into the fracture network than 40/70 mesh, indicating that doubling the proppant diameter increases settling and therefore hinders the slickwater proppant transport. The change in the dune height is low (9.4%) relative to the change in diameter.
5. A higher flow rate from 3% to 13%, depending on proppant size, has better proppant transport. This is because the faster the flow rate, the higher the drag force.
6. For hybrid proppant, the different sizes "median average diameters" (0.0150 inch for 40/70 mesh, 0.0074 inch for 100 mesh and 0.0380 inch for 14/40 mesh) provided 40% coverage of natural fractures of different widths while different densities (2.65 cc for 100 and 40/70 mesh, 1.054 cc for 14/40 mesh) provided 70% vertically propped area in each fracture compared to a single proppant size slurry.

4.5 Experimental Data Repeatability and Error Analysis

In order to prove an experiment, the ability to reproduce the results is critical as it directly proves the experiment and its' reliability of the produced laboratory data and the obtained conclusions. This was done by cautiously implementing and monitoring the experimental procedure to ascertain the accuracy of the generated data. The experimental apparatus was calculated and designed for accuracy as explained in Section 3.5.

The results were defined, and the error of margin was reduced and analyzed in the model. The first method of analyzing trended in terms of the proppant dune height in the main fracture with sensitivity to the change in the experimental values. The R2 values trended to a wide range of variables most of which were above 98% in Figure 4.20, which proved to be a highly reliable system with accurate results. In the sub-fracture groups, the R2 values trended above 95% in Figure 4.20, proving again that this was a highly reliable system. Also, the logical result trends acquired were easily explained by the laws of physics as was discussed in Section 4.1 – 4.4.

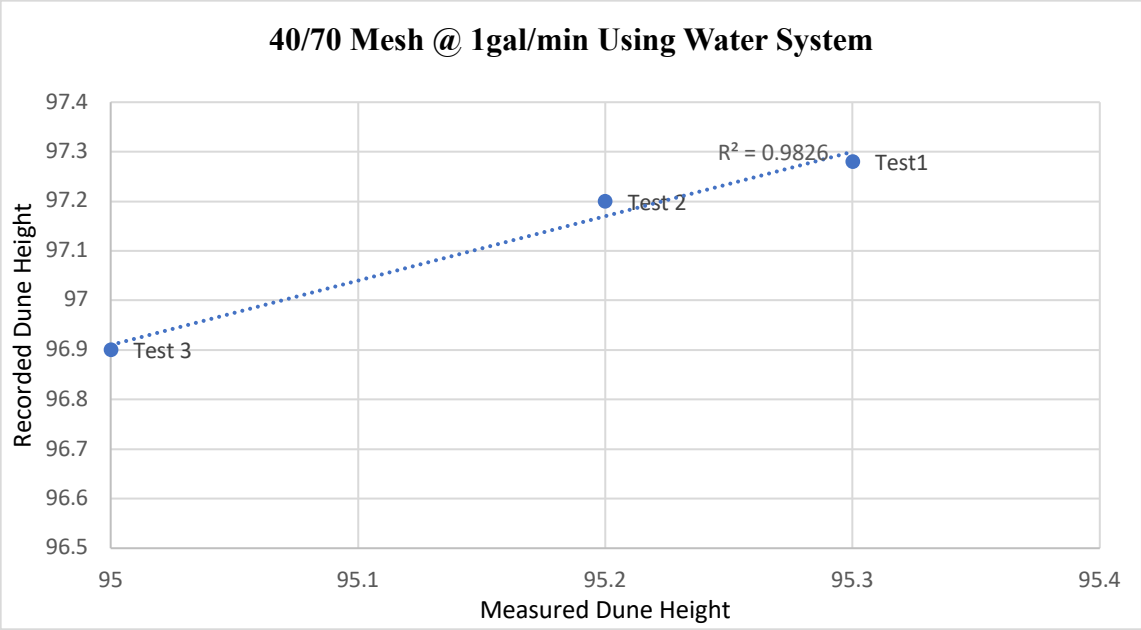

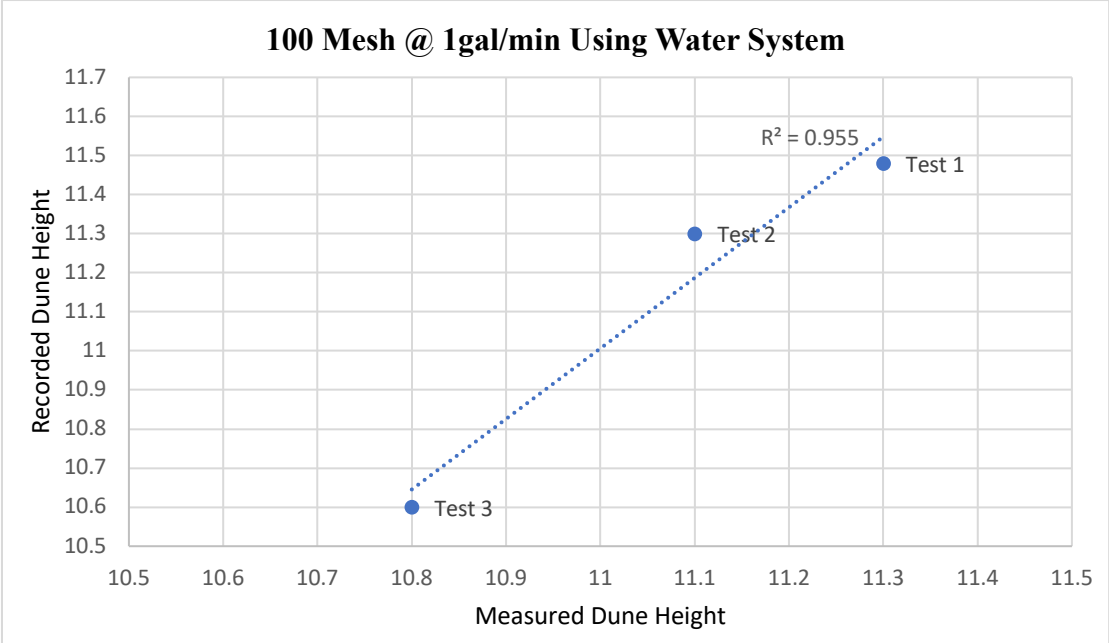

Figure 4.20: The top figure is the proppant dune height (%) of main fracture for 40/70 mesh at 1 gal/min. The bottom figure is the summation of proppant dune height of all sub-fractures for 100 mesh at 1 gal/min.

4.6 The Effects of Perforation Locations

In this section, the proppant transport behavior as it relates to slot entry location in the main fracture and sub-fractures has been analyzed. In Section 4.6.1, the proppant transport behavior in

the main fracture is analyzed when the slurry is pumped in through different perforation locations using two proppant sizes, two flow rates, and the water system. Section 4.6.2 focuses on how these parameters affected the proppant transport into the subsidiary fractures.

4.6.1 Main Fracture

In this study, there are two openings within the main slot representing different perforation locations; one at the base at 4 inches from the bottom of the slot and one at the highest point of the slot at 8 inches from the bottom of the slot. Twelve (12) experiments were used to assess the impact of these perforation locations (height) at the entrance of the main slot. The proppant sizes that were used were 40/70, 100 and 14/40 mesh. The average diameters of the proppants were 0.0150 inch 0.0074 inch, and 0.0380 inch, respectively. The densities of the proppants were 2.65 g/cm^3, 2.65 g/cm^3, and 1.054 g/cm^3, respectively. The concentration was 2 ppg for all runs, and flow rates were 1 gal/min and 2 gal/min. The experiments in this section were conducted using water only. Each experiment ran until the equilibrium height was reached in the slot network. During the experiment, snapshots were taken at 15, 25 and 35 minutes to capture the proppant transport behavior, dune height, and dune shape.

4.6.1.1 Proppant Transport Behavior

When the bottom perforation only was opened, the flow rate of slurry was fixed at 1 gal/min and 2 gal/min. As the slurry entered the perforation, there was an initial upward flow at low velocity. The flow was turbulent for about two minutes and later changed to effective laminar flow. As injection continued, two proppant transport mechanisms were prominent: (1) the suspended particles moved with the fluid while (2) settled particles rolled and slid towards the end of the slot. Once the deposition rate became constant, the proppant buildup increased by two inches every three minutes at a flow rate of 1 gal/min and one inch every three minutes at flow rate of 2 gal/min. Figure 4.21 shows that some of proppant was transported as suspended load while others were transported as bed-load. After the slurry left the perforation, it started to fall down to the bottom of the fracture because there was not enough lifting force to lift the proppant. On the bottom of the fracture, the bed-load rolled and slid due to the weight of the grains and low velocity. The proppant transport mechanisms observed with slurry flow from the bottom perforation were settling, rolling, sliding and saltation. The suspended height of the injected slurry was small and

therefore the settling rate of the particles was higher. The settled dune was closer to the perforation and as the injection time increased, the dune started to initiate the flow stream blocking issue.

The proppant dune continued to increase into a bank until equilibrium height was achieved, then the proppant spread further into the main fracture. The dune height increased until there was an increase in flow velocity, and then a vertical lift of proppants was observed. The particle-particle interaction lifted the proppants, and the low fluid viscosity caused them to fall to the bottom, as they traveled further, especially with flow rate of 1 gal/min. In conclusion, during injection from the bottom wellbore, the proppant dune was formed quickly and near the wellbore. At the lower flow rate, the settling was greater. For 100 mesh at 1 gal/min and 2 gal/min, the near wellbore dune heights at 15 minutes were 6 inch and 5 inch, respectively. For the second stage, at 1 gal/min between 15 minutes and 25 minutes of injection for 100 mesh, it was observed that the proppant dune height had reduced because of the erosion by the slurry. At 2 gal/min, the dune width and height increased, reaching equilibrium height and spread further into the fracture. For 40/70 mesh at 1 gal/min, the proppant dune height near the perforation location increased by 5.75 inch while there was no change at 2 gal/min. Figure 4.21 shows a sharp and more steep dune for the flow rate of 1 gal/min.

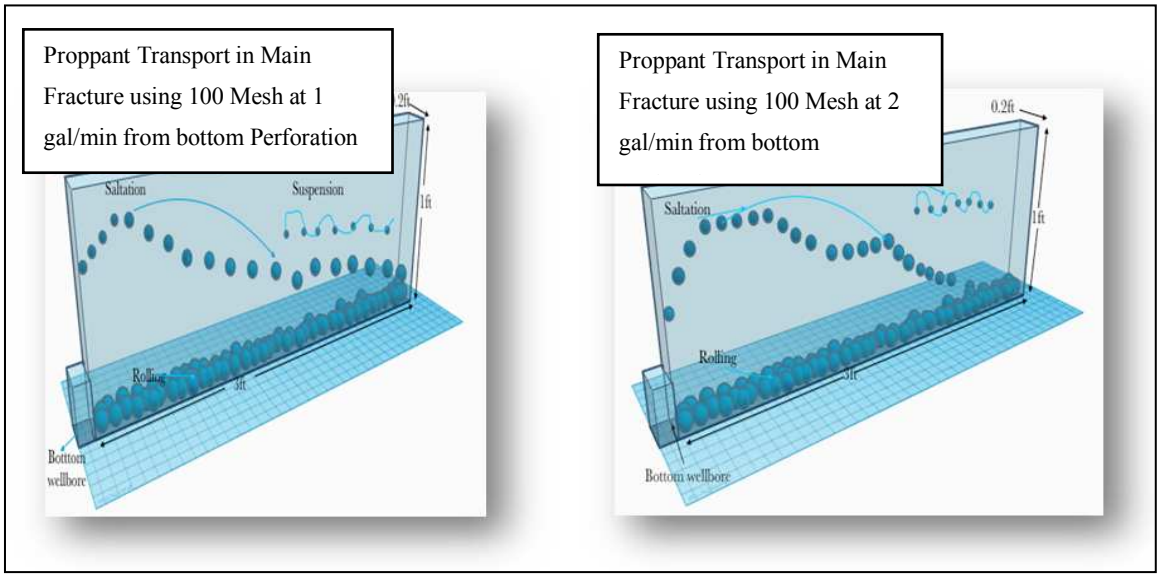

Figure 4.21: Illustration of the proppant transport mechanism in the main fracture using 100 mesh at one gallon per minute and two gallons per minute.

When the top perforation was opened, and the proppant entered the system, it initially behaved like the bottom perforation behavior. Over time, some of proppant grains accumulated

and fell to the bottom of the system. In higher concentrations, this behavior was more rapid. Two proppant motions were observed; individual grains moved with fluid and groups of proppant grains fell off in suspension. Over time, a bank of proppant built up at the bottom. Once the deposition rate became constant, the proppant buildup increased by one to two inches at three minutes intervals.

Figure 4.22 shows that some of the proppant travelled as a suspended load and others travelled as a bed-load. The proppant transport mechanisms observed with slurry flow from the top perforation were rolling, sliding, saltation and suspension. The heavier particles interacted with the side of the wall and fell to the bottom of the slot. The intermediate and smaller particles travelled with the fluid in form of saltation and suspension. Because of the available flow area, the lift force of the fluid acting on the particle was greater than the gravitational force and reduced its tendency to fall. Subsequently, as the slurry was injected from the top perforation, the particles accumulated at the bottom of the fracture. As the injection continued, the settled proppant reduced the flow area and increased the velocity of the flow with interaction between the particles. The interaction between the particles reduced their terminal velocity and increased the gravitational effects.

During the various experiments, two stages of proppant transport were observed. At the early stage of injection from the top entry point, a small dune with little effect from the flow stream was formed. At the lower flow rate, the settling is greater. For 100 mesh at 1 gal/min and 2 gal/min near the wellbore dune heights at 15 min were 11.75 inch and 9.5 inch, respectively. For the second stage, at 1 gal/min between 15 min and 25 minutes of injection for 100 mesh, the proppant dune height had reduced because of the erosion by the slurry. At 2 gal/min, the dune width and height increased, reaching equilibrium height and spreading further into the fracture and not blocking the flow field. For 40/70 mesh at 1 gal/min, the proppant dune height near the perforation location increased while there was no change at 2 gal/min.

With the bottom perforation open and the top perforation closed, the higher velocity increased the proppant transportability, increased the drag force, reduced the dune height by 57% and increased the dune length by 12%. The flow rate of 1 gal/min had the proppant dune height 44 % higher and 61% shorter than when pumped at 2 gal/min. At 1 gal/min, the drag force was lower, the proppant settled 22% faster and it clogged the flow field more readily.

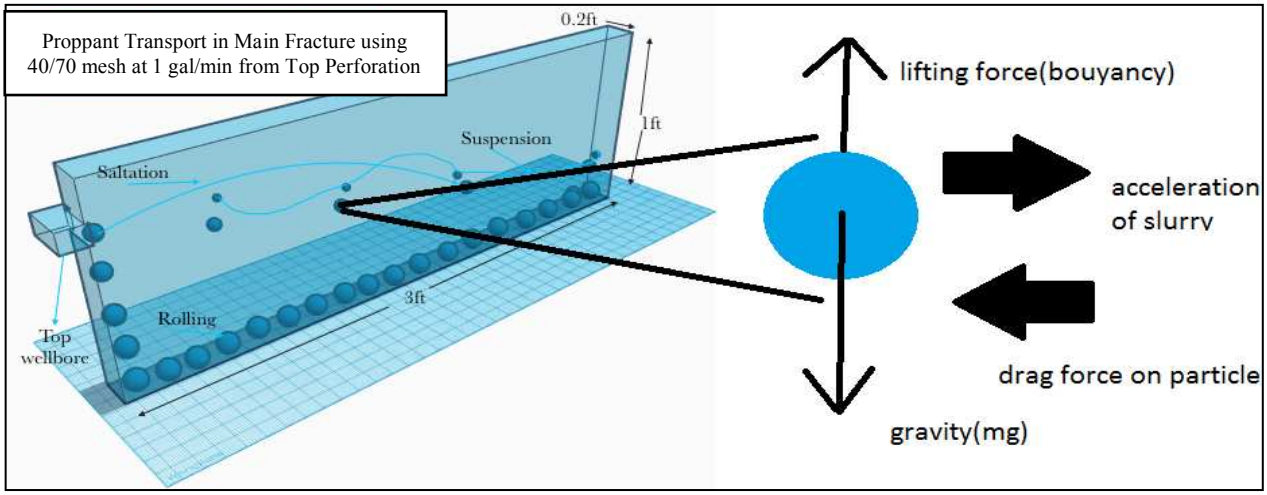

Figure 4.22: Illustration of the forces acting on a particle of 40/70 mesh.

4.6.1.2 Slickwater Proppant Dune Development

For the purpose of these analyses, the main fracture was divided into three sections: section A was near the slot entry point, (e.g. near the wellbore) and included the length of the main slot from the wellbore to sub-fracture B. Section B was measured along the main fracture from the sub-fracture B to the sub-fracture C. Section C was measured from sub-fracture C to the end of the main slot. Each of these three sections is one foot in length. It is important to note that for 40/70 mesh the equilibrium dune heights occurred at 35 minutes and 25 minutes for the flow rates of 1 gal/min and 2 gal/min, respectively. Tables 4.36 and 4.37 show the measured equilibrium proppant dune heights for the 40/70 mesh at the two flow rates as a function of the perforation location.

The results showed in Section A that at 1 gal/min the effect of pumping from the top perforation when the bottom perforation was closed showed a 15% decrease in the proppant dune height near the wellbore, with a 12% decrease in the proppant dune height in Section B; and in Section C there was a 3.8% decrease. Figure 4.23 demonstrates the difference in the proppant entry from the two perforation points and shows a gradual linear decline of settled proppants while pumping from the top perforation and a pyramid shape of settled proppants formed from the bottom perforation. When pumping at 2 gal/min from the top perforation, a parabolic dune was formed. Pumping from the bottom perforation yielded a linear dune as can be seen in Figure 4.24. The results show that in Section A pumping from the top perforation yielded a 58% higher dune

than pumping from the bottom perforation. In Section C, pumping from the bottom perforation yielded a 30% and a 40% higher dune height than pumping from the top perforation, respectively. The results showed that the effect of the perforation location was more prominent near the wellbore for both flow rates and fairly insignificant the further it was from the main slot entry at 1 gal/min.

Table 4.36: The equilibrium dune heights in inches for 40/70 mesh at 1 gal/min after 35 minutes of treatment

Perforation Locations	Section A	Section B	Section C
Top Perforation	8.25	7.50	6.50
Bottom Perforation	9.75	8.50	6.25

Table 4.37: The equilibrium dune heights in inches for 40/70 mesh at 2 gal/min after 25 minutes of treatment

Perforation Locations	Section A	Section B	Section C
Top Perforation	11.80	8.25	5.00
Bottom Perforation	5.00	11.80	8.25

The 100 mesh sand has a lower average diameter than the 40/70 mesh but the same specific gravity. It was also tested with two flow rates pumped into the top and bottom perforation locations. Tables 4.38 and 4.39 show the measured equilibrium dune heights from the laboratory experiments for the 100 mesh. Comparing results between the 40/70 mesh and the 100 mesh, the dune height results in sections pumping from the top perforation were: Section A yielded a 47% increase, Section B yielded a 31% increase, and Section C yielded a 17% increase. Figure 4.25 shows a pyramid shape with a linear decline of the settled proppants when transitioning from the top to the bottom perforation.

At a flow rate of 2 gal/min, pumping from the bottom perforation created a parabolic dune shape whereas pumping from the top perforation created a gradually declining linear dune shape as shown in Figure 4.26. Comparing results between the 40/70 mesh and the 100 mesh, the dune height results in sections pumping from the top perforation were: Section A yielded a 50% increase in height, Section B pumping yielded a 18% increase in height, and in Section C the dune heights were equal for both perforations. As with the 40/70 mesh, the results showed that the effect of the perforation location was more prominent near the wellbore and was insignificant the further it was from the main slot entry.

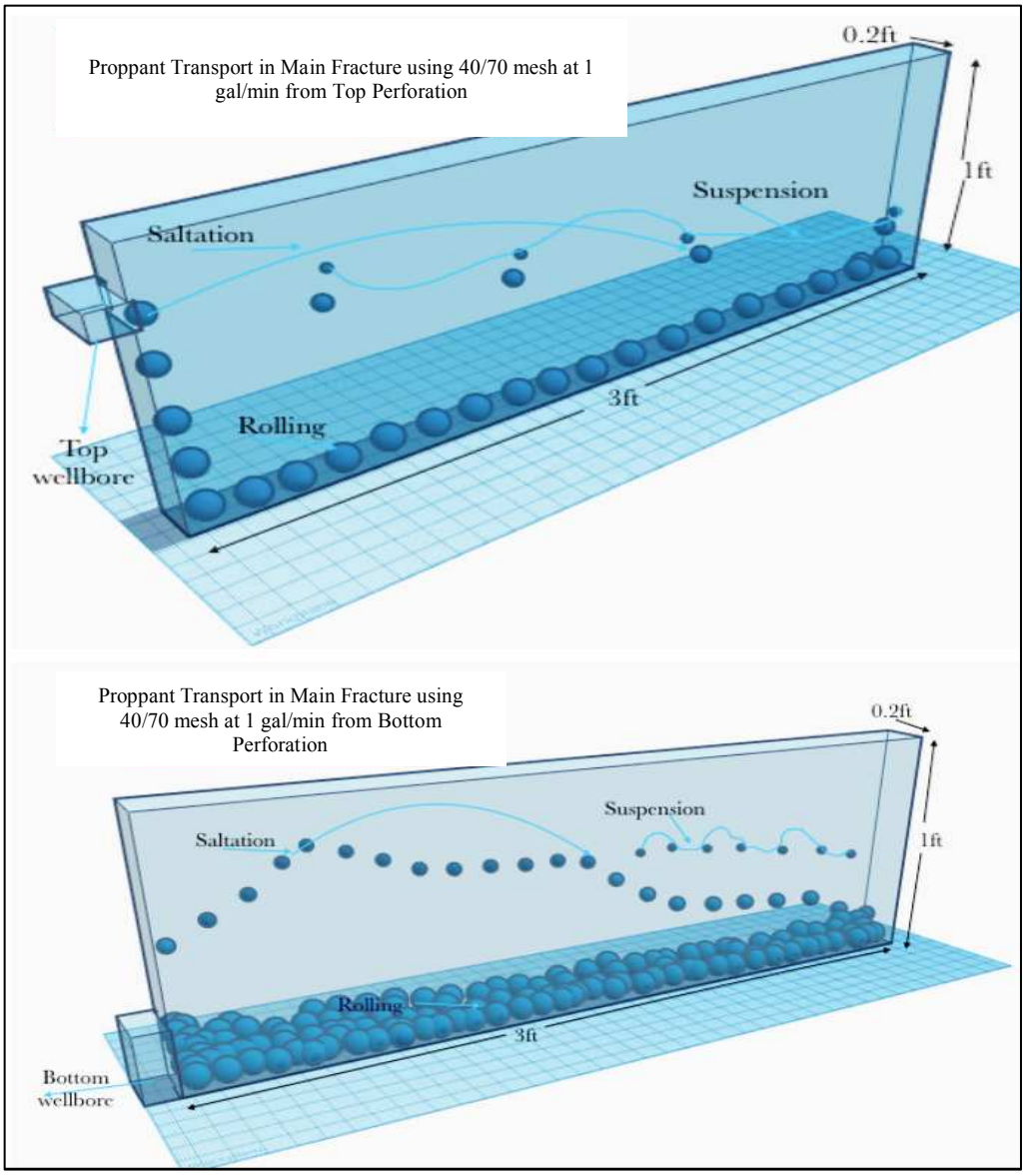

Figure 4.23: Top: the proppant transport behavior in the main slot of 40/70 mesh at one gallon per minute after 35 minutes of treatment while injecting from the top perforation. Bottom: the proppant transport behavior in the main slot of 40/70 mesh at one gallon per minute after 35 minutes of treatment while injecting from the bottom perforation.

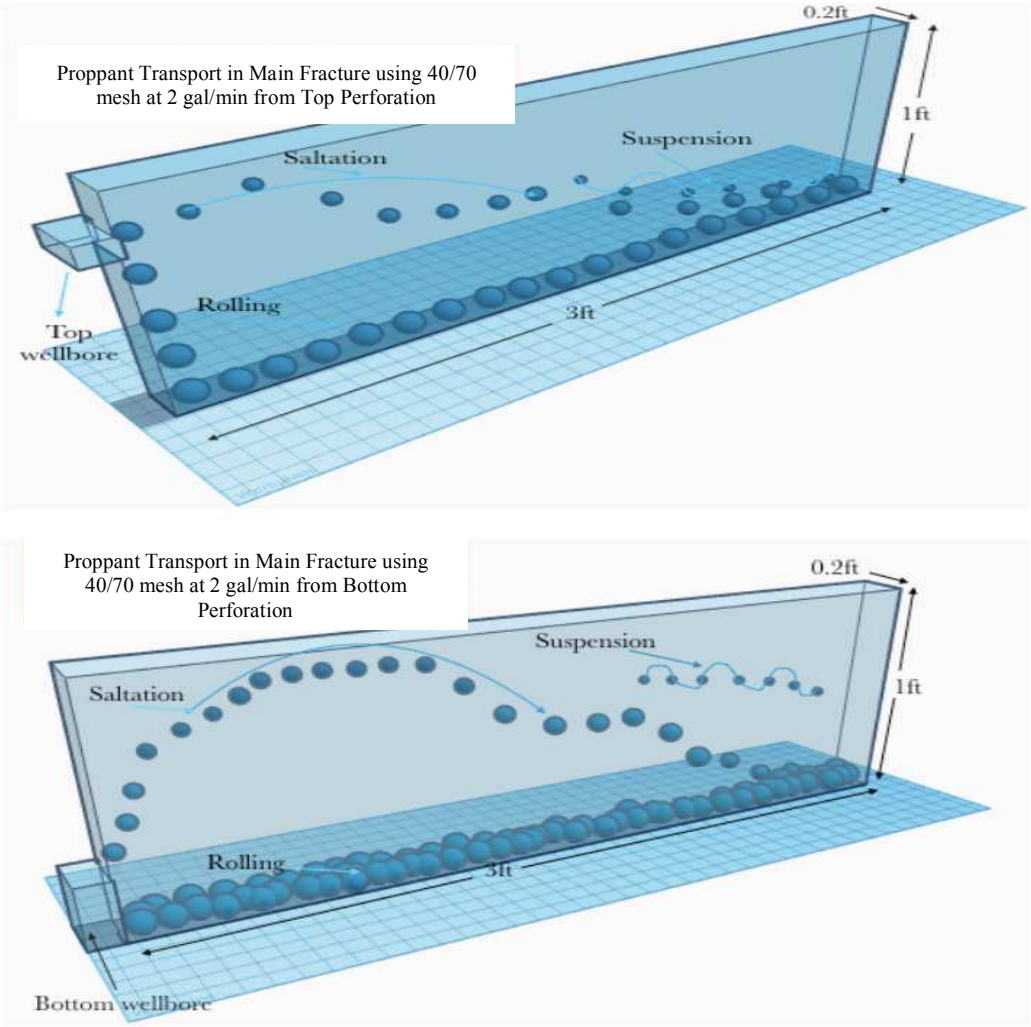

Figure 4.24: Top: the proppant transport behavior in the main slot of 40/70 mesh at two gallons per minute after 25 minutes of treatment while injecting from the top perforation. Bottom: the proppant transport behavior in the main slot of 40/70 mesh at two gallons per minute after 25 minutes of treatment while injecting from the bottom perforation.

Table 4.38: The equilibrium dune heights in inches for 100 mesh at 1 gal/min after 35 minutes of treatment

Perforation Locations	Section A	Section B	Section C
Top Perforation	11.40	9.75	4.50
Bottom Perforation	6.00	6.75	3.70

Table 4.39: The equilibrium dune heights in inches for 100 mesh at 2 gal/min after 25 minutes of treatment

Perforation Locations	Section A	Section B	Section C
Top Perforation	10.30	8.25	4.24
Bottom Perforation	5.25	10.00	4.25

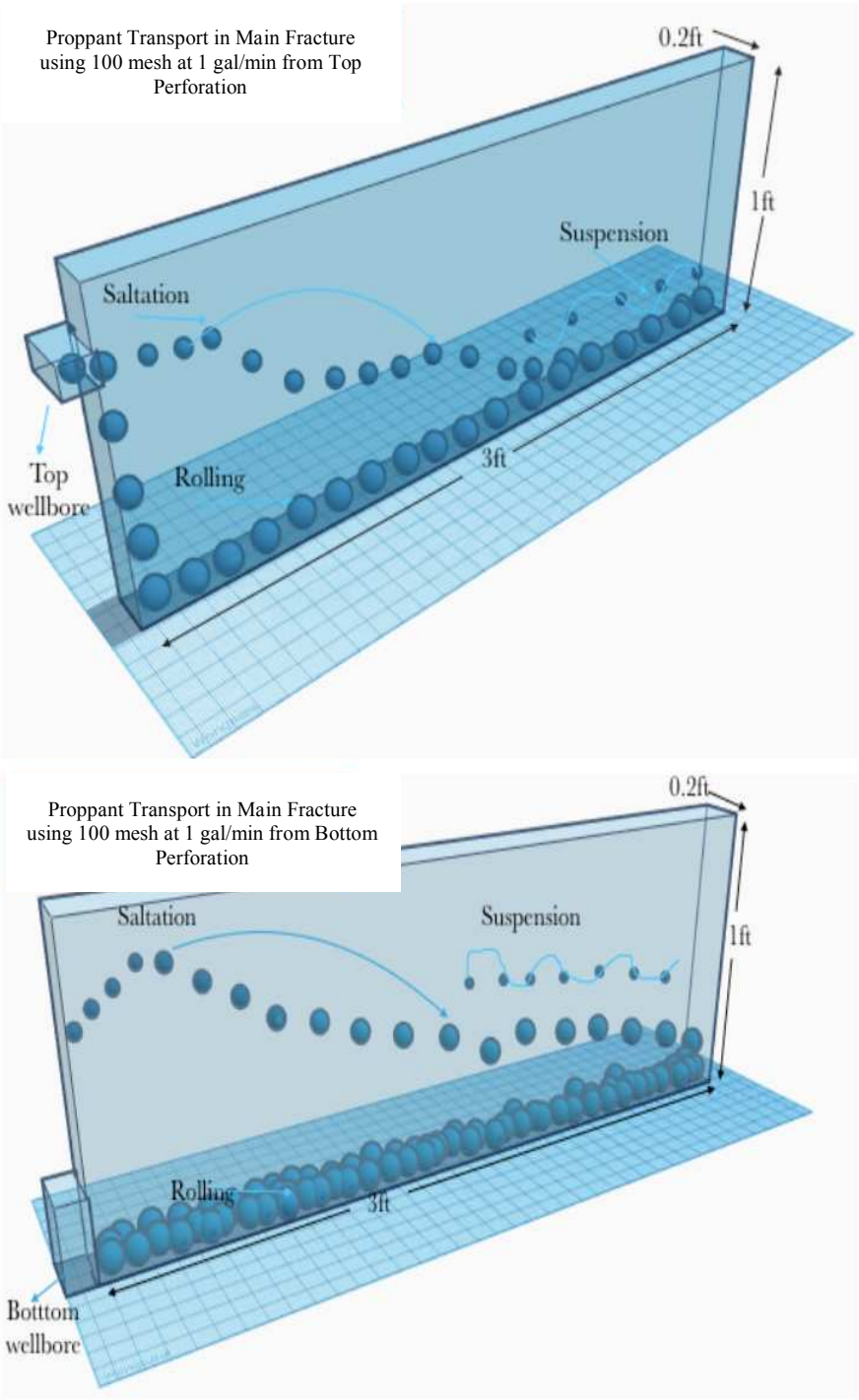

Figure 4.25: Top: the proppant transport mechanism in the main slot of 100 mesh at one gallon per minute after 35 minutes of treatment while injecting from the top perforation. Bottom: the proppant transport mechanism in the main slot of 100 mesh at one gallon per minute after 35 minutes of treatment while injecting from the bottom perforation.

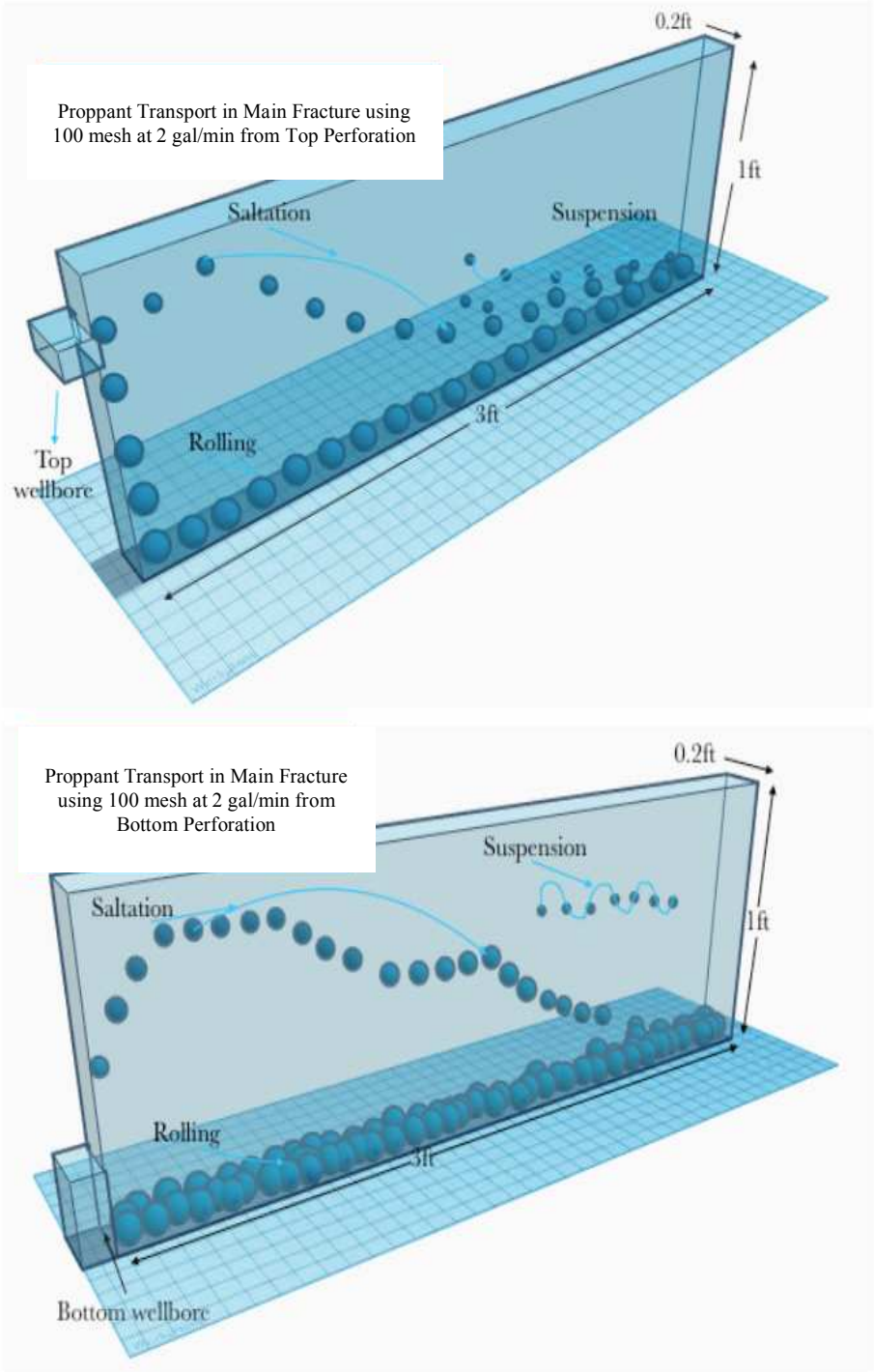

Figure 4.26: Top: the proppant transport mechanism in the main slot of 100 mesh at two gallons per minute after 25 minutes of treatment while injecting from the top perforation. Bottom: the proppant transport mechanism in the main slot of 100 mesh at two gallons per minute after 25 minutes of treatment while injecting from the bottom perforation.

4.7 Sub-fractures

Sub-fracture A is located in the middle of the primary fracture as shown in Figure 3.8. The transport mechanism in this sub-fracture was different from the other sub-fractures, because of its location from the main slot entry. It was perpendicular to the fluid flow direction. The transport of the proppant into the sub-fractures was harder from the bottom perforation because of the accumulated bed-load from the main fractures "rolled" with the lowest velocity into the sub-fractures. For sub-fracture A, when the slurry was injected from the bottom perforation, the dune height increased in the main fracture until the proppant load fell into the sub-fracture due to gravity. When injecting the slurry from the top perforation, the bed load transport and suspended load transport were dominant. The suspended load traveled around the corner with the carrying fluid into the sub-fractures while the bed load rolled and felled into the sub-fractures due to gravity. Because of the decreased flow area, the increased fluid velocity between the top of the dune and the top of the slot helped the proppant to turn the corner into the sub-fractures. A critical velocity or threshold velocity caused the proppant to turn the corner regardless of the perforation location. Tables 4.40 and 4.41 show the dune heights after 35 minutes of treatment for 100 mesh at 1 gal/min and 2 gal/min, respectively.

Sub-fracture A is divided into two sections: section A is the closest to the main fracture and section B is attached to section A at 90 degrees (see Figure 3.8). At the flow rate of 1 gal/min injection from the bottom perforation, the dune height was increased in section A by 19% and reduced in section B by 7%. According to the calculated volume of the settled proppants, pumping from the bottom perforation increased the volume of proppants by 62% (see Table 4.41). This shows that at a low flow rate of 1 gal/min using the bottom perforation, the rolling and erosion mechanisms of the settled proppants moved the proppant into the sub-fracture A. The proppants in the main fracture were eroded with increasing time when the velocity was at 1 gal/min.

Table 4.40: The equilibrium dune heights in inches for 100 mesh at 1 gal/min after 35 minutes of treatment

Perforation Locations	Section A	Section B
Top Perforation	5.25	3.50
Bottom Perforation	6.25	3.25

Table 4.41: The volume in inch^3 of proppant settled at 1 gal/min

Perforation Locations	Section A	Section B	Total
Top Perforation	2.8	1.50	4.35
Bottom Perforation	9.83	1.65	11.50

At the flow rate of 2 gal/min, injection from the top perforation increased the dune height in section A by 34% and section B by 43%. According to the calculated volume of settled proppants, pumping from the top perforation increased the volume of proppants by 62% (see Table 4.42). This means that when the flow rate is doubled using the top perforation, the proppants are carried into the sub-fracture A by suspension.

Table 4.42: The equilibrium dune heights in inches for 100 mesh at 2 gal/min after 25 minutes of treatment

Perforation Locations	Section A	Section B
Top Perforation	9.5	5.75
Bottom Perforation	6.25	3.25

Table 4.43: The volume in inch^3 of proppant settled at 2 gal/min

Perforation Locations	Section A	Section B	Total
Top Perforation	9.83	1.65	11.48
Bottom Perforation	2.85	1.50	4.35

For 40/70 mesh, since the average diameter of this proppant is twice the size of 100 mesh, more settling did occur. The dune heights for both flow rates are outlined in Tables 4.44 and 4.45. At the flow rate of 1 gal/min, injection from the bottom perforation increased the dune height in section A by 19% and reduced the dune height in section B by 7.6%. According to the calculated volume of settled proppants, pumping from the bottom perforation increased the volume of settled proppants by 0.3% (see Table 4.45). The transport mechanism for both perforations was rolling

and sliding. This is due to the settling tendencies of 40/70 mesh and the low drag force which is a result of the lower flow rate and the weak lifting force of water.

Table 4.44: The equilibrium dune heights in inches for 100 mesh at1 gal/min after 35 minutes of treatment

Perforation Locations	Section A	Section B
Top Perforation	4.25	3.00
Bottom Perforation	5.25	3.25

Table 4.45: The volume in inch^3 of proppant settled at 1 gal/min

Perforation Locations	Section A	Section B	Total
Top Perforation	4.93	1.50	6.43
Bottom Perforation	5.10	1.35	6.45

At the flow rate of 2 gal/min, injection from the top perforation decreased the dune height in section A by 36.6% and increased in section B by 13.3%. According to the calculated volume of settled proppants, pumping from the bottom perforation increased the volume of proppants by 35.5 % (see Table 4.47). This result was consistent with the theory that the 40/70 mesh when pumped from the bottom perforation settles quickly and travels further into the fracture by rolling. At higher flow rates, the force of newly injected proppants being pumped pushed the settled proppants further into the fracture. Suspension transport was not prominent due to three factors: (1) the weight of the proppant, (2) the viscosity of tap water was not sufficient in lifting the proppant particle, and (3) the particle-particle interaction caused the particles to settle faster.

Table 4.46: The equilibrium dune heights in inches for 40/70 mesh at 2 gal/min after 25 minutes of treatment

Perforation Locations	Section A	Section B
Top Perforation	4.75	3.75
Bottom Perforation	7.50	3.25

Table 4.47: The volume in inch^3 of proppant settled at 2 gal/min

Perforation Locations	Section A	Section B	Total
Top Perforation	4.65	1.35	6.00
Bottom Perforation	7.65	1.35	9.30

The geometry of sub-fracture B is presented in Figure 3.8. Its closeness to the main entry slot did affect the dune height and volume of proppant settled. Tables 4.48 and 4.49 show the 40/70 mesh proppant dune heights in sub-fracture B at 1 gal/min and 2 gal/min, respectively for both perforation locations. At the flow rate of 1 gal/min, injection from the bottom perforation increased the dune height in section A by 80.6% and in section B by 85.7%. According to the calculated volume of the settled proppants, pumping from the bottom perforation at 1 gal/min increased the volume of proppants by 10.1% (see Table 4.49). The dune height with the bottom perforation was higher because of the dominance of the rolling proppant transport mechanism.

Table 4.48: The equilibrium dune heights in inches for 40/70 mesh at 1 gal/min after 35 minutes of treatment

Perforation Locations	Section A	Section B
Top Perforation	1.50	0.50
Bottom Perforation	7.75	3.50

Table 4.49: The volume in $inch^3$ of proppant settled at 1 gal/min

Perforation Locations	Section A	Section B	Total
Top Perforation	4.30	1.60	5.90
Bottom Perforation	5.06	1.50	6.56

At the flow rate of 2 gal/min, injection from the top perforation decreased the dune height in section A by 30.9% and in section B by 21.1%. According to the calculated volume of the settled proppants, pumping from the bottom perforation increased the volume of settled proppants by 34.7% (see Table 4.51). This result suggests that the dominant mechanism is rolling, since the velocity was very low due to the slow particles movements that caused from blocking.

Table 4.50: The equilibrium dune heights in inches for 40/70 mesh at 2 gal/min after 25 minutes of treatment

Perforation Locations	Section A	Section B
Top Perforation	7.25	3.00
Bottom Perforation	10.50	4.75

Table 4.51: The volume in inch^3 of proppant settled at 2 gal/min

Perforation Locations	Section A	Section B	Total
Top Perforation	5.18	1.42	6.00
Bottom Perforation	8.35	1.58	9.93

For 100 mesh, Tables 4.52 and 4.53 show the dune heights after 35 minutes of the treatment for 100 mesh at 1 gal/min and 2 gal/min, respectively. Section A is the closest to the main fracture and section B is attached to section A at 60 degrees (see Figure 3.8). At the flow rate of 1 gal/min, injection from the bottom perforation increased the dune height in section A by 14.6 % and in section B by 6.7 %. According to the calculated volume of the settled proppants, pumping from the bottom perforation increased the volume of settled proppants by 17.6 % (see Table 4.53). The dominant transport mechanisms here were rolling, sliding, and suspension. Suspension is due to sub-fracture B's position from the main entry slot. Sliding is due to the erosional power of the injected slurry, and rolling is from the settled proppants.

Table 4.52: The equilibrium dune heights in inches for 100 mesh at 1 gal/min after 35 minutes of treatment

Perforation Locations	Section A	Section B
Top Perforation	8.75	3.50
Bottom Perforation	10.25	3.75

Table 4.53: The volume in inch^3 of proppant settled at 1 gal/min

Perforation Locations	Section A	Section B	Total
Top Perforation	5.79	1.73	7.52
Bottom Perforation	4.92	1.35	6.20

At the flow rate of 2 gal/min, injection from the top perforation increased the dune height in section A by 66.7% and reduced the dune heights in section B by 4%. According to the calculated volume of settled proppants, pumping from the top perforation increased the volume of

proppants by 12.5% (see Table 4.55). The result suggests that when using 100 mesh at 2 gal/min from the top perforation the transport mechanism is rolling and suspending. The suspension is due to the size of 100 mesh and the drag force from the flow rate. Also, since the sub-fracture B is so close to the main slot entry some of the pumped proppants are still in suspension and turned into sub-fracture B. The early settled proppants fell into sub-fracture B as more proppants were injected into the main fracture.

Table 4.54: The equilibrium dune heights in inches for 100 mesh at 2 gal/min after 25 minutes of treatment

Perforation Locations	Section A	Section B
Top Perforation	9.75	6.00
Bottom Perforation	3.25	6.25

Table 4.55: The volume in inch^3 of proppant settled at 2 gal/min

Perforation Locations	Section A	Section B	Total
Top Perforation	4.93	1.35	6.30
Bottom Perforation	4.16	1.35	5.51

Sub-fracture C is the furthest from the main slot entry and is attached to the main fracture at 120 degrees (see Figure 3.8). Tables 4.56 and 4.57 show the dune heights after 35 minutes of the treatment for 100 mesh at 1 gal/min and 2 gal/min, respectively. Section A is the closest to the main fracture, and section B is attached to section A at 60 degrees and section C is attached to section B at 90 degrees (see Figure 3.8). At the flow rate of 1 gal/min injecting from the bottom perforation, there was an increase of the dune height in section A by 39.3% and there were no changes in section B. Pumping from the top perforation increased section C's dune height by 15.45%. According to the calculated volume of settled proppants, pumping from the bottom perforation increased the volume of proppants settled by 17.9% (see Table 4.57). The lower flow rate impacted the amount of settlement when using the bottom perforation by enhancing the rolling mechanism.

Table 4.56: The equilibrium dune heights in inches for 100 mesh at 1 gal/min after 35 minutes of treatment.

Perforation Locations	Section A	Section B	Section C
Top Perforation	4.25	4.50	3.25
Bottom Perforation	7.00	4.50	2.75

Table 4.57: The volume in inch^{3}of proppant settled at 1 gal/min.

Perforation Locations	Section A	Section B	Section C	Total
Top Perforation	4.89	2.33	1.28	8.50
Bottom Perforation	6.30	2.55	1.50	10.35

At the flow rate of 2 gal/min injection from the top perforation, the dune height was increased in section A by 48.5% and increased section C by 25%. The bottom perforation increased the dune height of section B by 9.5%. According to the calculated volume of the settled proppants, pumping from the top perforation increased the volume of proppants by 15.2% (see Table 4.59). The results indicate that the increased flow rate increases the volume of the settled proppants in sub-fracture C from the top perforation. The dominant mechanism is turning a corner by means of suspension.

Table 4.58: The equilibrium dune heights in inches for 100 mesh at 2 gal/min after 25 minutes of treatment

Perforation Locations	Section A	Section B	Section C
Top Perforation	8.25	4.75	3.00
Bottom Perforation	4.25	5.25	2.25

Table 4.59: The volume in inch^3 of proppant settled at 2 gal/min

Perforation Locations	Section A	Section B	Section C	Total
Top Perforation	6.30	2.55	1.50	10.35
Bottom Perforation	5.40	2.03	1.35	8.78

For 40/70 mesh, Tables 4.60 and 4.61 show the proppant dune heights in sub-fracture C at 1 gal/min and 2 gal/min for both perforation locations with 40/70 mesh as proppant. At the flow rate of 2 gal/min, injection from the top perforation increased the dune height in section A by 25%, in section B by 12.5% and in section C by 8.3%. According to the calculated volume of the settled

proppants, pumping from the bottom perforation at one gallon per minute increased the volume of proppants by 14.3% (see Table 4.61).

Table 4.60: The equilibrium dune heights in inches for 40/70 mesh at 1 gal/min after 35 minutes of treatment.

Perforation Locations	Section A	Section B	Section C
Top Perforation	5.00	4.00	3.00
Bottom Perforation	3.75	3.50	2.75

Table 4.61: The volume in inch^3 of proppant settled at 1 gal/min.

Perforation Locations	Section A	Section B	Section C	Total
Top Perforation	3.38	1.89	1.37	6.64
Bottom Perforation	5.06	2.03	1.35	7.75

At the flow rate of 2 gal/min, injection from the bottom perforation decreased the dune height in section A by 39.2%, in section B by 18.2%, and in section C by 21.4%. According to the calculated volume of the settled proppants, pumping from the bottom perforation increased the volume of proppants by 15.6% (see Table 4.62). Rolling and sliding were the dominant mechanisms.

Table 4.62: The equilibrium dune heights in inches for 40/70 mesh at 2 gal/min after 25 minutes of treatment.

Perforation Locations	Section A	Section B	Section C
Top Perforation	4.50	4.50	2.75
Bottom Perforation	7.40	5.50	3.50

Table 4.63: The volume in inch^3 of proppant settled at 2 gal/min.

Perforation Locations	Section A	Section B	Section C	Total
Top Perforation	4.73	2.25	1.375	8.33
Bottom Perforation	6.19	2.33	1.35	9.87

During the experiments, different flow mechanisms were observed when the slurry was going into the sub-fractures and traveling through them. The 100 mesh travelled into sub-fractures B and A by suspension, sliding and rolling at 1 and 2 gal/min, while the 40/70 mesh traveled as a bed load into these sub-fractures. For sub-fracture C, the 100 mesh rolled and slid into the fracture

because of its distance from the main slot entry, even when the flow rate was doubled. This was due to sub-fracture C being angled against the direction of the flow, and the suspended proppants hitting the wall, causing settling and then ultimately sliding into the fracture. In the sub-fractures, the flow velocity decreased which caused the proppants to settle quicker as the drag forces became weaker. Also, the sub-fractures have a smaller width than the main fracture, which increased the settling rate because of more particle-particle and particle-wall contact. In the sub-fractures A and C, the proppant travelled by rolling and sliding, but the sub-fracture B was able to transport by suspension because it was in the direction of the flow. In conclusion, for the two perforation locations in terms of height, the obtained results showed the following:

1. As slurry was pumped from the top perforation, the particles experienced drag and buoyancy forces that cause the heavier particles to settle while lighter particles traveled further into the slot via suspension. When the slurry was pumped into the slot from the bottom perforation the 40/70 mesh settled 3 minutes faster and created a 20% larger dune than the 100 mesh. Although both proppant sizes have the same specific densities, their accumulated particles have a weight (gravity) that worked against the lifting force of the fluid.
2. When pumping from the top perforation, the concentration of the proppant in the slots increased as the injection time increased. Therefore, the lifting force of the fluid is not sufficient to move the particles. The increased concentration increases the velocity of the flow and results in more particle-particle and particle-wall interactions. When pumping from the bottom of the wellbore, the slurry flowed until the flow area was blocked. With more time the settled particles roll and slide until more particles are transported into the fracture to create larger dunes.
3. Observing the transport of the 40/70 mesh in the main slot and injecting from the bottom of the wellbore creates a parabolic dune while injection from the top of the wellbore creates a linear dune. As the slurry is injected from the top of the slot, the heavier particles interact with the side of the wall and fall to the bottom of the slot.
4. The intermediate and smaller particles travelled with the fluid in the form of saltation and suspension. Because of the available flow area, the lift force of the fluid acting on the particle is greater than the gravitational force and reduces its tendency to fall.

Subsequently, as the slurry is injected from the bottom of the perforation, the particles accumulate at the bottom of the fracture. As the injection continues the settled proppant reduces the flow area and increases the velocity of the flow and the interaction between particles. The interaction between the particles reduces their terminal velocity and increases the gravitational effects.

5. At 2 gal/min using the top of the wellbore, the drag force was higher than 1 gal/min. This did increase the number of particles that interacted with the wall of the fracture and settled at the bottom of the fracture. Therefore, there is more initial settling at 1 gal/min than at 2 gal/min in both the 40/70 and the 100 mesh than was expected.
6. Using the bottom of the wellbore, the higher velocity increased the proppant transportability, increased the drag force, reduced the dune height by 57% and increased the dune length by 12%. In conclusion, the distribution of the proppant is increased when the pump rate is raised.

CHAPTER 5

NUMERICAL MODELING RESULTS

This chapter describes numerical modeling of the proppant transport and proppant settling in the experimental fracture network. The numerical model used is called Fluent which is a module of the ANSYS software. Fluent is a powerful multi-physics computational fluid dynamics (CFD) software which uses Navier-Stokes flow equations as the transport model. While the model was used to simulate transport and particle settling in laboratory experiments, it can also be used in field applications. The transport model parameters include injection rate, proppant size and density, and fluid rheology (Newtonian and Non-Newtonian). Water and slickwater, at several concentrations of friction reducers, were used as the transport fluid.

Using the numerical model Fluent, the effect of particle size, particle density, injection rate, and fluid viscosity on proppant settling and the ultimate shape of the proppant dunes in the L- and V-shaped fractures was studied. Slickwater rheology was modeled as a non-Newtonian power-law fluid. The numerical model results indicated that fracture width and fluid viscosity had the most significant impact on proppant placement in the fractures while the sand size and density had a lesser impact on the distribution of the proppant in fractures. The fracture network geometry, such as bends and angles, had the least impact on the proppant transport and settling.

5.1 Modeling Description

This section describes modeling of proppant transport and proppant settling in the fracture network. The simulation cases of the CFD are divided in 18 different simulation runs, six runs for each fluid systems (water- slickwater at 1 gal/1000 gal friction reducer, and 2 gal/1000 gal of friction reducer) based on two different injection flow rates, 1 gal/min and 2 gal/min and three proppant sizes 40/70, 100, and 14/40 mesh. Figure 5.1 shows the models run and discussed in this chapter.

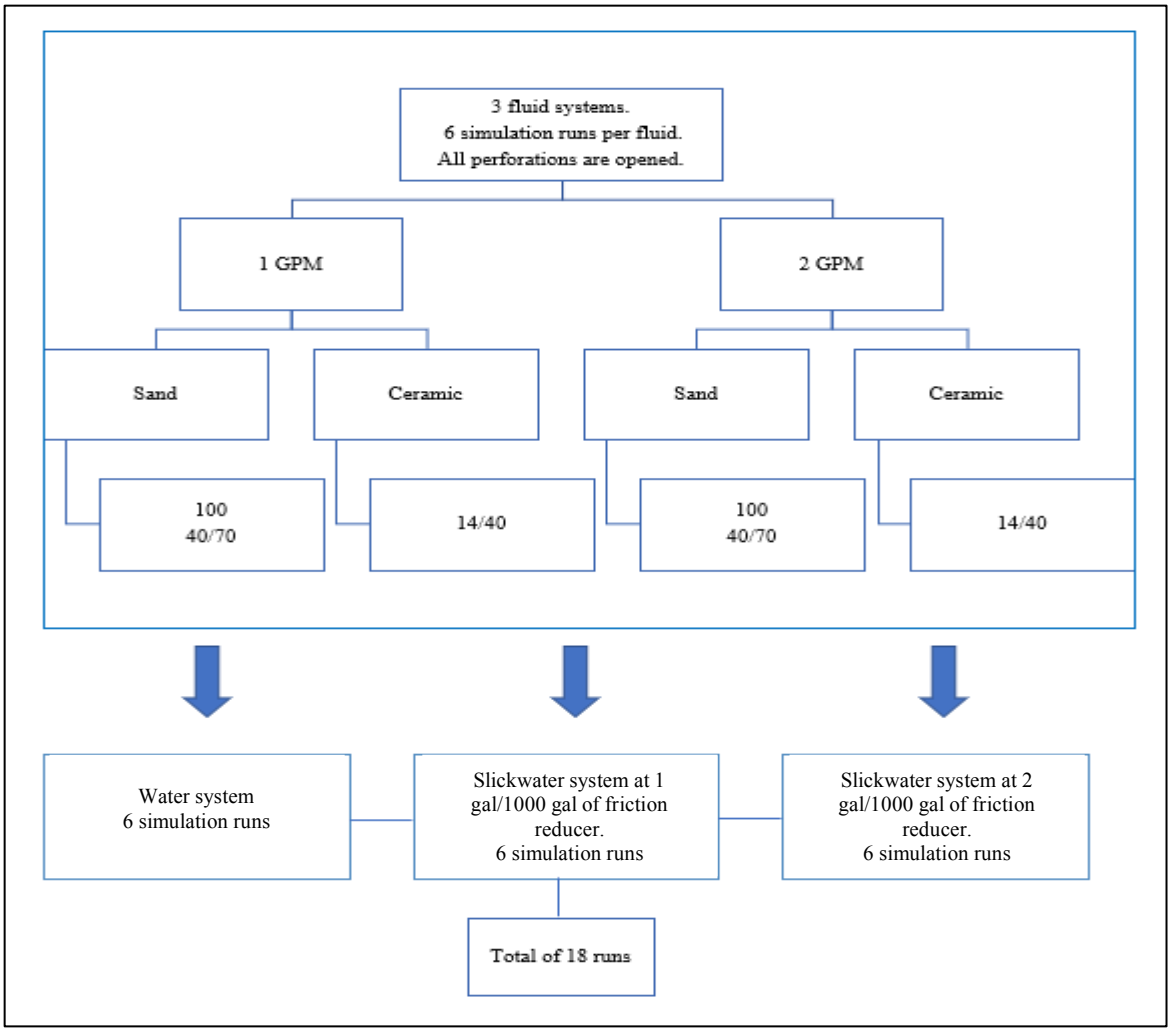

Figure 5.1: Simulation runs of different systems.

5.2 ANSYS Numerical Model

ANSYS software provides a comprehensive suite of computational fluid dynamic (CFD) software for modeling fluid flow problems. Specifically, it offers fluid flow analysis capabilities and provides tools needed to design and optimize new fluid equipment and to troubleshoot the existing installations. The primary ANSYS software products are ANSYS Fluent and ANSYS CFX with a wide range of applications: aerodynamics, combustion, hydrodynamics, particle dispersion, reacting flows, heat transfer, and much more. The ANSYS Fluent and ANSYS CFX graphics can show how fluid flow, particle flow, heat transfer, chemical reactions, combustion, etc. evolve with time.

5.3 Mathematical Modeling

The fracture width, height, and length in the experimental model are the same as what has been used in the laboratory experiments. SpaceClaim and DesignModeler modules were used to sketch the geometry of the fractures in 3D domain (Figure 5.2). The geometry was imported to the Fluent meshing system to generate the grid system for numerical modeling.

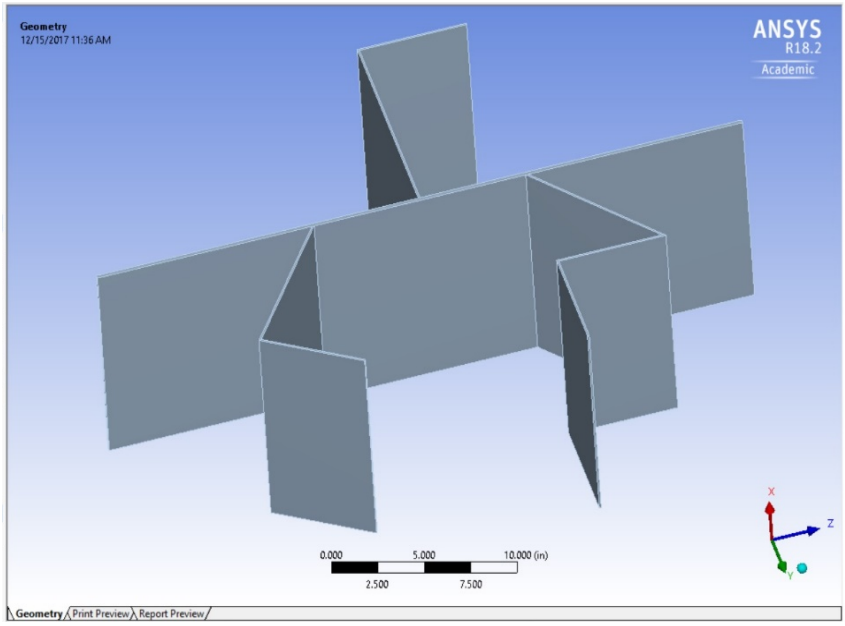

Figure 5.2: The sketch of the fracture network in the experiments.

The mesh size affects the accuracy and speed of the computation. Figure 5.2 shows the grid system devised for the numerical model. A fine mesh of uniform quadrilaterals (455,930) nodes was chosen over a coarse mesh to improve numerical accuracy; however, this caused a significant increase in computer memory and processing time.

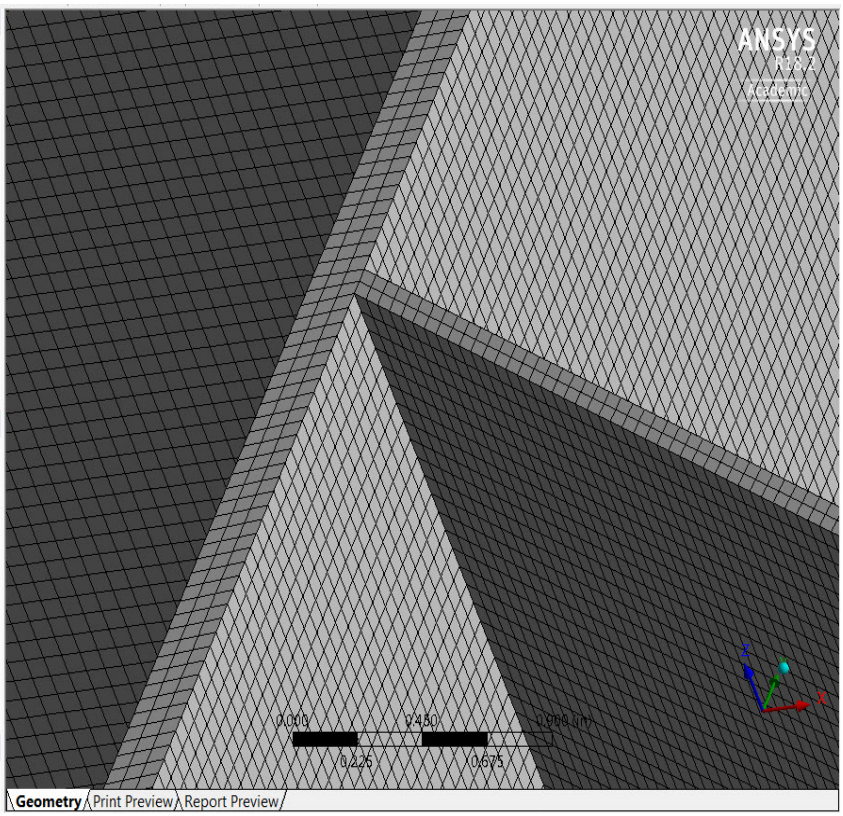

Figure 5.3: The grid system for the fracture network.

The Navier-Stokes (NS) equation (Eq. 5.1) was used to model proppant transport and settling in the laboratory experiments.

$$\rho\left(\frac{\partial v}{\partial t} + v.\nabla v\right) = -\nabla p + \mu\nabla^2.v + F \tag{5.1}$$

Where,

ρ = density of fluid, ML^{-3} $\left[\frac{\text{Mass}}{\text{Volume}}\right]$

v = velocity vector field , LT^{-1} $\left[\frac{\text{Length}}{\text{Time}}\right]$

p = pressure , FL^{-2} $\left[\frac{\text{Force}}{\text{Length 2}}\right]$

μ = viscosity , $ML^{-1}\ T^{-1}$ $\left[\frac{\text{Mass}}{\text{Length x Time}}\right]$

F = external force , F (= MLT^{-2}) $\left[\frac{\text{Mass x Length}}{\text{Time 2}}\right]$

The ANSYS module DDPM, the dense discrete phase model, was used for the proppant transport and distribution in the fracture network, and the Euler granular code was used to model

proppant settling. Both Eulerian and Lagrangian coordinates are used in the numerical model. The Eulerian coordinate is a fixed coordinate while the Lagrangian coordinate follows the flow of the phase front (i.e., front tracking as in the Buckley-Leverett displacement calculations). Mathematically, this can be explained using the following equation:

$$\underbrace{\frac{\partial f}{\partial t}}_{\substack{\text{Eulerian}\\ \text{Time Derivative}\\ \text{in Fixed}\\ \text{Coordinates}}} + \vec{v}.\nabla f = \underbrace{\frac{Df}{Dt}}_{\substack{\text{Lagrangian}\\ \text{Time Derivative}\\ \text{in Moving}\\ \text{Coordinates}}} \tag{5.2}$$

Where, $\vec{v}$ is the stream velocity and f a function such as the density of proppant particles.

As mentioned earlier, the Eulerian granular model was used to simulate proppant transport in fractures. In this model, the proppants and carrying fluid are treated as separate phases. While each phase follows its own mass, momentum and energy conservations, the transport between different phases is counted via interfacial terms. For instance, the granular model uses interfacial terms to account for collisional and frictional effects, and the drag coefficients are based on single particle drag plus the concentration principles. The wall effects are also included.
The mass balance of the fluid phase in the transport model is:

$$\frac{\partial}{\partial t}\left(\alpha_f \rho_f\right) + \nabla.\left(\alpha_f \rho_f \overrightarrow{V_f}\right) = \sum_{p=1}^{n}\left(\dot{m}_{pf} - \dot{m}_{fp}\right) \tag{5.3}$$

Where,

α_f = volume fraction component of phase f (dimensionless)

$\overrightarrow{V_f}$ = velocity of phase f, LT^{-1} $[\frac{\text{Length}}{\text{Time}}]$

ρ_f = density of f, ML^{-3} $[\frac{\text{Mass}}{\text{Volume}}]$

$\dot{m}\_pf$ = mass transfer from phase p to f, LT^{-1} $[\frac{\text{Length}}{\text{Time}}]$

$\dot{m}_{fp}$ = mass transfer from phase f to p, LT^{-1} $[\frac{\text{Length}}{\text{Time}}]$

Similarly, the momentum balance for the fluid phase is:

$$\frac{\partial}{\partial t}\left(\alpha_f \rho_f \overrightarrow{V_f}\right) + \nabla.\left(\alpha_f \rho_f \overrightarrow{V_f}\overrightarrow{V_f}\right) = -\alpha_f \nabla \mathrm{p} + \nabla.\bar{\bar{\tau}}_f + \alpha_f \rho_f \overrightarrow{g} + \sum_{p=1}^{n}\left[K_{pf}\left(\overrightarrow{V_p} - \overrightarrow{V_f}\right) + \dot{m}_{pf}\overrightarrow{V_{pf}} - \dot{m}_{fp}\overrightarrow{V_{fp}}\right] + \left(\vec{F}_f + \vec{F}_{lift,f} + \vec{F}_{wl,f} + \vec{F}_{vm,f} + \vec{F}_{td,f}\right) \quad (5.4)$$

Where,

$\overrightarrow{g}$ = acceleration due to gravity , $\mathrm{LT}-2$ $\left[\frac{\text{Length}}{\text{Time 2}}\right]$

$\bar{\bar{\tau}}_f$ = the stress − strain tensor which is calculated with the following equation:

$\bar{\bar{\tau}}_f = \alpha_f \mu_f\left(\nabla\overrightarrow{V_f} + \nabla\overrightarrow{V_f}^{T}\right) + \alpha_f\left(\lambda_f - \frac{2}{3}\mu_f\right)\nabla.\overrightarrow{V_f}\bar{\bar{I}}$

μ_f = shear viscosity of f, $\mathrm{ML^{-1}\ T^{-1}}$ $\left[\frac{\text{Mass}}{\text{Length x Time}}\right]$

λ_f = bulk viscosity of f , $\mathrm{ML^{-1}\ T^{-1}}$ $\left[\frac{\text{Mass}}{\text{Length x Time}}\right]$

$K_{pf},\ K_{fp}$ = interphase momentum exchange coefficient , $\mathrm{ML^{-3}T^{-1}}$ $\left[\frac{\text{Mass}}{\text{Volume x Time}}\right]$

$\vec{V}_{fp}, \vec{V}_{pf}$ = interphase velocity , $\mathrm{LT^{-1}}$ $\left[\frac{\text{Length}}{\text{Time}}\right]$

$\vec{F}_f$ = external body fluid , F (= $\mathrm{MLT^{-2}}$) $\left[\frac{\text{Mass x Length}}{\text{Time 2}}\right]$

$\vec{F}_{lift,f}$ = the lift force of the f , F (= $\mathrm{MLT^{-2}}$) $\left[\frac{\text{Mass x Length}}{\text{Time 2}}\right]$

$\vec{F}_{wl,f}$ = wall friction (dimensionless)

$\vec{F}_{vm,f}$ = virtual mass force (dimensionless)

$\vec{F}_{td,f}$ = turbulent dispersion force (dimensionless)

The conservation of momentum for the particle phase (subscript p) is:

$$\frac{\partial}{\partial t}\left(\alpha_p \rho_p \overrightarrow{V_p}\right) + \nabla.\left(\alpha_p \rho_p \overrightarrow{V_p}\overrightarrow{V_p}\right) = -\alpha_p \nabla p - \nabla p_p + \nabla.\bar{\bar{\tau}}_p + \alpha_p \rho_p \overrightarrow{g} + \sum_{p=1}^{n}\left[K_{fp}\left(\overrightarrow{V_f} - \overrightarrow{V_p}\right) + \dot{m}_{fp}\overrightarrow{V_{fp}} - \dot{m}_{pf}\overrightarrow{V_{pf}}\right] + \left(\vec{F}_p + \vec{F}_{lift,p} + \vec{F}_{wl,p} + \vec{F}_{vm,p} + \vec{F}_{td,p}\right) \quad (5.5)$$

Where,

p_p = pressure of particle , $\mathrm{FL^{-2}}$ $\left[\frac{\text{Force}}{\text{Length 2}}\right]$

K_{fp} = momentum exchange coeffient , $\mathrm{ML^{-3}T^{-1}}$ $\left[\frac{\text{Mass}}{\text{Volume x Time}}\right]$

$\vec{F}_p$ = external body particle , F (= $\mathrm{MLT^{-2}}$) $\left[\frac{\text{Mass x Length}}{\text{Time 2}}\right]$

$\vec{F}_{lift,p}$ = the lift force of the p , F (= $\mathrm{MLT^{-2}}$) $\left[\frac{\text{Mass x Length}}{\text{Time 2}}\right]$

$\vec{F}_{wl,p}$ = wall friction (dimensionless)

$\vec{F}_{vm,p}$ = virtual mass force (dimensionless)

$\vec{F}_{td,p}$ = turbulent dispersion force (dimensionless)

The Syamlal et al. (1993) equation was used to calculate particle pressure:

$$p_p = 2\rho_p(1 + e_{pp})\alpha_p^2 g_{0,pp}\theta_p \quad (5.6)$$

e_{pp} = coefficient of restitution for particle collisions (dimensionless)

$g_{0,pp}$ = radial distribution function (dimensionless)

θ_p = granular temperature, K

$$\bar{\bar{\tau}}_p = \alpha_p\mu_p\left(\nabla\overrightarrow{V_p} + \nabla\overrightarrow{V_p}^T\right) + \alpha_p(\lambda_p - \tfrac{2}{3}\mu_p)\nabla.\overrightarrow{V_p} \quad (5.7)$$

$$\mu_p = \mu_{p,col} + \mu_{p,kin} + \mu_p, fr \quad (5.8)$$

$$\mu_{p,col} = \tfrac{4}{5}\alpha_p^2\rho_p d_s g_{0,pp}(1 + e_{pp})\left(\tfrac{\theta_p}{\pi}\right)^{\frac{1}{2}} \quad (5.9)$$

$$\mu_{p,kin} = \frac{\alpha_p\rho_p d_p\sqrt{\theta_p\pi}}{6(3-e_{pp})}\left[1 + \tfrac{2}{5}(1 + e_{pp})(3e_{pp} - 1)\alpha_p g_{0,pp}\right] \quad (5.10)$$

The frictional component of particle shear velocity is based on Johnson et al. (1990) formula:

$$\mu_p, fr = 0.1\alpha_p\frac{(\alpha_p - \alpha_{p,\min})^n}{(\alpha_p,max - \alpha_p)^c}sin\emptyset \quad (5.11)$$

Where,

$\emptyset$ = angle of internal friction [degree]

n = 2 and c = 5 (Ocone et al.1993)

d_p = particle diameter, m [Length]

Bulk viscosity is based on Lun et al. (1984):

$$\lambda_p = \tfrac{4}{3}\alpha_p^2\rho_p d_s g_{0,ss}(1 + e_{pp})\left(\tfrac{\theta_p}{\pi}\right)^{\frac{1}{2}} \quad (5.12)$$

The trajectories of the discrete particle phase are calculated by integrating the force balance on the particle in a Lagrangian reference frame. The force balance equates the forces acting on the particle with the particle inertia (Eq. 5.13).

$$\frac{du_p}{dt} = F_D(u - u_p) + \frac{gx(\rho_p - \rho)}{\rho_p} + F_x \tag{5.13}$$

Where,

$F_x = acceleration\ term\ \left(\frac{force}{unit\ particle}\right)$

$F_D(u - u_p) = drag\ force\ per\ unit\ particle\ mass$

$F_D = \frac{18\mu}{\rho_p d_p^2} \frac{C_D Re}{24}$

u = fluid phase velocity (m/sec) $[\frac{\text{Length}}{\text{Time}}]$

u_p = particle velocity (m/sec) $[\frac{\text{Length}}{\text{Time}}]$

μ = fluid viscosity (kg/m. sec) $[\frac{\text{Mass}}{\text{Length x Time}}]$

ρ = fluid density (kg/m^3) $[\frac{\text{Mass}}{\text{Volume}}]$

ρ_p = density of particle (kg/m^3) $[\frac{\text{Mass}}{\text{Volume}}]$

d_p = particle diameter (m) [Length]

$Re = \frac{\rho d_p |u_p - u|}{\mu}$

Particle motion is described as:

$$\frac{dx}{dt} = u_p \tag{5.14}$$

$$\frac{du_p}{dt} = \frac{1}{\tau_p}(u - u_p) + a \tag{5.15}$$

Where,

a = acceleration terms due to all forces except drag

The particle velocity at a new location is calculated from:

$$u_p^{n+1} = u^n + e^{-\frac{\Delta t}{\tau_p}}(u_p^n - u^n) - a\tau_p\left(e^{-\frac{\Delta t}{\tau_p}} - 1\right) \tag{5.16}$$

New particle location is calculated as:

$$x_p^{n+1} = x_p^n + \Delta t\left(u^n + a\tau_p\right) + \tau_p\left(1 - e^{-\frac{\Delta t}{\tau_p}}\right)\left(u_p^n - u^n - a\tau_p\right) \quad (5.17)$$

The Euler implicit discretization is:

$$\frac{(u_p^{n+1} - u_p^n)}{\Delta t} = \frac{1}{\tau_p}\left(u^* - u_p^*\right) + a^n \quad (5.18)$$

$$u_p^* = \frac{1}{2}\left(u_p^n + u_p^{n+1}\right) \quad (5.19)$$

$$u^* = \frac{1}{2}\left(u^n + u^{n+1}\right) \quad (5.20)$$

$$u^{n+1} = u^n + \Delta t u_p^n . \nabla u^n \quad (5.21)$$

New particle velocity at the new location n+1 is:

$$u_p^{n+1} = \frac{u_p^n\left(1 - \frac{1\Delta t}{2\tau_p}\right) + \frac{\Delta t}{\tau_p}\left(u^n + \frac{1}{2}\Delta t u_p^n . \nabla u^n\right) + \Delta t a}{1 + \frac{1\Delta t}{2\tau_p}} \quad (5.22)$$

In the numerical model, the fracture geometry and grid are fixed in space thus they are specified as data. Then, the proppant distribution and movement in the fracture are tracked as continuum using Lagrangian coordinates (front tracking).

The proppant transport was modeled using a diameter distribution method of Rosin-Rammler, which uses minimum, maximum, and average diameter of proppants to generate proppant distribution. The proppants used were 40/70, 100, and 14/40 mesh. The CFD modeling uses proppant and fracturing fluid as two separate components in a single fluid mixture (the slurry), and the viscosity of the mixture is calculated based on the kinetic theory of granular flow.

5.4 Laboratory Models and Numerical Modeling

In this research, three different viscosities were used to represent three different fracturing fluids 1 cp, 12 cp and 15 cp. In hydraulic fracturing, the fluid leakage from such fluids could cause significant water blockage and lower matrix permeability in pores at the fracture face regions in tight reservoirs. However, in the experimental apparatus, the fracture surfaces were impermeable to the fracturing fluids. The fracture in the experimental model was initially filled with fracturing fluid without proppant, and there was one injection inlet and four production outlets. The inlet

flow rates were 1 gal/min (8 ft/min) and 2 gal/min (16 ft/min), and the injection time was 35 min for 1 gal/min and 25 min for 2 gal/min. The proppant concentration was 2 ppg. The experimental model was designed to investigate the impacts of the following parameters on proppant transport: fluid viscosity, proppant density, proppant size, and injection rate. The parameters used in the model runs are shown in Table 5.1.

Table 5.1: Parameters Used In Numerical Modeling Based on Experimental Measurements

Property	Symbol	Unit	Value
Particle diameter	d_p	inch	0.0394, 0.0331, 0.0278, 0.0234, 0.0197, 0.0165, 0.0139, 0.0177, 0.0098, 0.0083, 0.0070, 0.0059
Particle density	ρ_p	lb/ft^3	165.43, 165.43, 65.50
Fluid density	ρ	lb/gal	8.33, 11.80, 14.80
Fluid dynamic viscosity	μ	cp	1, 12, 15
Fluid injection rate	v_{in}	ft/s	8, 16
Particle injection volumetric concentration	c_p	ppg	2
Time step size(s)	Δt	s	0.001
Injection time	t	s	1500, 2100
Number of time steps	N	unitless	3000

5.5 Model Flowchart

Figure 5.4 shows the numerical model flowchart.

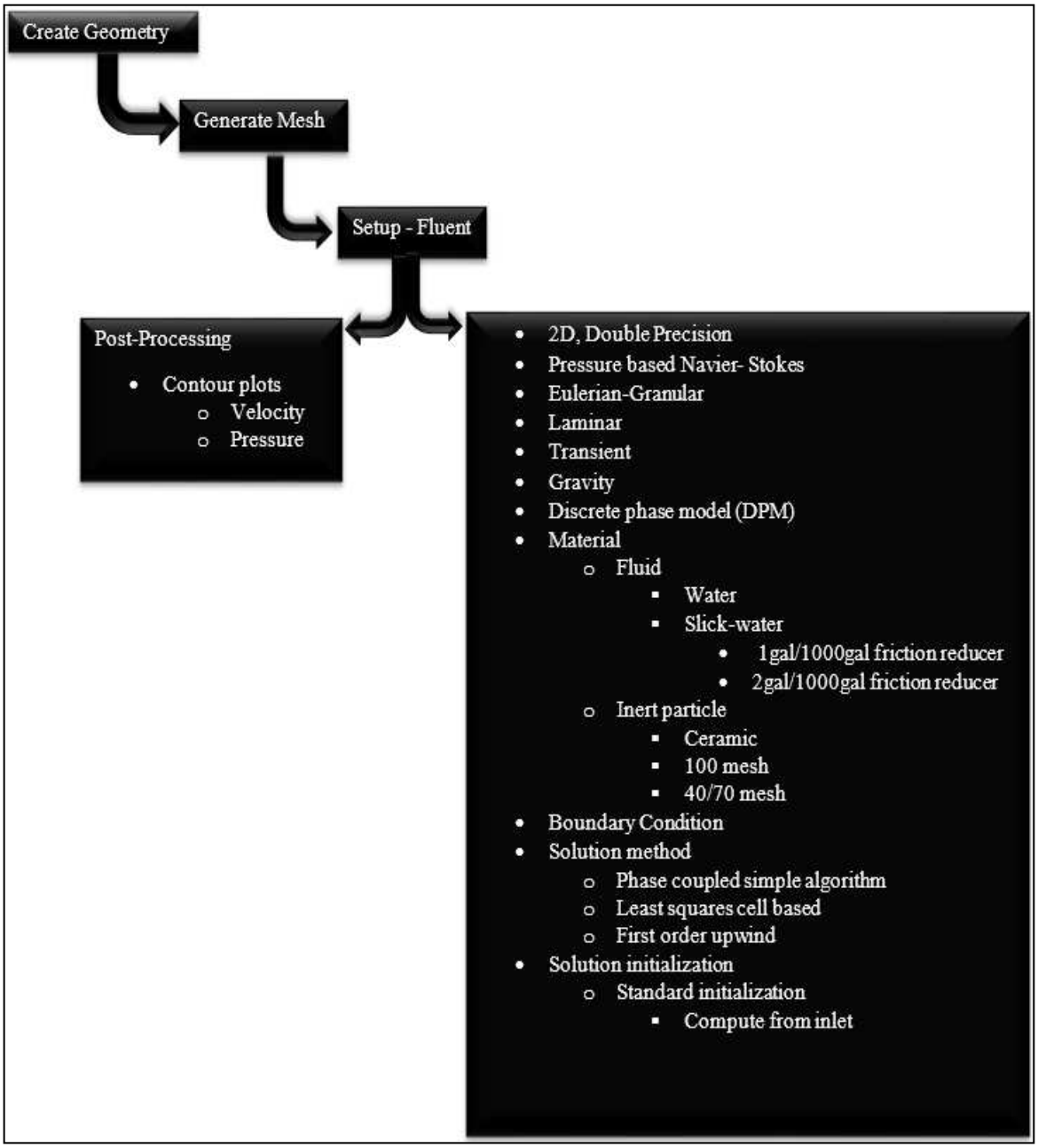

Figure 5.4: Numerical Model Flowchart.

5.6 Numerical Model Results

This section discusses the impact of fluid viscosity, proppant size and density, and injection rate on proppant transport in the fracture network.

5.6.1 General Observations

Figure 5.5 presents the slurry velocity field and the corresponding Reynolds number after 1500 seconds of the slurry injection for a numerical experiment. These plots indicate decreasing slurry concentration along the length of the fracture because of proppant settling.

Figure 5.6 shows the proppant amount for every particle size at 1500 seconds of injection and a proppant bed in the entire fracture network. Several additional runs were conducted in a similar manner but with different input parameters. These experiments demonstrate the propagation of varying size-dunes. The runs also show that smaller proppants propagate faster than the larger ones. In the sub-fracture groups, the numerically modeled proppant transport was similar to the experimental model.

5.6.2 The Impact of Fluid Viscosity

Figure 5.7 shows the numerical model results of using three different fluid systems: (1) The left panel is particle distributions of 40/70 mesh using water system. (2) The right panel is particle distributions of 40/70 mesh using slickwater at 1 gal/1000 gal of friction reducer. (3) The bottom panel shows particle distributions of 40/70 mesh using slickwater at 2 gal/1000 gal of friction reducer. All panels show a rate of at 2 gals/min. Specifically, the numerical model indicated that higher viscosity treating fluids suspend proppants better in the stream because of larger drag forces, resulting in more effective transport of the proppants.

Specifically, comparing the laboratory experimental results with the ANSYS model numerical simulation results leads to the following observations:

1. Proppant concentration in the experiment and ANSYS numerical simulation are similar in the entire fracture network.

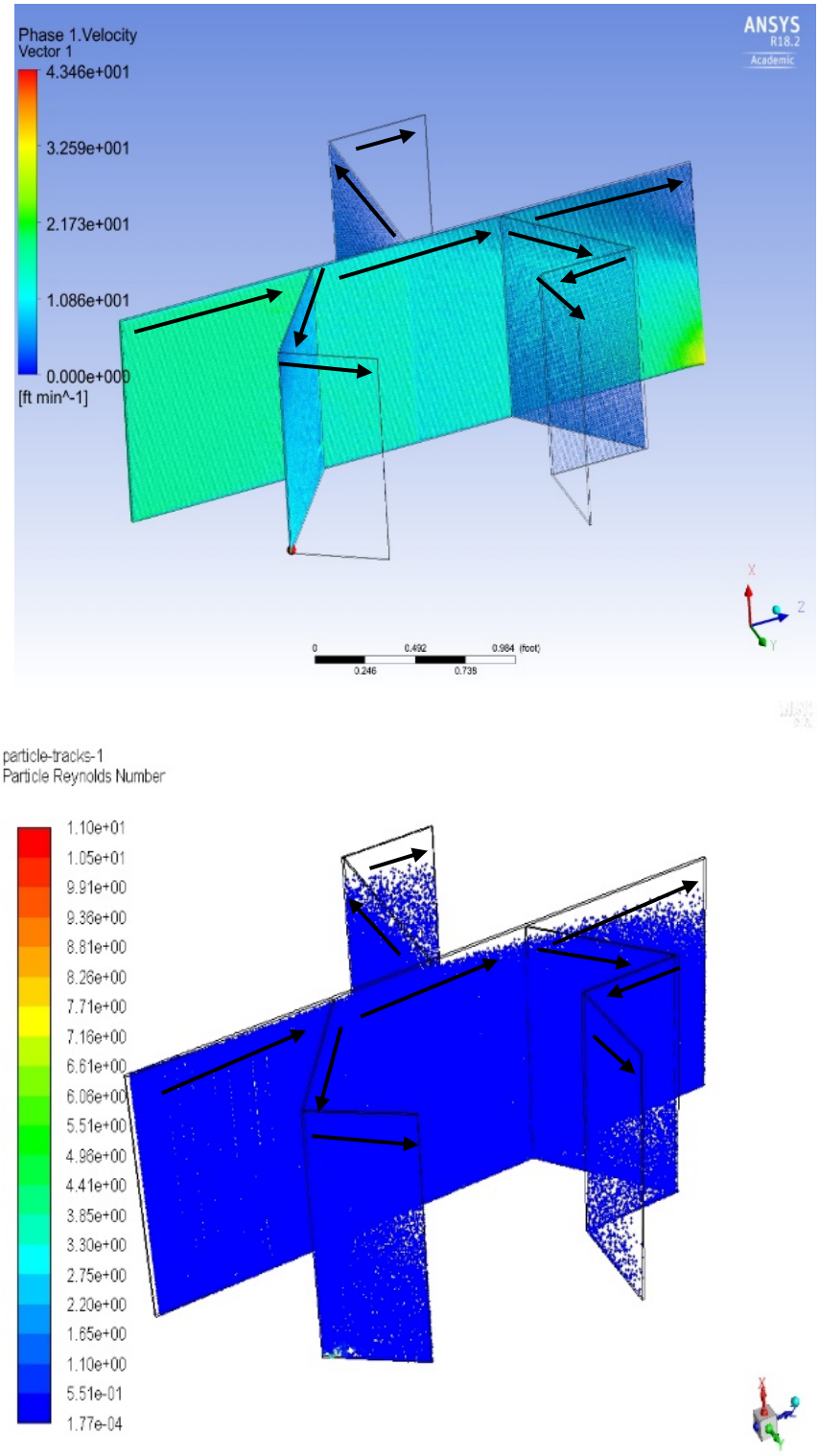

Figure 5.5: The top diagram presents the velocity field (in ft/min) in the fracture network, at 1500 seconds, for 100 mesh proppant in slickwater, consisting of 2 gallons of friction reducer per 1000 gallons of water, at 2 gal/min of injection. The bottom diagram shows the Reynolds numbers for flow in the fracture network.

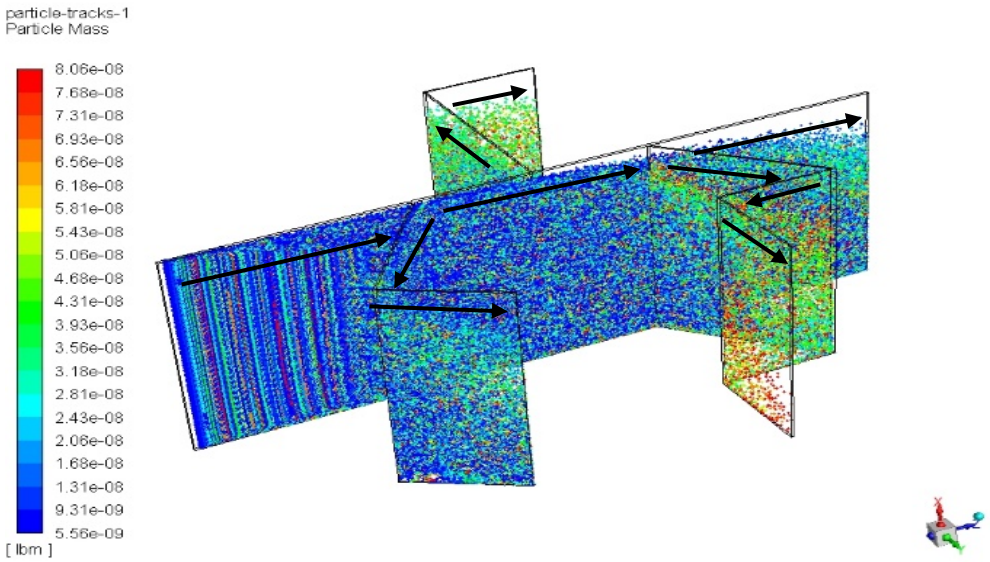

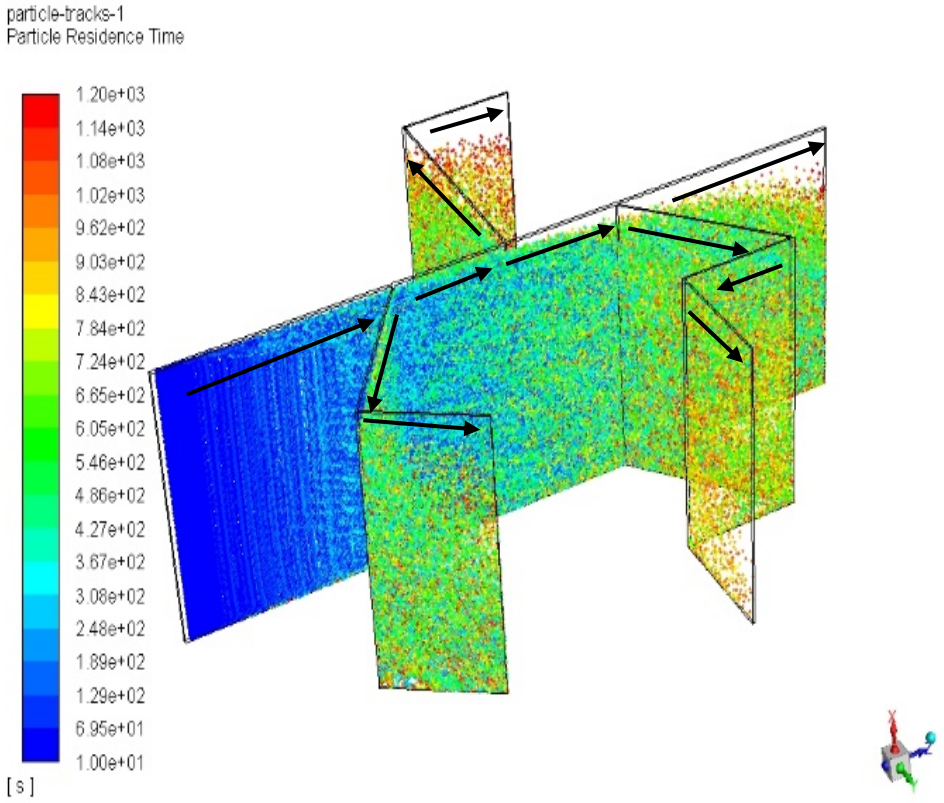

Figure 5.6: The top diagram shows the distribution of particle mass for the same system as shown in Figure 5.5. The bottom diagram presents the particle residence time.

2. The sub-fractures, both in the experiment and ANSYS numerical model, have lower propped fracture heights for the low viscosity fracturing fluids. The ANSYS yielded propped height of 2% - 30% in the sub-fractures compared to the laboratory experiments which resulted in differences of 7% - 15%.
3. ANSYS simulation indicated that the high viscosity fracturing fluids transport proppants more effectively in sub-fractures.
4. Both the numerical and experimental results indicate that acute fracture angles lower the sand entry rate which impacts the quality of the proppant placement in the fractures.
5. The proppant transport path follows the flow streamlines; therefore, it is sensitive to the degree of branching and turning. For instance, the numerical model indicated that acute angles yielded 3-5% less flow into the branch compared to the obtuse angles which yielded 10-15%. On the other hand, the experimental research showed 5-8% in the acute angles and 10-23% in the obtuse angles.
6. The numerical model indicated that the 15 cp viscosity fluid yielded a higher propped height than the 1cp viscosity fluid - 30% for the 15 cp fluid and 2% for 1 cp fluid.

5.6.3 The Impact of Proppant Size and Density

The sand proppant used for the experiments were 40/70 and 100 mesh, while the ceramic proppant was 14/40 mesh of ultra-light weight. The numerical model indicated that the diameter of the proppant affects the settling rate and proppant transport in slickwater slurries. Heavier proppants are harder to lift and so they settle readily to the slot bottoms. The larger the diameter, the greater the proppant settling leading to less effective transport in the fractures.

Figure 5.8 shows the simulation results using three proppant sizes**.** The upper panel is particle distributions for the 100 mesh proppant, the middle panel is particle distributions for the 40/70 mesh proppant, and the lower panel shows particle distributions for the 14/40 mesh proppant. All simulations were conducted using 1 gal friction reducer/1000 gal of water at 1 gal/min.

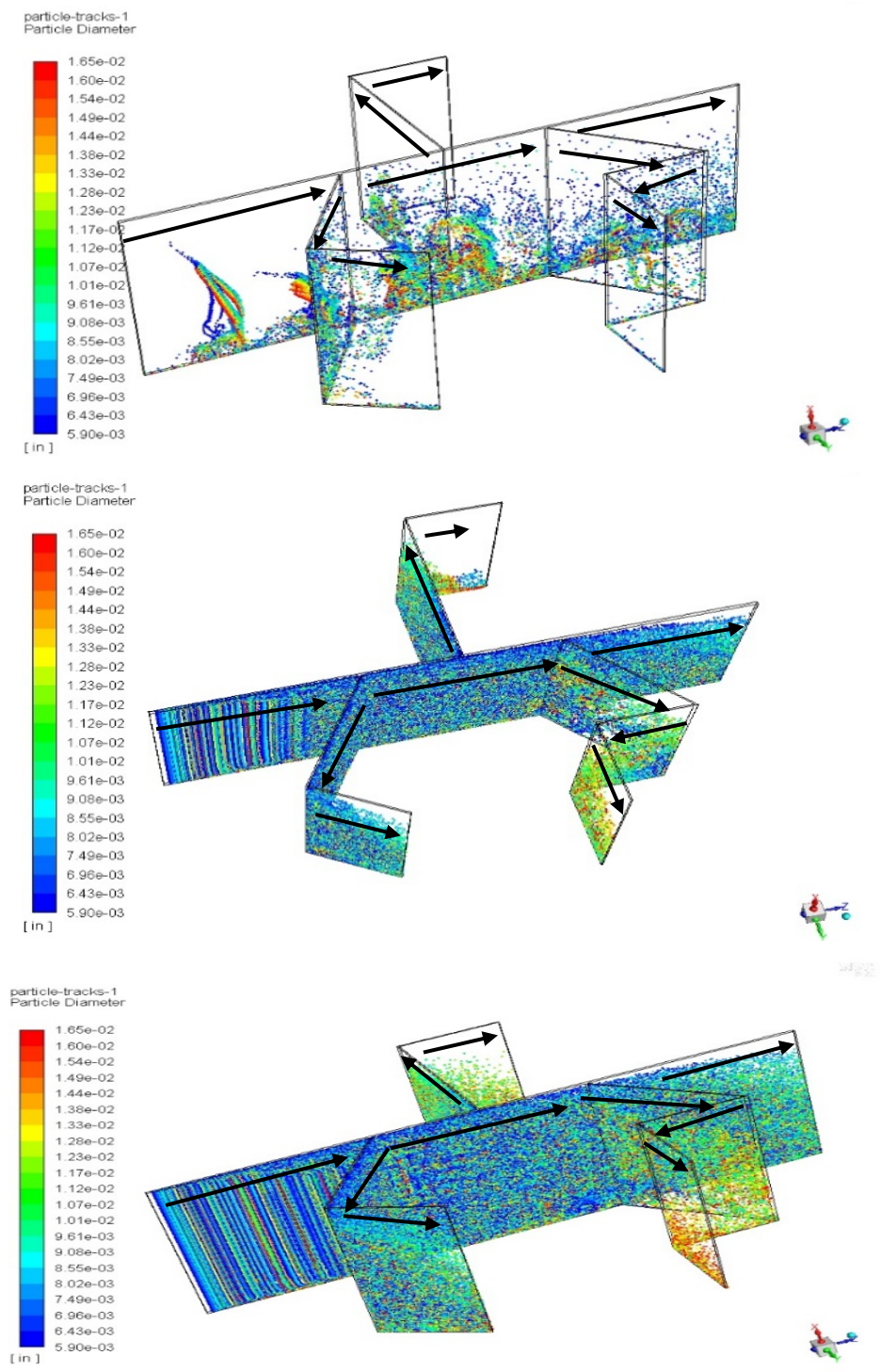

Figure 5.7: This figure shows the results of using three different fluid systems. The top panel is particle distributions of 40/70 mesh using water system. The middle panel is particle distributions of 40/70 mesh using slickwater at 1 gal/1000 gal of friction reducer. The bottom panel shows particle distributions of 40/70 mesh using slickwater at 2 gal/1000 gal of friction reducer. The simulation and experiments were conducted at 2 gal/min.

Comparing the laboratory results with the ANSYS simulation results led to the following observations:

1. The low viscosity fluid experiments indicated that the 40/70 mesh proppant underwent more settling than the 100 mesh proppant near the wellbore.
2. The ANSYS simulation of low viscosity fluid yielded settling of 40% compared to the laboratory experiments of 49%.
3. The high viscosity fluid experiments indicated that the onset of settlement happened further away and was not close to the wellbore.
4. The low viscosity fluid yielded better transport for the 100 mesh proppant than the 40/70 mesh proppant.
5. The numerical model indicated that the 40/70 mesh in the low-viscosity fluid yielded a much higher propped height than the 100 mesh. Also, the numerical model yielded 8% compared to laboratory experiments which resulted 9.4%.
6. In the numerical model, the high fluid viscosity yielded a more even proppant distribution consistent with the experimental results.
7. In the numerical model of the low viscosity fluid transport**,** the ultra-light weight proppant settled in the fracture network while experiments indicated that there was no settlement.
8. In the numerical model of the low viscosity fluid, the ultra-light weight proppant had a greater propped height than the denser sand in the main fracture. The numerical simulation yielded 20% for the ultra-light weight, which offer much better vertical coverage area of proppant.
9. In the numerical model of the low viscosity fluid, the ultra-light weight proppant had a greater propped height than the dense sand in the sub-fractures. The numerical simulation yielded 45% for the ultra-light weight, which offer much better vertical coverage area of proppant.

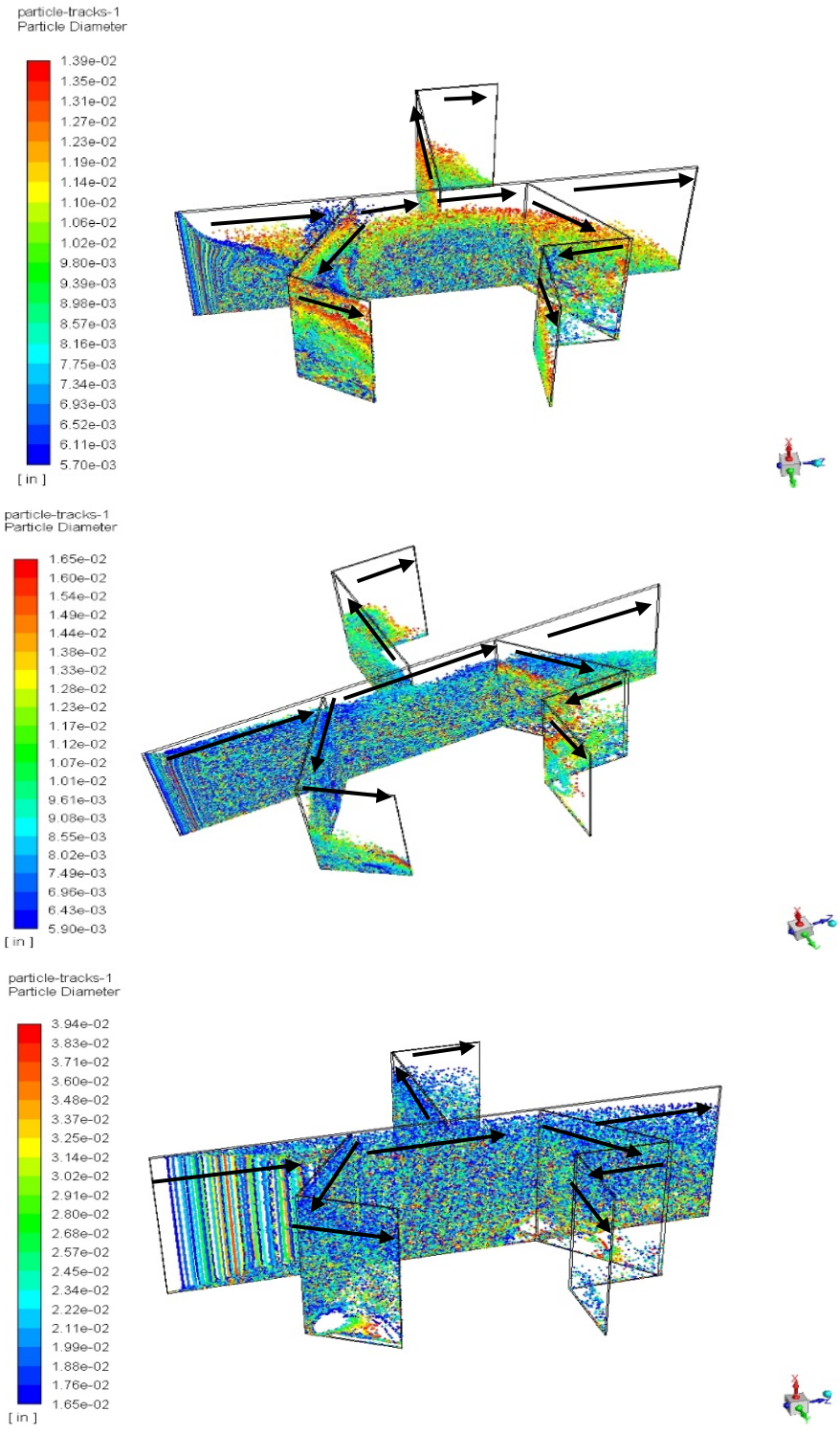

Figure 5.8: This figure shows the results of using three different proppant sizes. The upper panel is particle distributions of 100- mesh. The middle panel is particle distributions of 40/70. The lower panel shows particle distributions of 14/40 mesh. All panels were conducted using slickwater at 1 gal/1000 gal of friction reducer at 1 gal/min.

5.6.4 The Impact of Injection Rate

The numerical model indicates that the injection rates affects the settling rate and the transport of the proppant in slickwater slurries. The lower injection rates result in lower horizontal flow velocities which reduce the travel distance of the proppant. The high injection rates have higher horizontal velocities; thus, leading to suspending more proppants in the stream. The high injection rates also yielded higher propped height in the sub-fractures and reduced the settlement in the main fracture.

Figure 5.9 shows the numerical results for proppant transport using two flow rates. The left panel is particle distributions for 40/70-mesh proppant at 1 gal/min in water. The right panel is particle distributions for 40/70- mesh proppant at 2 gal/min in water.

Comparing the laboratory experimental results with the ANSYS numerical simulation results lead to the following similar observations:

1. Increasing injection rate had an impact on enhancing slickwater proppant transport due to the higher drag and lifting force caused by the higher velocity fluid.
2. High injection rates yielded higher propped height in the sub-fracture groups.
3. The numerical simulation resulted of 42% settlement of the proppant at 1 gal/min compared to the laboratory experiments of 55%. When the injection rate was raised to 2 gals/min, the settlement of proppant increased to 60% compared to the laboratory experiments 80%.
4. High injection rates resulted less settlement in the main fracture.
5. The laboratory experiments showed that 95% settled out in the main fracture for 1 gal/min and when the pump was increased to 2 gals/min the settlement was only 87.5%. The ANSYS simulation yielded settling of 90% and 70% for 1 gal/min and 2 gal/min, respectively.

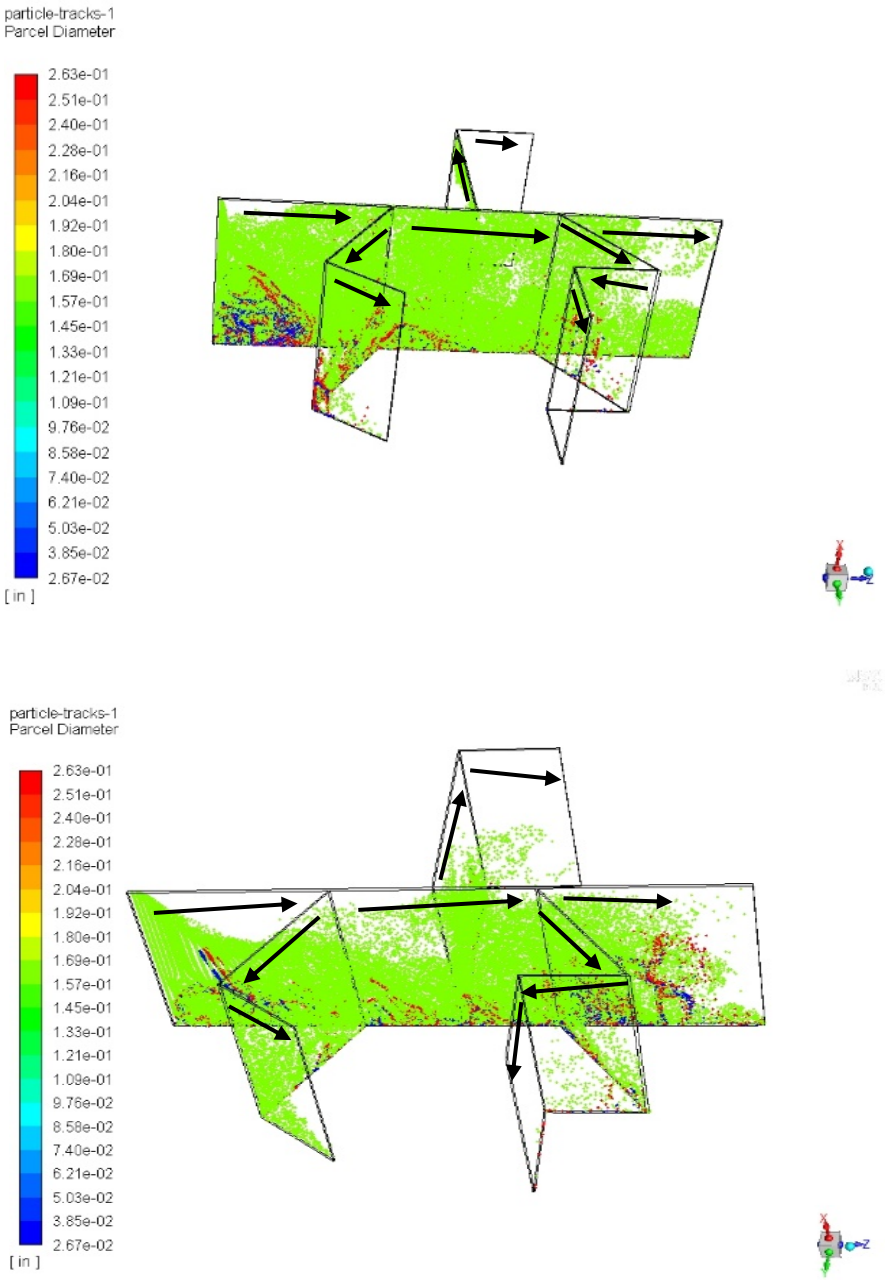

Figure 5.9: This figure shows the results of using two different flow rates. The top panel is particle distributions at 1 gal/min. The bottom panel is particle distributions at 2 gal/min. All panels were conducted using water system for 40/70- mesh proppant.

CHAPTER 6

EXPERIMENTAL AND MODELING DISCUSSION

Hydraulic fracturing has become a very viable way to extract oil and gas from the unconventional low permeability shale reservoirs. Slickwater treatments have become a preferred method of stimulation for these low permeability shale reservoirs. Sweep stages with ramp-up schedules have been used to prevent the early proppant screen-out during these treatments (Olson 2011). In low permeability reservoirs, the main reason for fracturing is to maximize flow and production of the hydrocarbons to travel freely to the wellbore and up to the surface making wells economically viable. The fracture length and the fracture conductivity are the two main variables which directly affect the success of a hydraulic fracture treatment.

6.1 Implication of the Complex Fracture Networks

The goal of this research is to reduce the speculation of proppant transport in an en echelon natural fracture system. The geometry angles chosen for study were 60, 90, and 120 degrees (Smith et al. 2015). This was done to mimic a set of extension fractures that are aligned en echelon and rotated away from the joint axis. Features on the surface of a natural fracture provide information about the fracture's origin. Rib marks are curved features perpendicular to the lines of hackle of the fracture face. These features indicate extensional fracturing, which is opposed to slickenside lineation that indicates shear fracturing. The fractures are associated with faults, folds, and igneous intrusions. Conjugate shear fractures form in a fault zone at roughly 60 degrees. Also, syncline fractures are often parallel to the fold axis, whereas the fold at the peak of an anticline makes a high angle roughly at 120 degrees (Savalli and Engelder 2004). With the above in mind, this is why these angles have been chosen to experiment with, as they are very similar to natural fractured formations. In the performed computer modeling, it was found that the proppant transport was sensitive to acute angles and less sensitive in obtuse angles, which coincides with Warpinski and Teufel (1987). They showed that joints and faults do affect the hydraulic fracture geometry and the fracture growth by hindering the proppant transport. This was found to be true in both the modeling and the experimental work performed as part of this research.

There is a lot of concern in the industry in regards to the final propped fracture lengths and the associated proppant transport. It is not known as to how much of the fractures are propped, un-

propped, or just partially propped. Three scenarios have been presented by Cipolla et al. (2008) for the proppant placement in complex networks. The first was that the proppant is evenly distributed throughout the complex fracture networks. This was found to be true in these experiments when using a slickwater solution of 2 gal/1000 gal of friction reducer (refer to Section 4.1.1.3). The second was that the proppant is concentrated in a dominant primary fracture only (Section 4.1.1.3). This was found to be true in this experiment when just water was used. The third was that the proppant settles and gets distributed in a pillar-like structure. This also occurred when hybrid proppant was used with the same slickwater solution above in this experiment. According to this research, it was found that different hybrid proppant sizes provided 40% better coverage of natural fractures of different widths while different densities provided 70% better propped vertical area in each individual fracture.

6.2 Implications of Proppant Transport Factors in the Fracture Network

This experimental research sets out to define and reduce speculation in the transport of proppant occurring in complex fracture networks. The proppant transport in networks was studied in the past by Kern et al. (1959) who studied proppant transport in water. In the early stages of injection in their work, using water only, it was found that the proppant settled near the wellbore. The developed proppant dunes increased in height until equilibrium occurred. Equilibrium is when all of the injected proppant moves past the established dune and further into the fracture. The experimental results of Sahai et al. (2014), Brannon et al. (2006) and Barree and Conway (1995), all agree with the results of Kern et al. (1959). This experimental work also agrees with their results using a water system. In this work, the slickwater with friction reducer results showed that the proppant settled ahead or at the beginning of the fracture leaving a void and then forming a dune behind the void. Then the dune increased until it reached equilibrium height and the remaining injected proppant moved further into the other fractures.

In regards to impermeable walls and secondary fractures, research has been done by Sahai et al. (2014) and Alotaibi et al. (2015) with proppant transport in subsidiary fractures. They used Plexiglas sheets which were also used by Babcock et al. (1967) to create primary and secondary fractures. This research agrees with their work including 1) proppant flows into the secondary fractures because of the fluid flow rate and transport is also affected by gravity; 2) smaller proppant was observed to be dominant in the secondary fracture slots, where as the larger proppant particles

were found mainly in the primary fracture when using the water system only; and, 3) larger proppants were observed to be in the secondary slots when using slickwater with friction reducer which created more even distribution in these secondary slots.

According to Gadde et al. (2004) and Southard (2006) slickwater transport is dependent on eight factors including: 1) slurry velocity 2) fracture width, 3) fluid density 4) fluid viscosity 5) proppant diameter 6) proppant shape 7) proppant density and 8) proppant concentration. He states that these factors vary in their magnitude and their effect on the proppant transport. This current research also agrees with Gadde and Sharma's research. When the proppant diameter is increased, it led to a higher proppant settlement rate and reduced the transportability. This effect was due to the size and weight of the larger particles that contributed to more friction on the walls combined with more particle-particle interactions, which hindered their respective velocities and resulted in more settling (Liu and Sharma 2005). Other critical factors included the combination of the proppant with the fluid density. These values contributed to the net force between gravity and the buoyancy forces acting upon the proppants. When the gravity force is higher than the buoyancy force, then the proppant settles. This leaves the need to have a lifting force provided by the slurry through higher pump rate to overcome the gravity force and maintain the proppant in a state of suspension. If the buoyance force is equal to the gravity force, the particles remain in suspension even without fluid flow Patankar et al. (2002).

The specific transport mechanisms should be discussed to clarify how the proppant is transported into the fracture network. Proppant transport in low viscosity fluids is achieved after the equilibrium dune height is reached, as evaluated experimentally by Patankar et al. (2002). Their study said the transport takes three forms including rolling, saltation, and suspension. These mechanisms take place at the same time after equilibrium is reached but the way they carry different grain sizes further into the fractures does differ. Rolling and sliding mechanisms occurs for two reasons: 1) the proppant is the largest size/weight which gravity pulls downward to the bottom to settle, and 2) the high drag and lifting forces that are exerted by the slurry on the proppant causes them to roll forward in the direction of the slurry movement. This is the slowest form of transport. The action of rolling and sliding takes place at a dune height where the slurry velocity is high enough to create sufficient drag and lift (Dey 1999).

Saltation is a transport mechanism which requires that the flow velocity be high enough to supply a lifting force that overcomes the weight of the proppant grain which lifts it from the dune while traveling in a forward motion with sufficient slurry drag forces. The lifting force occurs when the flow of the slurry is greater than the grain weight and the flow underneath the grain is greater than the flow above the grain. The lifting force begins to lose its' strength as the grain travels further away from the dune and loses its' upward motion due to the gravity force which pulls it downwards.

Suspension transport occurs when the grains are usually small in their nature and the fluid or slurry exerts a very high drag and lifting force. The grains are transported in this manner due to their small size and weight which causes them to remain suspended in the slurry. These particles keep moving until the slurry losses its' high velocity. Alotaibi et al. (2015) conducted a detailed experiment with primary, secondary and tertiary fractures. He had a very detailed description of the dune sizes and lengths. He noted also three transport mechanisms as did Dey (1999), Southard (2006), and Patankar et al. (2002). This study concurs with all four of these studies in the observation of these different transport mechanisms.

Proppant transport into the secondary fractures occurs in the form of a stabilized proppant dune with a traction carpet, also referred to as a fluidized bed. The proppant movement into the secondary slots, which are at angles to the main slot, occurs when the pump rate is higher than the primary slot can maintain. This forces the proppant to flow into the secondary slot. Additionally, the proppant falls or rolls from the primary slot into the secondary slot due to the effect of gravity. The experimental results showed that the proppant buildup in the secondary slot only occurred after the dune was built up in the primary slot, which coincides with (Sahai 2012).

According to Sahai (2012), the secondary fractures that were further away from the wellbore showed that the proppant was transported by gravity only. This was due to the fact that the effective flow rate to these more distant fractures was lower than the necessary threshold rate. Since the effective flow rates at the secondary fractures that are closer to the wellbore would be higher, the proppant can be expected to turn the corner. This points to the conclusion that to have good proppant transport into the secondary fractures, a higher velocity profile is needed. This research also agrees with Sahai et al. (2014), who stated the proppant buildup in the secondary slots was observed to be dependent on the dune buildup in the primary slot. It should be noted that

in this work, the secondary fractures that reached equilibrium proppant dune heights were highly dependent on the total amount of proppant pumped during the experiment.

6.3 Impacts of Slot Entry

In this study, there were two major impacts in regard to entry points that were found. The first impact occurred when two entry points were opened. It was found that the higher fluid viscosity (2 gal/1000 gal) of friction reducer combined with a pump of 2 gal/min transported the proppant most efficiently into the sub-fracture groups of secondary, tertiary, and quaternary fractures up from volumes of 20 to 36%. The higher slurry viscosity had the ability to transport proppant of all sizes into all of the sub-fracture groups.

In the second impact of this experiment, only one of the perforations was opened while the other was closed at different heights of 4 inches and 8 inches from the base of the slot. Experiments were performed using different proppant sizes and densities of proppant with water only. The results viewed were related to the volume of the settled proppant, the dune shape, the slurry density, flow behavior and the transport mechanism. The results showed that when the slurry was pumped from the top perforation there was a lot of drag and the buoyance forces that caused the heavier particles to settle out, while the lighter particles travelled further in the slot through suspension. Also, when the slurry was pumped into the bottom perforation using 40/70 mesh, the proppant settled three minutes faster and created a 20% larger dune than did the 100 mesh. The particles had the same gravity weight worked against the lifting force of the fluid. The slurry flowed until the area was blocked and with more time the settled particles rolled and slid into the fracture which created larger dunes.

Also, with the 40/70 mesh injecting from the bottom, it was noted that the dune shape was parabolic, while injecting from the top created a linear dune. When the slurry was injected from the top slot the heavier particles interacted with the side of the wall and fell to the bottom. The intermediate and finer particles traveled with the fluid in the form of suspension and saltation. This is because the fluid force acting on the particles was greater than the gravitational forces and reduced the tendency of the particles to fall. When the injection was from the bottom slot, the particles accumulated at the bottom of the fracture. As the injection continued, the settled proppant reduced the flow, increased the velocity of the flow, and also the interaction between the particles.

This interaction between the particles reduced their velocity which increased the gravitational effects. In theory, the faster flow rate yields a higher drag or lift force. As the flow was increased from 1 gal/min to 2 gal/min, the drag force was higher in both the top and bottom perforations. There was more initial settling using 1 gal/min injection rate compared to the 2 gal/min rate. In the bottom perforation, using the higher pump rate increased the drag force and the transportability plus reduced the dune height by 57%. It also increased the dune length by 12%, leading to the conclusion that the proppant distribution is increased when the pump rate is raised.

6.4 Modeling Implications

The modeling performed as part of this research was found to be similar to the results of those in Li et al. (2016). The CFD modeling results discussed in Chapter 5 are very similar to Li et al. (2016) results in that increased slurry flow also increased the proppant transport into the secondary fractures. Li et al. (2016) had only two fractures, where as in this research there are four fractures. In this research, it was also found that the proppant transport is sensitive to branching in respect to the proppant turning corners and entering the sub-fracture groups. Also, the viscosity had a significant effect on the transport of the proppant in that the higher viscosity yielded more proppant in the sub-fracture groups. The low viscosity in wide fractures showed significantly less proppant in the fractures compared with the high viscosity slurry which yielded more proppant in all the fractures and was less sensitive to the width of the fractures. The proppant density and size also affected the proppant transport in that the smaller sizes and lower density proppants had less settling and had a substantially higher propped area in the fracture. Higher injection rates also yielded higher propped height in the fractures.

Li et al. (2016) investigated the proppant transport into different sub-fractures at different angles as was done in this experiment. They also used primary and secondary fractures as was done in this experiment. They used three flow rates including 1.32 gpm, 1.98 gpm, and 2.64 gpm. They also changed the angles in the secondary fracture which greatly affected the proppant distribution and found lower flow rates resulted in higher proppant amounts in the secondary fractures. When the angle of the secondary fracture was increased, it reduced the proppant in the secondary fracture and also affected the amount of the proppant in the main fracture. When Li et al. used smaller particles, the dune lengths were found to be shorter. When they increased the injection rate, they found that the proppant in the main fracture was reduced but increased in the

secondary or subsidiary fractures. They also found when using larger diameter proppant along with increased injection rates that the slurry or proppant was increased in the secondary fracture and reduced in the primary fracture, which coincides with this research.

Referring to Alotaibi et al. (2015), they observed that the secondary fractures are essential to the duning of the fractures, but the tertiary fractures did not contribute to estimating the duning of the fractures in respect of the dune height and the dune length. This experiment was found to be contrary to Alotaibi in that good conductivity was found also in the secondary, tertiary, and quaternary fractures when high viscosity combined with high fluid rate was used. However, Alotaibi et al. (2015) did say that the secondary fracture depended on the amount of proppants that were injected to reach an equilibrium height. This experiment showed that slickwater can transport proppant into the secondary and tertiary fracture that are closer to the wellbore. Keep in mind that Alotaibi et al. (2015) used only water as the transport mechanism where in this experiment there are three slurries.

As this experiment used different weights and sizes of proppants, it should be mentioned that the densities of the proppants do have an effect on the transportability of the proppants. The weights of proppant range from sand at 2.65 g/cc to the other proppants which range from 1.0 g/cc for the ultra-light weight proppant to more than 3.0 g/cc which is for sintered bauxite (Rickards et al. 2006). Ultra-light weight proppant showed no settling at all in the fracture network, even when it was used in the water system. The 100 mesh sand proppant showed better transport to the fracture network than 40/70 mesh. This shows that doubling the proppant diameter increases settling and therefore hinders the slickwater proppant transport. The change in the dune height is a low 9.4% relative to the change in diameter. Sieve analysis showed that the 100 mesh had 35% more segregation than the 40/70 mesh.

The sizes of the proppants do influence or have an effect on the proppant transport and how well the fracture is held open or sustained which is mandatory for good fluid flow or conductivity. The sizes of the proppants are determined by using meshes of a certain size which only allow particles that can pass through the screen size to obtain the exact size of proppants that are to be used. The larger size of proppant does increase the fracture conductivity while the smaller proppants transport better. Sand and ceramic proppants are the most commonly used in the hydraulic fracturing process. Ottawa sand is a very widely used product that is in use today because

it is well rounded, mono-crystalline, and maintains conductivity evenly when it is subjected to high stresses (Rickards et al. 2003). Other sand proppants range in shape from angular to more spherical grain shapes. As stated previously, sand proppants have a density of 2.65 g/cc while the ultra-light weight proppant can be as low as 1.0 g/cc (Rickards et al. 2006). In this experiment the results found were the same as Liu and Sharma (2005) that increasing the size or diameter of the proppant increased the settling rate of the proppant in the fracture. This reduced the transportability of the proppants as the larger sizes are heavier thus the settling occurs which creates larger dune areas. It was noted that the larger sizes interacted with themselves and the walls of the fracture causing increased settling. This also coincides with this study using water, and slickwater with a low concentration of friction reducer. However, when the friction reducer was doubled combined with double the pump rate, these forces were overcome, and much better propping occurred inside all the fractures. Alotaibi et al. (2015) also noted in their experiment that the larger sizes of proppant did hinder the propped area and affected the Equilibrium Dune Length (EDL) as the proppants traveled in a "Hindered Settling Mechanism" as it was termed. They noted that the lateral distance covered by the larger proppant was shorter but that increasing the velocity of the slurry also increased the distribution of the dune length and the erosional effect which was not lost when he used the 100 mesh. Tsai et al. (2013) found that if the density of the proppant is equal to the carrying fluid, then proppant can be transported further into the fracture. If the proppant has a higher specific gravity, then the proppant settles and forms dunes quicker. They stated that the increase in flow rate will decrease the settlement of the proppant by increasing the drag forces. They concluded that smaller proppant should be injected before heavier proppant to maintain conductivity near the wellbore. Slurry transport was modeled using fracture shear and leak-off of the fracturing fluids without taking into account the gravitational effect, particle-particle and fluid-particle interaction Miller et al. (2008). Tsai et al. (2013) studied proppant transport using the effect that particles have on each other and the effects fluids have on particles.

Blyton et al. (2015) investigated the proppant distribution in a fracture using a CFD-DEM coupling method. Their method involved using a modified Navier-Stokes equation, the momentum equation, and the continuity equation. They modeled the interaction between particles and fluids using the force of the particle on the fluid and the force of the fluid on the particle for every cell. This experiment agrees with Tsai et al. (2013) both in the modeling and in the experiment.

Chang et al. (2016) noted that when ceramic proppants were used there was an appreciable higher conductivity achieved due to a uniform size and smoothness that packed in the fracture much better than sand proppants. He also noted that the concentration of this proppant affected the conductivity. He noted that a decreased concentration produced increased conductivity using two different sizes of proppants, which were 40/70 and 100 mesh. They noted that the larger size proppants are necessary or essential to maintain the fracture in an open position. He also claimed that increasing the viscosity improved the benefits or packing of the smaller proppants in the fracture. The low settling of the 100 mesh created longer and higher dunes. He recommended using a mixed size of proppants to achieve good conductivity with an effective transport to and inside the fracture. Woodworth and Miskimins (2007) also agreed with Chang et al. (2016) in the respect of using lower concentrations. Wu and Wang (2006) also addressed sizes and shapes of grains like sands which are more susceptible to drag forces because their shapes are angular which is agreed upon in this study also. The angular grains do interact with the walls and do show higher settling tendencies Southard (2006).

Zhang et al. (2017) used the rectangular domain with non-slip boundaries to model proppant transport mechanisms. They observed that when proppant is injected, it settles at the bottom of the fracture and a proppant dune forms. Due to the size of the domain, the proppant settles in a small amount of time. They used high injection rates that caused the dune to be flat and wide-spread across the fracture. The initial results of Zhang et al. (2017) showed a settled proppant bed-load, a high concentration of slurry above the bed-load and a clear fluid layer. They characterized the transport as suspension, fluidization and settlement. This current study agrees with these results.

During sieve analysis, it was observed that the 100 sand mesh showed higher proppant segregation based on proppant sizes (around 35%) than the sieved 40/70 sand mesh. Based on the sieve analysis and the results of the laboratory tests carried out with two flow rates and one concentration of proppant, it was noticed that the resultant proppant distribution was different across the fracture network. Also, this was dependent on the flow rates across the fracture intersection and the proppant sieve distribution. This agrees with Sahai (2012) results where he used different pump rates and proppant concentrations with 100 mesh and 30/70 mesh. Slurries that have higher velocities do have better proppant transportability and they build shorter dunes with longer lengths (Brannon et al. 2006). This is because of the higher drag and lift forces that

were applied though higher velocities. There is a critical velocity where the proppant stops settling or reaches the equilibrium dune height whereby all the injected proppant is transported further inside the fractures and sub-fractures. In slickwater slurries, the viscosities are usually very low. So, suspension of the proppant is not expected at low velocities. However, when the velocity is increased or doubled as in this experiment, the drag force was increased, and more proppant was transported into the fractures which agrees with Southard (2006). This study also agrees with these results.

The following are the results of Alotaibi's et al. (2015) experiment: 1) the height of the dune depends on the velocity of the slurry, 2) higher velocity increases erosional effect on the proppant dune, and 3) higher velocity improves the transport of proppant into the subsidiary fractures. Their results showed that increasing the velocity by 11% caused a 0.7% reduction of the equilibrium dune length. Doubling the flow rate resulted in approximately 5% reduction of EDL. Alotaibi et al. (2015) concluded that increasing the velocity does not significantly affect the settling tendencies of slickwater. At higher velocities the dune loses its erosional power due to the nearly horizontal dune surface. His recommendation for optimum result is the increase of flow rate and decrease of proppant concentration. This study agrees with Alotaibi's results in respect to increasing the flow rates to obtain more proppant transport and reduces the dune height by 7.89%, 12.93% and 16.17% of the three fluid systems involved in this research. However, this study just used one concentration, whereas Alotaibi used various concentrations.

The drag force of the fluid controls the horizontal transport of the proppant. This means that at a higher injection rate, the proppant is dragged for a longer distance. With higher pump rates, the location near the wellbore is free of settled proppant because of the erosional power of the high velocity slurry entering the fracture. The downside of using high injection rates will be the reduction of fracture conductivity near the wellbore (Zhang et al. 2017). Chang et al. (2016) also indicates that the higher rates enable the proppant to travel longer distance before settling. Lower treatment rates result in higher duning of the proppant. Also, higher treatment rate reduces the treatment time. Chang et al. (2016) observed that higher flow rates yielded longer flat dunes and increased horizontal propped area.

For the simulations in this work, an open-hole wellbore is utilized. It involved pumping the slurry from the whole left side boundary of the rectangular domain. Zhang et al. (2017)

experimented using an open-hole wellbore. The first group of the injected proppants settled at the bottom of the fracture tip. With time, the tip fracture is blocked, and the simulation is forced to stop at a premature time. The proppant transport mechanism is dependent on the injection rate, fluid viscosity, perforations, and proppant characteristics Zhang et al. (2017).

The presence of pre-existing fractures and joints is to be taken into account to adequately capture the proppant transport process. Mack et al. (2014) observed that the proppant flowed more readily into sub-fractures that were orthogonal to the direction of the flow in the main fracture at high flow-rates. Lab results from Sahai et al. (2014) shows that below the threshold velocity, suspended proppant will not turn into the sub-fractures. The proppant with a smaller diameter has a higher chance of being transported into sub-fractures.

A minimum velocity is required to transport proppant into the sub-fractures. The minimum velocity is dependent on the fracture width and the particle size. When the particle gets to an intersection, it is subjected to a drag force that is related to the diverging flow into the sub-fracture. The particle begins to move in the direction of the drag flow, if the drag force is strong enough, then the particle will flow into the sub-fracture (Chang et al. 2016). This experimental and modeling work both agree with the above authors in that the proppant transport behaviors and the factors that affected the proppant transport behaviors and settlement are the same.

High viscosity fluid created wider dunes and caused a stronger fluidization mechanism. This will increase the time it takes for the proppant dune to achieve equilibrium height. Proppant transport is heavily dependent on fluid viscosity. A small change in viscosity can affect placement and transport of proppant (Zhang et al. 2017). Chang et al. (2016) also observed from their results that higher viscosity enhanced transport and lower viscosity enhanced fracture conductivity. Overall, the scaled results of this experimental study suggest that the proppant does get transported into the complex fracture networks and is dependent on the combined effects of pump rate, proppant concentration, amount of proppant pumped and proppant size. This study agrees with above results and even more as this study used tertiary and quaternary fractures and had the same results.

By using or considering the results of the transport behavior parameters in these experiments and the results of others found in literature, future fracture treatments can be made to

obtain much better packed fractures that yield a more perfect conductivity to achieve maximum flow of the formation's hydrocarbons.

CHAPTER 7

CONCLUSIONS AND FUTURE WORK

In this research, laboratory experiments and computer simulations were carried out to better understand proppant transport using a prototype of complex fracture networks. This chapter provides the conclusions and recommendations for future work. The experimental results are analyzed to provide field recommendations and applications.

7.1 Conclusions

This work initially set out to add to the studies of Sahai et al. (2014) and Alotaibi et al. (2015) to verify that proppant could be transported into the tertiary and quaternary fractures with have good propping in all fractures. The overall impact of this study proves that good propping of all fractures can be achieved with maximum pump rate using either hybrid mixes of proppant or ceramic proppant with its uniform shape and weight which has the potential improve well productivity. Listed below are twelve overall conclusions obtained from this work.

Sections 7.1.1- 7.1.3 provides several conclusions made from the results of the laboratory experiments and the ANSYS Fluent modeling. These conclusions are observations made from the results presented in Chapter 4 and Chapter 5.

7.1.1 Laboratory Results with Two Perforations Open

1. Increased fluid viscosity improved the slurry transport into the sub-fracture groups by increasing the transportability of the proppant from 20 to 36% with even distribution in the sub-fracture groups.
2. Doubling the concentration of the friction reducer proved to yield better results than doubling the pump rate. These two factors combined, especially doubling the flow rate, proved to yield the best results in delivering the most proppant to all the sub-fracture groups.
3. Proppant size did prove to be a factor in good transport of proppant into all fractures. The best use of size is to have a mixture of sizes or hybrids to obtain the best results in fracture packing or propping. The smaller proppants travel further and remain suspended, due to their weight, to reach the further recesses which improved the propped area.

4. Water exhibited the highest settling of the slurry because it had no carrying capacity to keep the proppant lifted in the slurry to be transported into subsidiary fractures.

7.1.2 Laboratory Results with One Perforation Open and One Perforation Closed

1. Pumping from the top perforation yielded higher settling of the slurry in the primary fracture, but with time and continued pumping, the concentration of proppant in the slots did increase. This proves the lifting force was not enough to move the particles into the sub-fracture groups.
2. Pumping from the bottom perforation showed that the slurry flowed until the flow area was blocked, but with more injection time, the settled particles rolled and slid until more particles were transported into the fracture, creating larger dunes.
3. In both scenarios, the proppant transport is increased with the doubling of the pump or injection rate delivering more proppant to all groups of fractures. These experiments showed that the distribution of the proppant was increased when the pump rate was raised. Higher velocity increased the proppant transportability, increased the drag force, reduced the dune height by 57%, and increased the dune length by 12%.

7.1.3 ANSYS Fluent Results

1. Fluid flow is sensitive to branching and turning corners into the sub-fractures and sensitive between the hydraulic and the natural fracture.
2. Fracture width had a significant impact on the proppant transport especially for the low viscosity fluids, which didn't have the lifting capacity for the particles. The high viscosity fluid fracture fluid was far less impacted by the fracture width and wound up with a similarly propped fracture shape in each branch.
3. Viscosity had a significant impact on the proppant transport. The higher viscosity fluid propped the fracture significantly better when compared to low viscosity fluids.
4. Particle size had a significant impact on the propping of the fractures with the smaller particles propping better with less settling compared to larger particles which had more settling. Also, light-weight proppants showed to have the least amount of settling of all proppants due to their size, weight, and uniform shape.

5. The highest possible flow injection rate combined with the best viscous fluid using either light-weight proppants or mixed proppants yields the best uniform pack of proppant.

7.2 Future Work

As water was first used in the fracturing process with sand as proppant, today's needs are to design the best overall slurries to get the most well propped fracture and to achieve the best conductivity. The use of more viscous slickwater has improved the fracturing process dramatically and still needs further research and investigation to provide better transport, better proppant mixes or hybrids slurries, with the best overall or correct flow rates. There is a need to understand the process of fracturing totally to complete these goals and know what is needed in each area of the world. Below is a list of recommended topics for future research projects in this area:

1. There needs to be research done on all studies related to this subject in the use of proppants, their sizes, weights, concentrations, flow mechanisms, pump rates, etc. A catalog of such results would allow others to easily see what has been lacking and pursue areas that have not been addressed until everything has been researched to improve our total knowledge and understanding of the fracturing process.
2. There are still items such as varying the concentrations of sand with proppant sizes, proppant densities, flow rates which still need to be researched and the results cataloged.
3. Evaluation of erosional effects on the proppants, both small and large, with the effects of one on the other.
4. Research can be done to understand the convection effects of different sand concentrations and their weight variations between the pumping stages.
5. Use slots that are not uniform so as to simulate natural occurring fractures.
6. More research should be done in the fracturing networks using secondary, tertiary, and quaternary fractures that are closer to natural fractures (micro-fractures) in formations and compare them to this work.
7. Attempt to make research models as close as possible to the fractures that are in a natural well which would make the research more productive. The use of inclined vertical angles would apply here.
8. Use the hybrid proppants that are now being used in the industry to discover the best parameters (size and density) and compare them with the results in our research lab.

9. More studies need to be conducted on the slickwater proppant transport using different densities than were done in this study and compare them.
10. Evaluate proppant density on the proppant settlement while keeping the proppant shape and proppant size the same. In this study, two different proppant densities were used while the proppant shape and size were not constant. Other studies need to be done and then compared with these results.
11. Evaluations need to be done with viscosities between 1-20 cp to prove or disapprove this work especially in the sub-fracture groups as fluid viscosity does enhance the transportability of the proppants. The results should show the enhancement of the proppants distribution inside the fractures.
12. Evaluate different flow rates to determine the minimum flow rate needed for the proppants to turn the corners into the sub-fractures. Determine which the optimal rate is if possible.
13. Vary the width of the sub-fractures. That is, instead of just having the sub-fractures with the same width, each sub-fracture can have its own width.
14. The fluid viscosity can be varied for the experiments conducted at different perforation locations. In this study, water only was used. However, instead of using just water, slickwater at different concentrations should be used to better understand the effect of perforation location on the proppant transport behavior.
15. The geometry of the domain used in ANSYS should be more complex to better simulate proppant transport.
16. Using the ANSYS software, the secondary, tertiary, and quaternary slots should be programmed in the modeling with different angles. This way the results from the experiments can be compared to the simulation results.
17. In the ANSYS software, the perforation locations (heights) were not programmed in the software in this study. In the future simulations these need to be programmed to obtain comparable results to the experiments.
18. In the ANSYS software use different input values of the same parameters that were used in this study to obtain different results and compare them to this study.

NOMENCLATURE

B = Magnetic field strength, (volt × s[$\frac{\mathrm{M}\times\mathrm{L}^2}{T^2\times\mathrm{EC}}$])

d_{sol} = solid particle diameter, *L* (ft)

E = Induced voltage, (volts) $\mathrm{E} = [\frac{\mathrm{M}\times\mathrm{L}^2}{T^2\times\mathrm{E.C}}]$

fv = proppant volume fraction (unitless)

fvM = maximum fraction for a mobile slurry (unitless)

g = gravitational acceleration $\frac{L^2}{T}$ (ft2/s)

h = slot height, *L* (ft)

H = fracture height, *L* (ft)

h = height of the fracture, *L* (m)

K = Factor set-calibration factor, ($1/m^2$) $[\frac{1}{L^2}]$

k = permeability of the formation, $MLT^{-2}A^{-2}$ (md)

k = consistency index $\frac{M}{LT^2}$ (lbf-sn/ft2)

K' = consistency index, $\frac{M}{LT^2}$ lb-secn/ft^2

kf = permeability of the fracture, $MLT^{-2}A^{-2}$ (md)

L = Distance between the two electrodes, (meter) [L]

n = flow behavior index (dimensionless)

n = flow behavior index (unitless)

N_{Ref} = Reynolds number for fluid (Dimensionless)

q = injection rate, $\frac{L^3}{T}$ (ft^3/sec)

Q = Fluid volumetric flow rate, (m^3/sec)

Q' = injection rate $\frac{L^3}{T}$ (gal/min)

t = time, *T* (seconds)

VF = Fluid velocity, (m/s) $[\frac{\mathrm{L}}{\mathrm{T}}]$

w = fracture width, *L* (ft)

w	=	slot width, *L* (ft)
W	=	fracture width, *L* (in.)
Xf	=	half-length of the fracture, *L* (ft)
μ_{base}	=	viscosity of the base fluid, $\frac{M}{LT}$ (cp)
μ_{slurry}	=	viscosity of the slurry, $\frac{M}{LT}$ (cp)
f_v	=	volume fraction of solids (unitless)
u_∞	=	velocity of the fluid, $\frac{L}{T}$ (ft/sec)
u_L	=	velocity in the slurry, $\frac{L}{T}$ (ft/sec)
u_{sol}	=	solid particle velocity, $\frac{L}{T}$ (ft/sec)
τ_y	=	shear stress, $\frac{M}{L^2}$ (lb/ft^2)
ρ	=	density of the fluid $\frac{M}{L^3}$ (kg/m3)
ρ_f	=	fluid density, $\frac{M}{L^3}$ (lb/gal)
ρ_{sol}	=	solid particle density, $\frac{M}{L^3}$ (lb/gal)
p	=	pressure, $\frac{M}{LT^2}$ (psi)
d	=	diameter of the fracture width, *L* (m)
δt	=	change in the velocity with time, *T* (seconds)
δw	=	change in the velocity with respect to the fracture width, *L* (ft)
δx	=	change in the velocity in the fracture in the x-direction, *L* (ft)
δy	=	change in the velocity in the fracture in the y-direction, *L* (ft)
ρ	=	density of the fluid $\frac{M}{L^3}$ (lb/gal)
β	=	exponent (unitless)
γ	=	shear rate, $\frac{1}{T}$ (sec^{-1})
μ	=	viscosity of fluid, $\frac{M}{LT}$ (cp)
μ	=	viscosity (kg/m.sec)
μa	=	apparent viscosity, $\frac{M}{LT}$ (cp)

ABBREVIATIONS

DFA = Dune to fracture area ratio

EDL = Equilibrium dune level

VFD = Variable frequency drive

RPM = Revolutions per minute

CFD = Computational Fluid Dynamics

SRV = Stimulated reservoir volume

TSO = Transmission System Operator

EDH = Equilibrium dune height

TCF = Trillion cubic feet

DTD = Dune to total Dune area ratio

DHFH = Dune height to fracture height ratio

FR = Full Requirements

SI METRIC CONVERSION FACTORS

Measurement	**Value**	**Unit**
Barrel (bbl.) ×	1.589873 E-01	m3
Ft (ft) ×	3.048 E-01	m
Gallon (gal.) ×	3.78541 E-03	m3
Pound (lb.) ×	4.53592 E-01	Kg
Inch (in.) ×	2.54 E-02	m
Millimeter (mm) ×	1.0 E-03	m

REFERENCES

Abass, H. H., Al-Mulhem, A. A., Alqam, M. H., and Khan, M. R. 2006. Acid Fracturing or Proppant Fracturing in Carbonate Formation? A Rock Mechanics View. Presented at the SPE Annual Technical Conference and Exhibition, San Antonio, Texas, 24-27 September. SPE-102590-MS. https://doi.org/10.2118/102590-MS.

Al-Muntasheri, G. A. 2015. A Critical Review of Hydraulic-Fracturing Fluids for Moderate- to Ultralow-Permeability Formations Over the Last Decade. SPE Prod & Oper 29 (4): 243–260. SPE-169552-PA. https://doi.org/10.2118/169552-PA

Alotaibi, A. 2015. Slickwater Proppant Transport in Complex Hydraulic Fracture Networks: New Experimental Study and Scalable Correlations Development. Doctoral dissertation, Colorado School of Mines. Golden, Colorado (2015).

Alotaibi, A., and Miskimins, L. 2015. Slickwater Proppant Transport in Complex Fractures: New Experimental Findings & Scalable Correlation. Presented at the SPE Annual Technical Conference and Exhibition, Houston, Texas, 28-30 September. SPE-174828-MS. https://doi.org/10.2118/174828-MS.

Babcock, R.E., Prokop, C.L., and Kehle, R.O. 1967. Distribution of Propping Agents in Vertical Fractures. Presented at the Spring Meeting of the Mid-Continent District, API Division of Production, New Orleans, Louisiana, March. API-67-207.

Barree, R.D., and Conway, M.W. 1994. Experimental and Numerical Modeling of Convective Proppant Transport, SPE paper 28564, presented at the 1994 Annual Technical Conference & Exhibition, New Orleans, LA, September 25-28.

Barree, R.D. and Conway, M.W. 1995. Experimental and Numerical Modeling of Convective Proppant Transport. Journal of Petroleum Technology 47 (3): 216-222. SPE-31068-PA. http://dx.doi.org/10.2118/28564-PA.

Biot, M. A. and Medlin, W. L. 1985. Theory of Sand Transport in Thin Fluids. Presented at the SPE Annual Technical Conference and Exhibition, Las Vegas, Nevada, 22-25 September. SPE-14468-MS. http://dx.doi.org/10.2118/14468-MS.

Blyton, C., Gala, D. and Sharma, M. 2015. A Comprehensive Study of Proppant Transport in a Hydraulic Fracture. Presented at SPE Annual Technical Conference and Exhibition, Houston, Texas, 28-30 September. SPE-174973-MS. https://doi.org/10.2118/174973-MS.

Boggs, S., Jr, Y. I., Kwon, G. G., and Goles et al. 2002. Is quartz cathodoluminescence color a reliable provenance tool? A quantitative examination: Journal of Sedimentary Research,

72(3), pp.408-415.

Brannon, H.D., Wood, W.D., and Wheeler, R.S. 2006. Large Scale Laboratory Investigation of the Effects of Proppant and Fracturing Fluid Properties on Transport. Presented at the International Symposium and Exhibition on Formation Damage Control, Lafayette, Louisiana, and 15-17 February. SPE-98005-MS. http://dx.doi.org/10.2118/98005-MS

Cabrejos, F. J., and Klinzing, G. E., 1994, "Pick Up and Saltation Mechanisms of Solid Particles in Horizontal Pneumatic Transport," J. Powder Technol., 79(2), pp. 173–186.

Carman, P. C., Cawiezel, K.E.: "Successful Breaker Optimization for Polyacrylamide Friction Reducers in Slickwater Fracturing, "PE 106162, 2007 SPE Hydraulic Fracturing Technology Conference, College Station, Tx, USA, 29-31 January 2007.

Chang, O., Dilmore, R. and Wang, J. 2016. Model development of proppant transport through hydraulic fracture network and parametric study. Journal of Petroleum Science and Engineering 150 pp.224-237.

Cipolla, C. L., Warpinski, N. R., Mayerhofer, M. J., Lolon, E., & Vincent, M. C. 2008. The Relationship between Fracture Complexity, Reservoir Properties, and Fracture Treatment Design. SPE Annual Technical Conference and Exhibition, Denver, Colorado, 21-24 September. SPE-115769-MS. doi: https://doi.org/10.2118/115769-MS.

Clark, P. E. and Courington, T. J. 1994. Visualization of flow into a vertical fracture. Presented at the SPE Permian Basin Oil and Gas Recovery Conference. Midland, TX, March 16–18. SPE-27692-MS. https://doi.org/10.2118/27692-MS.

Clark, P. E.and Zhu, Q. 1994. Fluid flow into vertical fractures from a point source. Presented at the SPE Annual Technical Conference and Exhibition. New Orleans, LA, September 25–27. SPE-28509-PA. https://doi.org/10.2118/28509-PA.

Cleary, M. P. and Fonseca, A. Jr. 1992. Proppant convection and encapsulation in hydraulic fracturing: Practical implications of computer and laboratory simulation. Presented at the SPE Annual Technical Conference and Exhibition, Washington, DC, October 4–7. SPE-24825-MS. https://doi.org/10.2118/24825-MS.

Clifton, R., and Wang, J. 1988. Multiple fluids, proppant transport, and thermal effects in three-dimensional simulation of hydraulic fracturing. Presented at the SPE Annual Technical Conference and Exhibition, Houston, Texas, 2-5 October. SPE-18198-MS. https://doi.org/10.2118/18198-MS.

Curtis, J. B., 2002, Fractured shale-gas systems: AAPG Bulletin, v. 86, no. 11, p. 1921–1938.

de Pater, C.J., Cleary, M. P., Quinn, T.S., Barr, D.T., Johnson, D.E., and Weijers, L., 1994, Experimental Verification of Dimesional Analysis for Hydraulic Fracturing, SPE paper 24994, SPE Production and Facilities, November 1994, pg. 230-238.

Dey, S. 1999. Sediment Threshold. Applied mathematical modeling 23 (5): 399-417. http://dx.doi.org/10.1016/S0307-904X(98)10081-1.

Fourar, M., S. Bories, R. Lenormand, and P. Persoff, Two-Phase Flow in Smooth and Rough Fractures: Measurement and Correlation by Porous-Medium and Pipe Flow Models, Water Resour. Res., 29(11), pp. 3699-3708, 1993.

Gadde, P.B., Liu, Y., Norman, J., and Sharma, M.M., 2004, Modeling Proppant Settling in Water-Fracs. presented at the SPE Annual Technical Conference and Exhibition, Houston, TX, 26-29 September. SPE-89875-MS.

Gadde, P. B. and Sharma, M. M. 2005. The impact of proppant retardation on propped fracture lengths. Presented at the SPE Annual Technical Conference and Exhibition, Dallas, Texas, 9-12 October. SPE-97106-MS. http://dx.doi.org/10.2118/97106-MS.

Ghyben, W. B. 1988. Nota in verband metde voorgenomen putboring nabij Amsterdam-Tijdsch. Van Kouinglijk Instituut Van Ingenieurs 5:8–22, No 1073.

Gidley, J.L., Holditch, S.A., Nierode, D.E. et al. 1989. Postfracture Formation Evaluation. In Recent Advances in Hydraulic Fracturing, 12. Chap. 15, 317. Richardson, Texas: Monograph Series, SPE.

Hammond, P. (1995). Settling and slumping in a Newtonian slurry, and implications for proppant placement during hydraulic fracturing of gas wells. Chemical Engineering Science,50(20), 3247-3260. doi:10.1016/0009-2509(95)00152-u.

Hanks, R.W, Rue, H. C. Eng. Chem. Fundam. 1966. Matrix Isolation Spectroscopy. International Conference on Matrix Isolation Spectroscopy,5, 558.

Harris, P., Morgan, R. and Heath, S. 2005. Measurement of Proppant Transport of Frac Fluids. Presented at the SPE Annual Technical Conference and Exhibition, Dallas, Texas, 9-12 October. SPE-95287-MS. https://doi.org/10.2118/95287-MS.

Herzberg A (1901) Die Wasserversorgung einiger Nordseebäder. J. Gasbeleucht. Wasserversorgung 44:815–819

Johnson, P. C., Nott, P. and Jackson, R. 1990. Frictional-collisional equations of motion for particulate flows and their application to chutes. J. Fluid Mech 210, 501–535.

Kaufman, P., Penny, G. and Paktinat, J. 2008. Critical Evaluations of Additives Used in Shale Slickwater Fracs. In: SPE 119900, SPE Shale Gas Production Conference, 16–18, Society of Petroleum Engineers, Irving, Texas

Kern, L.R., Perkins, T.K., and Wyant, R.E. 1959. The Mechanics of Sand Movement in Fracturing. Presented at the Annual Fall Meeting of Society of Petroleum Engineers, Houston, TX, 5-8 October. SPE-1108-G. http://dx.doi.org/10.2118/1108-G.

King, G. E. 2010. Thirty Years of Gas Shale Fracturing: What Have We Learned? Presented at the SPE Annual Technical Conference and Exhibition, Florence, Italy, 19–22 September. SPE-133456-MS. https://doi.org/10.2118/1110-0088-JPT.

Kresse, O., Cohen, C., Weng, X., Wu, R. and Gu, H. 2013. Numerical Modeling of Hydraulic Fracturing in Naturally Fractured Formations. 45th US Rock Mechanics/Geomechanics Symposium, San Francisco, California, 26-29 June. 11-363 ARMA.

Kundert, D., & Mullen, M. 2009. Proper Evaluation of Shale Gas Reservoirs Leads to a More Effective Hydraulic-Fracture Stimulation. Presented at SPE Rocky Mountain Petroleum Technology Conference, Denver, Colorado, 14-16 April. SPE-123586-MS. https://doi.org/10.2118/123586-MS

Li, N., Li, J., Zhao, L., Luo, Z., Liu, P. and Guo, Y. 2016. Laboratory Testing on Proppant Transport in Complex-Fracture Systems. SPE Production & Operations. SPE-181822-PA. https://doi.org/10.2118/181822-PA.

Liu, Y. and Sharma, M.M. 2005. Effect of fracture width and fluid rheology on proppant settling and retardation: an experimental study. Presented at the Annual Technical Conference & Exhibition, Dallas, TX, 9-12 October. SPE-96208-MS. https://doi.org/10.2118/96208-MS.

Lun, C.K., Savage, S.B., Jeffrey, D.J., 1984. Kinetic theories for granular flow: inelastic particles in coquette flow and slightly inelastic particles in a general flow field. Journal of Fluid Mechanics 140, 223-256.

Mack, M., Sun, J. and Khadilkar, C. 2014. Quantifying proppant transport in thin fluids: theory and experiments. Presented in SPE Hydraulic Fracturing Technology Conference, Woodlands, TX, 4–6 February. SPE-168637-MS. https://doi.org/10.2118/168637-MS.

Miller, C., Waters, G. and Rylander, E. 2008. Evaluation of production log data from horizontal wells drilled in organic shales. SPE North American Unconventional Gas Conference and Exhibition, paper SPE 144326-MS, 23 p.

Mobbs, A. T., and Hammond, P. S. 2001. Computer simulations of proppant transport in a hydraulic fracture. SPE Prod. Facil., pages 112–121, 2001.

Moody, L. F. 1944. Friction factors for pipe flow. Transactions of the ASME 66 (8): 671–684.

Nabi, M., Vriend, H. J.,Mosselman. E., Shimizu. Y. 2012. Detailed simulation of morphodynamics: 1 Hydrodynamic model. Water Resources. Res., 48, W12523.

Nolte, K. G. (1988). Discussion of examination of a cored hydraulic fracture in a deep gas well. SPE Production & Facilities 8(03), 159–164. SPE 26302.

Novotny, E. J. 1977. Proppant Transport. Paper SPE 6813 presented at the SPE Annual Technical Conference and Exhibition, Denver, Colorado, 9-12 September. SPE-6813-MS. https://doi.org/10.2118/6813-MS.

Ocone, R., Sundaresan, S. and Jackson, R. 1993. Gas-particle flow in a duct of arbitrary inclination with particle-particle interaction. Fluid Mechanics and Transport Phenomena 39, 1261-1271

Olga, K., Xiaowei, W., Dimitry, C., Romain, P. and Charles, C. 2013. Effect of Flow Rate and Viscosity on Complex Fracture Development in UFM Model. Presented at the ISRM International Conference for Effective and Sustainable Hydraulic Fracturing, Brisbane, Australia, 20-22 May. ISRM-ICHF-2013-027.

Olson, K., Southwestern Energy, 2011, Personal Communication.

Palisch, T.T., Vincent, M.C., and Handren, P.J. 2010. Slickwater Fracturing: Food for Thought. SPE Production & Operations 25 (3): 327-344. SPE-115766-PA. https://doi.org/10.2118/115766-MS.

Patankar, N. A., Joseph, D. D., Wang, J., Barree, R. D., Conway, M., and Asadi, M. 2002. Power law correlations for sediment transport in pressure driven channel flows. International Journal of Multiphase Flow 28 (8): 1269-1292. http://dx.doi.org/10.1016/S0301-9322(02)00030-7.

Rickards, A.R., Brannon, H.D., Wood, W.D., and Stephenson, C.J., 2003, High Strength, Ultralightweight Proppant Lends New Dimensions to Hydraulic Fracturing Applications, SPE 130 paper 84308, presented at the 2003 SPE Annual Technical Conference and Exhibition, Denver, October 5-8, 2003.

Rickards, A.R., Brannon, H.D., and Wood, W.D. 2006. High Strength, Ultralightweight Proppant Lends New Dimensions to Hydraulic Fracturing Applications. SPE Production & Operations 21 (2): 212-221. SPE-84308-PA. http://dx.doi.org/10.2118/84308-PA.

Rimassa, S. M., Howard, P. R. and Blow, K. A. 2009. Optimizing Fracturing Fluids From

Flowback Water. Presented at the SPE Tight Gas Completions Conference, San Antonio, Texas, USA, 15-17 June 2009. SPE-125336-MS. http://dx.doi.org/10.2118/125336-MS

Sahai, R. 2012. Laboratory Evaluation of Proppant Transport in Complex Fracture Systems. MS thesis, Colorado School of Mines, Golden, Colorado (October 2012).

Sahai, R., Miskimins, J. L., and Olson, K. E. 2014. Laboratory Results of Proppant Transport in Complex Fracture Systems. Society of Petroleum Engineers. Presented at the SPE Hydraulic Fracturing Technology Conference, Woodlands, Texas, 4-6 February. SPE-168579-MS. http://dx.doi.org/10.2118/168579-MS.

Sampaio, J. 2016. Drilling fluid laboratory manual Colorado School of Mines.

Savalli, L., and Engelder, T. (2004). Mechanisms controlling rupture shape during subcritical growth of joints in layered rocks. Geological Society of America Bulletin, 117 (3), DOI: 10.1130/B25368.1

Schein, G.W., Carr, P.D., Canan, P.A., and Richey, R., 2004, Ultra Lightweight Proppants: Their Use and Application in the Barnett Shale, SPE paper 90838, presented at SPE Annual Technical Conference and Exhibition held in Houston, Texas, U.S.A, September 26-29, 2004.

Shah, S. and Asadi, M. 1997. Fracturing fluid characterization: State-of-the-art facility and advanced technology. sponsored by Gas Research Institute under contract 5091-211-2114 and the U.S. Department of Energy under contract DE-FC21-92MC29077 Presented at the Natural gas conference, Houston, Texas, 24-27 March.

Shields, A. 1936. Anwendung der ahnlichkeitsmechanik und der turbulenzforschung auf die geschiebebewegung. Mitteilungen der Preussischen Versuchsanstalt fur Wasserbau und Schiffbau 26 (1): 5-24.

Smith, B. L., Baig, A. M., Urbancic, T., and Viegas, G. F. 2015. En echelon Fracture Growth in Shales During Hydraulic Stimulation. Agu Fall Meeting Abstracts. 2015.

Smith, M. B., Klein, H. H. 1995. Practical Applications of Coupling Fully Numerical 2-D transport Calculation With a PC-Based Fracture Geometry Simulator. Society of Petroleum Engineers paper 30505, 1995

Smith, M. and Montgomery, C. 2015. Hydraulic fracturing. CRC Press.

Southard, J. 2006. An Introduction to Fluid Motions, Sediment Transport, and Current Generated Sedimentary Structures. MIT Open Courseware, 1 September 2006, http://ocw.mit.edu/courses/earth-atmospheric-and-planetary-sciences (accessed 5 September 2017).

Steward, D.B., 2013. George P. Mitchell and the Barnett shale. Journal of Petroleum Technology 65.11 (2013): 58-68.

Stokes, G.G. 1851. On the Effect of the Internal Friction of Fluids on the Motion of Pendulums. Mathematical Proceedings of the Cambridge Philosophical Society 9 (8): 287.

Sun, Y., Wu, Q., Bai, B. and Ma, Y. 2013. The Flow Behavior of Friction Reducer in Microchannels During Slickwater Fracturing. Presented at the SPE Production and Operations Symposium, Oklahoma City, Oklahoma, USA SPE-164476-MS. http://dx.doi.org/10.2118/164476-MS

Syamlal, M., W. Rogers, and T. J. O'Brien. 1993. MFIX documentation: Theory guide. DOE/METC-94/1004, DE9400,097, 49 pp., U.S. Dep. of Energy, Washington, D. C.

Tomac, I. and Gutierrez, M., 2016. Coupled hydro-thermo-mechanical modeling of hydraulic fracturing in quasi-brittle rocks using BPM-DEM. Journal of Rock Mechanics and Geotechnical Engineering.

Tsai, K., Fonseca E., Degaleesan, S. and Lake, E. 2013. Advanced computational modeling of proppant settling in water fractures for shale gas production, SPE J. **18**, 50-56.

Unwin, A. T. and Hammond, P. S. 1995. Computer simulations of proppant transport in a hydraulic fracture. Presented at the Society of Petroleum Engineers Western Region Meeting, Bakersfield, California, 8-10 March. SPE-29649-MS. https://doi.org/10.2118/29649-MS.

US Department of Energy: "Modern Shale Gas Development in the United States: A Primer," US Department of Energy, 2010.

U.S. Energy Information Administration (EIA), 2013 Dry Natural Gas Production (Million Cubic Feet). 30 Nov. 2013.

U. S. Energy Information Administration (EIA), 2011. Technically Recoverable Shale Oil and Shale Gas Resources: An Assessment of 137 Shale Formations in 41 Countries outside the United States. 21 June 2011, https://www.eia.gov/pressroom/presentations/newell_06212011.pdf (accessed 30 September 2017).

Warpinski, N., Kramm, R., Heinze, J. and Waltman, C. 2005. Comparison of Single-and Dual-Array Microseismic Mapping Techniques in the Barnett Shale. 2005. Presented at the SEG Annual Meeting, Houston, Texas, 6-11 November. SEG-2005-1261.

Warpinski, N.R. and Teufel, L.W., 1987, Influence of Geologic Discontinuities on Hydraulic Fracture Propagation, Journal of Petroleum Technology, 1987, vol. 39, no. 2, pg. 209-220.

White, G. L. 1964. Friction Pressure Reducers in Well Stimulation. Journal of Petroleum Technology 16 (8): 865 - 86810.2118/802-PA

Woodworth, T.R. and Miskimins, J.L. 2007. Extrapolation of laboratory proppant placement behavior to the field in slickwater fracturing applications. Presented at the 2007 SPE Hydraulic Fracturing Technology Conference, College Station, Texas, 29-31 January. SPE-106089-MS. http://dx.doi.org/10.2118/106089-MS.

Wu, W. and Wang, S. 2006. Formulas for sediment porosity and settling velocity. Journal of Hydraulic Engineering 132 (8): 858-862. http://dx.doi.org/10.1061/(ASCE)0733- 9429 (2006) 132:8 (858).

Zhang, G., Gutierrez, M. and Li, M. 2017. Numerical simulation of transport and placement of multi-sized proppants in a hydraulic fracture in vertical wells. Granular Matter, 19(2).

Zhong Jianhua, Liu Shengxin, Ma Yinsheng, et al. 2016. Macro-fracture mode and micro-fracture mechanism of shale. Petroleum Exploration and Development, 2016, 42(2): 242–250.